UNIVERSITY OF CALIFORNIA
SANTA CRUZ

NOVEL MOLECULAR ISOTOPE PROXIES IN BIVALVES FOR RECONSTRUCTING SPATIAL AND TEMPORAL BIOGEOCHEMICAL CYCLING IN MARINE ECOSYSTEMS

A dissertation submitted in partial satisfaction
of the requirements for the degree of

DOCTOR OF PHILOSOPHY

in

OCEAN SCIENCES

by

Natasha L. Vokhshoori

December 2021

The Dissertation of Natasha L. Vokhshoori
is approved:

_____
Professor Matthew D. McCarthy, Chair

_____
Professor Ana Christina Ravelo

_____
Researcher Nancy Prouty

_____
Researcher Torben Rick

_____
Peter Biehl
Vice Provost and Dean of Graduate Studies

Table of Contents

List of Figures

List of Tables

ABSTRACT

Novel molecular isotope proxies in bivalves for reconstructing spatial and temporal biogeochemical cycling in marine ecosystems

by

Natasha L. Vokhshoori

Novel molecular isotope proxies measured in bivalve tissues represent a wide range of approaches for tracing ecological and climatological change through time and space. In comparison to other oceanographic data used to reconstruct modern and past biogeochemical cycles (e.g., marine sediment cores), chemical signals preserved in sessile, filter-feeding mollusks record climate and ecological signals directly in the context of a local environment. As global planetary warming accelerates climate change, marine ecosystems are exhibiting vastly different responses in terms of nutrient availability, phytoplankton community composition, and fundamental baseline biogeochemical cycles. Responses are particularly dynamic in highly variable coastal regions, underscoring the need for creating detailed, local historical and geologic records to understand how specific ecosystems and regions have responded to past climatic regime shifts.

In my dissertation, I have developed a set of novel approaches that couple bulk and compound-specific isotopes of amino acids (CSI-AA) in multiple bivalve tissues (shell and soft tissue) to reconstruct the *integrated* biogeochemical histories of environment in which bivalves grow. These new integrative isotope techniques are particularly valuable for environments with extreme variability (e.g., nearshore margins), those that are very difficult to sample (e.g., the deep-sea), or as new paleo reconstruction approaches which can be used with any reasonably preserved shell sample from either sediment cores or archaeological sites.

Key findings include: the development of a novel suite of geochemical proxies for tracing chemosynthetic production in spatially heterogenous, deep-sea methane cold seeps,

including for the first time quantifying the amount of nitrogen obtained through heterotrophic filter-feeding vs. chemoautotrophy in a chemosymbiotic bivalve (Chapter 1). These new geochemical proxies can now be applied to any remnant bivalve shell to reconstruct the biogeochemical histories of often times transient methane seep systems. Next, I tested and calibrated CSI-AA proxy approaches in shell matrix protein (Chapter 2) to develop preserved bivalve shell as a bioarchive across multiple environments. I compared isotope patterns in three different bivalve species from two coastal ecosystems (littoral and estuary) and show that the well-established ecological isotope proxies (niche width, baseline $\delta^{13}C$ and $\delta^{15}N$, trophic level, and resource contribution) calibrated in bivalve soft tissue are directly transferred and preserved to shell protein matrix. However, in this chapter I also show that past CSI-AA trophic level calculations are fundamentally inaccurate and propose a new mollusk-specific trophic level equation required for both soft tissue and shell, linked to consistently compressed trophic discrimination factors and shell isotope routing. Finally, to determine the fidelity of isotope signals in ancient bivalve shell, I tested the preservation of bulk and CSI-AA isotope values and patterns in a suite of archaeological shells spanning a wide range of time periods between the middle to late Holocene and depositional preservation environments (Chapter 3). I show that even in subfossil shells whose bulk isotopes are strongly diagenetically altered, CSI-AA proxies are intact across almost 6 kyr of preservation. This work quantitively demonstrates CSI-AA preservation in the insoluble shell matrix protein of bivalves and sets the stage for using bivalve shell as bioarchives for CSI-AA parameters, to reconstruct paleoecological histories of nearshore systems with far more detail and precision that has ever been possible.

To Mark

the rock star to my sea star

***

“The journey of a thousand miles begins with a single step.”

- Lao-tzu

Acknowledgements

My deepest thanks to my advisor Matthew McCarthy and his unwavering commitment to mentor me, even after all these years. I am also grateful to my committee members Christina Ravelo, Torben Rick, and particularly Nancy Prouty, their feedback on my research helped to improve each project and reach it to completion. Special gratitude is extended to Stephanie Christensen, our lab manager, whose professionalism and kindness was always a pleasure to be around. And thank you to the rest of the UCSC Stable Isotope Lab, Dyke Andreasen and Colin Carney for working with me to produce the best data possible.

I would not be here without the friendship and support of the McCarthy Lab: Matt McCarthy, Steph Christensen, Brett Tipple, Yuan Shen, Hilary Close, Hope Ianiri, Beryl DeLong, Eve Pugsley, Danielle Glynn, Ily Iglesia and Taylor Broek. Our lab meetings were always too long but really inciteful. Conferences were more fun as a lab group, thanks for the memorable times in Puerto Rico! Throughout my PhD career, I had the pleasure of mentoring several highly talented undergraduate students, some of whom completed Senior Theses with me: Jade MacMillan, Laurel Teague, Alexander Bailess and Brennan Popovic.

This work was made possible by the support from (in alphabetical order): ARCS Foundation Scholar Award, Friends of Seymour Center, Future Leaders of Coastal Science Award, Hammett Fellowship, Mathais UC Reserve Research Fund, Myer's Oceanographic and Marine Biology Trust and United States Geological Survey.

The first chapter of this dissertation includes a reprinted version of previously published work:

Vokhshoori, N. L., McCarthy M. D., Close H. G., Demopoulos A. W. J., & Prouty N. G. (2021). New geochemical tools for investigating resource and energy functions at deep-sea cold seeps using amino acid δ15N in chemosymbiotic mussels (*Bathymodiolus childressi*). Geobiology, 00, 1–17. https://doi.org/10.1111/gbi.12458

Matthew D. McCarthy and Nancy G. Prouty supervised this project, Hilary Close and Amanda Demopoulos are also contributing co-authors, but the analysis and writing of this paper were substantially my own.

The second chapter of this dissertation contains a reprint of submitted work in review:

Vokhshoori, N.L., Tipple, B.J., Teague, L., Bailess, A., & McCarthy, M.D. Calibrating bulk and amino acid $\delta^{13}C$ and $\delta^{15}N$ isotope ratios between bivalve soft tissue and shell for reconstructing paleoecological archives. Submitted October 2021 to *Palaeogeography, Palaeoclimatology, Palaeoecology*.

Matthew D. McCarthy supervised this project, Brett Tipple, Laurel Teague and Alexander Bailess are also contributing co-authors. Again, the analysis and writing of this manuscript were substantially my own.

Introduction

Climate regime shifts due to natural oscillations, such as El Niño Southern Oscillation and Pacific Decadal Oscillation, or anthropogenic-driven ocean warming can have major impacts nutrient availability, phytoplankton community composition, and fundamental biogeochemical cycles in marine systems. A classic case study of natural oscillation phenomenon is in the Pacific Ocean where over the past 50 years historical observations have documented movement from a cool “anchovy regime” to a warm “sardine regime” and back to an anchovy regime. This natural variation was found to be directly linked to fluctuations in sea surface temperature and change in thermocline slope (Chavez et al. 2003). Characterizing natural biochemical cycle variation, especially in the face of human-induced planetary warming and resource extraction, is therefore critical to understanding ecosystem function in response to climate forcing. Moreover, coastal ecosystem response to climate anomalies can be highly localized (Jacox et al. 2016, Sakuma et al. 2016, Starko et al. 2019). However, most regions of the ocean lack highly detailed historical/geological oceanographic data to resolve site-specific or localized change.

Geologic records for reconstructing past ocean climate are traditionally derived from marine sediment cores. Yet in highly dynamic regions such as coastal upwelling systems, or otherwise inaccessible ephemeral chemosynthetic deep-sea habitats, preserved organic matter in sediment cores may be too crude in resolution for capture the level of detail required to understand rapid system change. Specifically, sinking algal particles are subjected to advection, microbial resynthesis, and physical degradation before it is deposited and buried on the seafloor, leading to variability in organic supply at any specific location. In all such environments, an archive that can capture the level of detail of precise location, together with high temporal resolution, is critical to understanding rapid change. Bivalves (oysters, mussels, clams) are sessile, filter-feeders of particles from the local, ambient water column, and

therefore are unambiguous for the habitat they are recording. Bivalves (or mollusks in general) are also some of the most abundant macroinvertebrates in benthic marine ecosystems, and their shelly hard parts preserve well in archaeological middens and also within sediments. As such, they represent ideal archives for developing novel isotope proxies that can be used for understanding integrated nutrient and primary producer dynamics, and broader change in the biogeochemical cycling of carbon and nitrogen at the base of marine food webs in both time and space.

Stable isotope analysis of carbon ($\delta^{13}C$) and nitrogen ($\delta^{15}N$) are highly informative measurements for reconstructing biogeochemical cycles and ecosystem variability. Whole tissue, or bulk isotope values in an organism reflects a combination of the isotopic composition at the base of the food web in which they forage, as well as diet composition. Consumers typically have higher isotope values than their food source due to physiologically mediated isotope discrimination, which occurs during assimilation and tissue synthesis. However, trophic discrimination factors (TDFs) can vary strongly for bulk isotopes (0 to 3‰ for $\delta^{13}C$, and 2 to 5‰ for $\delta^{15}N$; Vanderklift & Posnard 2003, DeNiro & Epstein 1978), introducing substantial uncertainty in any ecosystem trophic assessment derived from bulk isotope data alone.

In order to untangle the sometimes confounding effects of a mixed diet from variation in the composition of primary producers (i.e. baseline), compound-specific isotopes of amino acids (CSI-AA) for both carbon ($\delta^{13}C_{AA}$) and nitrogen ($\delta^{15}N_{AA}$) have been developed in recent years as a suite of novel molecular isotope proxies for ecosystem and paleo-oceanographic studies. The development of CSI-AA proxies is based on observed trophic isotope fractionation behavior as well as fundamental evolutionary pathways for protein synthesis.

Animals must acquire essential amino acids (EAAs) directly from their diet to build and maintain proteinaceous tissues, and thus the $\delta^{13}C$ values of this class of AAs show little to no fractionation with trophic transfer up the food chain (Howland et al. 2003, McMahon et al. 2015). The unique isotopic “fingerprint” of compounds synthesized by primary producers (Larsen et al. 2009) is therefore also preserved up the food chain for which C sources can

be reconstructed from a consumer (e.g. Larsen et al. 2013). For $\delta^{15}N_{AA}$, certain AAs undergo isotopic enrichment due to significant transamination and deamination linked to the central glutamate pool (McMahon & McCarthy 2016), and are termed "trophic AAs" (e.g. glutamic acid, proline), while other AAs (e.g. phenylalanine) show little isotopic discrimination with trophic level and are termed "source AAs" (McClelland & Montoya 2002, Popp et al. 2007, Chikaraishi et al. 2009), which can directly indicate $\delta^{15}N_{baseline}$ values in a system. Taken together, CSI-AA of C and N have proven to be highly informative in ecological and geochemical studies. The most notable is the ability to estimate trophic level (TL), measure the isotope value at the base of the food-web (i.e. baseline) and characterize primary-producer groups all from a consumer's tissue. Further, other CSI-AA parameters have also been developed for microbially influenced systems to measure degradation or degree of microbial resynthesis ($\sum V$; McCarthy et al. 2007), and now for the first time to identify unique signatures for tracing chemosynthetic bacterial source in deep-sea systems (see Chp. 1). Overall, while bulk isotope analysis is relatively inexpensive to run, thereby allowing for larger sample numbers important for addressing ecological questions such as trophic plasticity of a community or group, CSI-AA provides far more detailed information to understand changes in both ecosystems and biochemical processes driving isotope patterns.

Thesis Overview

This thesis aims to develop and apply a set of novel approaches coupling bulk and amino-acid compound-specific stable isotope analysis in multiple bivalve tissues to reconstruct the integrated biogeochemical histories of any environment in which bivalves are found.

These new integrative isotope techniques will be particularly valuable for environments with extreme variability (e.g., nearshore margins), those that are very difficult to sample (e.g., the deep sea), or as new paleoenvironmental reconstruction techniques where preserved shell can be sampled from sediments, subfossil, or archaeological sites.

The following questions provide the main framework of my thesis:

1. *How well do bivalve tissue isotope values reflect base of the food web processes, and record primary producer community composition?*
2. *Are there tissue-specific calibrations required for utilizing ancient shells as bioarchives?*
3. *How does diagenesis affect amino acid isotope signals in ancient shell archives?*

With my newly developed geochemical proxies and tissue-specific calibrations, future research will then be able to investigate the changes in nitrogen sources and primary production for different marine ecosystems and through time.

To explore these research questions, this dissertation is divided into three chapters. Chapter 1 explores the spatial heterogeneity in the trophic ecology of deep-sea chemosynthetic mussels from methane seeps along the US Atlantic Margin. I analyzed bulk $\delta^{15}N$ and $\delta^{13}C$, and the $\delta^{15}N_{AA}$ values in the gill and adductor tissue, and compare these data to analogous data from littoral mussels as a heterotrophic ocean endmember. I then developed a new approach to quantify the amount of heterotrophic filter-feeding vs. chemoautotrophy in seep mussels in such environments. Chapter 2 is a methodological study aimed at ground-truthing the use of CSI-AA proxies in mussel shell. I explore and then calibrate the isotopic offsets between soft tissue and shell matrix organic matter in bivalves from different coastal ecosystems (e.g. littoral, estuarine), setting the stage for applying CSI-AA-based parameters for paleo-ecological reconstructions of nearshore systems. Chapter 3 incorporates calibrations from Chapter 2 and analyzes the bulk and amino acid $\delta^{13}C$ and $\delta^{15}N$ changes occurring in archaeological mussel shell from the California Channel Islands to test potential impacts of diagenesis and/or contamination. The overall goal is to determine if such subfossil shells which are diagenetically altered can still preserve unaltered AA signatures, and so be used for ecological reconstructions and to investigate the molecular level mechanisms driving observed changes in bulk isotope values.

References

Chavez, F.P., Ryan, J., Lluch-Cota, S.E., Ñiquen, M. (2003) From anchovies to sardines and back: multidecadal change in the Pacific Ocean. Science 299, 217–221.

Chikaraishi, Y., Ogawa, N.O., Kashiyama, Y., Takano, Y. and others (2009) Determination of aquatic food-web structure based on compound-specific nitrogen isotopic composition of amino acids. Limnol Oceanogr Methods 7: 740−750

DeNiro, M.J., Epstein, S. (1978) Influence of diet on the distribution of carbon isotopes in animals. Geochim Cosmochim Acta 42:495−506

Howland, M.R., Corr, L.T., Young, S.M.M., Jones, V. and others (2003) Expression of the dietary isotope signal in the compound-specific $\delta^{13}C$ values of pig bone lipids and amino acids. Int J Osteoarchaeol 13:54−65

Jacox, M.G., Hazen, E.L., Zaba, K.D., Rudnick, D.L., Edwards, C.A., Moore, A.M., Bograd, S.J. (2016) Impacts of the 2015–2016 El Niño on the California Current System: Early assessment and comparison to past events, Geophys. Res. Lett., 43, 7072–7080, doi:10.1002/2016GL069716.

Larsen, T., Taylor, D.L., Leigh, M.B., O'Brien, D.M. (2009) Stable isotope fingerprinting: a novel method for identifying plant, fungal, or bacterial origins of amino acids. Ecology 90:3526−3535

Larsen, T., Ventura, M., Andersen, N., O'Brien, D.M., Piatkowski, U., McCarthy, M.D. (2013) Tracing carbon sources through aquatic and terrestrial food webs using amino acid stable isotope fingerprinting. PLoS ONE 8, e73441.

McCarthy, M.D., Benner, R., Lee, C., Fogel, M.L. (2007) Amino acid nitrogen isotopic fractionation patterns as indicators of heterotrophy in plankton, particulate, and dissolved organic matter. Geochim. Cosmochim. Acta 71, 4727–4744.

McClelland, J.W., Montoya, J.P. (2002) Trophic relationships and the nitrogen isotopic composition of amino acids. Ecology 83:2173−2180

McMahon, K.W., McCarthy, M.D. (2016) Embracing variability in amino acid δ15N fractionation: mechanisms, implications, and applications for trophic ecology. Ecosphere 7: e01511

Popp, B.N., Graham, B.S., Olson. R.J., Hannides, C., Lott, M.J. (2007) Insight into the Trophic Ecology of Yellowfin Tuna, *Thunnus albacares*, from Compound- Specific Nitrogen Isotope Analysis of Proteinaceous Amino Acids*. Terrestrial Ecology* 1: 173–190.

Starko, S., Bailey, L.A., Creviston, E., James, K.A., Warren, A., Brophy, M.K., Danasel, A., Fass, M.P., Townsend, J.A., Neufeld, C.J. (2019) Environmental heterogeneity mediates scale-dependent declines in kelp diversity on intertidal rocky shores. PLoS ONE 14: e0213191.

Vanderklift, M.A., Ponsard, S. (2003) Sources of variation in consumer-diet ^{15}N enrichment: a meta-analysis. Oecologia 136:169−182

Chapter 1

Geochemical tracers of nitrogen chemosynthesis in seep mussels

"Captain Nemo pointed to this prodigious heap of shellfish, and I saw that these mines were genuinely inexhaustible, since nature's creative powers are greater than man's destructive instincts."

- Jules Verne, *Twenty Thousand Leagues Under the Sea*

***

What exists is out of reach and very deep. Who can fathom it?

- Ecclesiastes 7:24

Reprinted with permission from Wiley, the following contains material that was published in *Geobiology* on June 2021:

New geochemical tools for investigating resource and energy functions at deep-sea cold seeps using amino acid $\delta^{15}N$ in chemosymbiotic mussels (*Bathymodiolus childressi*)

Natasha L. Vokhshoori, Matthew D. McCarthy, Hilary G. Close, Amanda Demopoulos and Nancy G. Prouty

Abstract: In order to reconstruct the ecosystem structure of chemosynthetic environments in the fossil record, geochemical proxies must be developed. Here, we present a suite of novel compound-specific isotope parameters for tracing chemosynthetic production with a focus on understanding nitrogen dynamics in deep-sea cold seep environments. We examined the chemosymbiotic bivalve *Bathymodiolus childressi* from three geographically distinct seep sites on the NE Atlantic Margin and compared isotope data to non-chemosynthetic littoral mussels to test whether water depth, seep activity, and/or mussel bed size are linked to differences in chemosynthetic production. The bulk isotope analysis of carbon ($\delta^{13}C$) and nitrogen ($\delta^{15}N$), and $\delta^{15}N$ values of individual amino acids ($\delta^{15}N_{AA}$) in both gill and muscle tissues, as well as $\delta^{15}N_{AA}$-derived parameters including trophic level (TL), baseline $\delta^{15}N$ value ($\delta^{15}N_{Phe}$), and a microbial resynthesis index (ΣV), were used to investigate specific geochemical signatures of chemosynthesis. Our results show that δ15NAA values provide a number of new proxies for relative reliance on chemosynthesis, including TL, ∑V, and both $\delta^{15}N$ values and molar percentages (Gly/Glu mol% index) of specific AA. Together, these parameters suggested that relative chemoautotrophy is linked to both degree of venting from seeps and mussel bed size. Finally, we tested a Bayesian mixing model using diagnostic AA $\delta^{15}N$ values, showing that percent contribution of chemoautotrophic versus heterotrophic production to seep mussel nutrition can be directly estimated from $\delta^{15}N_{AA}$ values. Our results demonstrate that $\delta^{15}N_{AA}$ analysis can provide a new set of geochemical tools to better understand mixotrophic ecosystem function and energetics, and suggest extension to the study of ancient chemosynthetic environments in the fossil record.

1.1 Introduction

Nitrogen biogeochemical cycling in deep-sea chemosynthetic environments such as methane cold seeps and hydrothermal vents is highly mediated by microbial life (Paerl & Pinckney, 1996). The ability for resident organisms to assimilate a wide variety of nitrogen sources allows for these ecosystems to be remarkably productive and widespread. The interactions between chemosynthetic- and photosynthetic-based ecosystems appear to be greater than previously realized (see Review by Levin et al., 2016), with the importance of chemosynthetic production potentially extending into certain fisheries (Grupe et al., 2015; Levy & Lee, 1988; Seabrook et al., 2019).

At both ancient and modern vents and seeps, animal–bacterial chemosymbiotic pairings are important for converting chemical energy into food resources for the surrounding ecosystem and tend to be dominated by a limited number of invertebrate megafaunal taxa (Aharon, 1994; Levin, 2005). One of the most abundant genera found in modern vents and methane seeps is bathymodiolin mollusks, a sub-family within Mytilidae and endemic to chemosynthetic habitats, that can exploit chemical energy percolating from the seafloor from biogenic methanogenesis by hosting methanotrophic bacterial endosymbionts in their gill tissues (Lee & Childress, 1994; Lee & Childress, 1995). Bathymodiolus spp. are therefore an important link in the trophic transfer of energy to surrounding benthic food webs. However, their feeding ecologies are not fully understood. While methane acts as both an energy source and carbon source for building macromolecules, sources of nitrogen (N) for chemosynthetic production in symbionts are less known, especially given the heterogeneity of seep activity between sites (Bourque et al., 2017). *Bathymodiolus childressi* are mixotrophic, relying on chemosymbiosis with its methanotrophic endosymbionts (Lee & Childress, 1994; Lee & Childress, 1995) while still maintaining a functional gut for hetero-trophic filter feeding (Page et al., 1990; Pile & Young, 1999). This allows the seep mussel to potentially meet its N demands

from a variety of sources, including dissolved inorganic nitrogen (DIN; e.g., NH4+, NO3−) or diazotrophy via its endosymbionts and suspended and sinking particulate organic matter (POM) via filter feeding. However, what is not known is what environmental conditions may influence the reliance on heterotrophy versus chemo-symbiosis and thus its effect on biogeochemical cycles. New approaches to quantitatively estimate degree of bathymodiolin reliance on heterotrophy versus chemosymbiosis could shed light on the relative importance of photosynthetic production in chemosynthetic environ-ments, and vice versa, across multiple environments from present to the geologic past, where protein is preserved in shell and carbonates in some cases chemosynthetic clam beds are found as early as middle to late Eocene (~40 Mya; Kiel, 2010).

Common tools for tracing organic C and N sources include bulk isotopes of organic carbon ($\delta^{13}C$) and nitrogen ($\delta^{15}N$). Typically, $\delta^{13}C$ values between −40‰ and −80‰ reflect methane-derived organic carbon, a function of the discrimination of ^{13}C during methanogen-esis in sediments. Bulk $\delta^{13}C$ and $\delta^{15}N$ values are invaluable tools in ecological studies to compare differences in trophic niches of species (Jackson et al., 2011) and for assessing environmental gradients (Graham et al., 2010). However, it is more difficult to trace nitrogen sources and nutrient cycling using bulk isotopes alone because bulk $\delta^{15}N$ values represent the combined signal of trophic effects and baseline N source in a system. In particular for heterogeneous environments, it can therefore be especially difficult to interpret bulk isotope values alone. For example, *B. childressi* from methane seeps in the Gulf of Mexico were found to have $\delta^{15}N$ bulk values between −18.0‰ and 5.0‰ (MacAvoy et al., 2008), and −2.2‰ and 4.5‰ for the USAM (Demopoulos et al., 2019), a range that is ambiguous in terms of distinguishing the influence of heterotrophy compared to differences in baseline $\delta^{15}N$ values of the DIN pool (Becker et al., 2014).

Compound-specific isotopes of amino acids (CSI-AA) of nitrogen ($\delta^{15}N_{AA}$) offer an entirely new dimension source of information beyond bulk isotope values, because they independently estimate both the trophic level of an animal and simultaneously the baseline isotope value of its N source from a single sample. In addition, $\delta^{15}N_{AA}$- based indices have been developed to simultaneously trace microbial sources (e.g., ΣV; McCarthy et al., 2007). This new information is based on the differential fractionation of specific AA with trophic transfer (McClelland & Montoya, 2002). $\delta^{15}N_{AA}$ values from marine samples fall within three canonical biochemical groupings: trophic AAs (fractionate strongly and predictably with trophic transfer), source AAs (show little to no fractionation with trophic transfer), and threonine (displays a unique inverse fractionation) (reviewed by McMahon & McCarthy, 2016). These three groupings are the basis for CSI-AA proxies which have been developed for baseline $\delta^{15}N$ values and trophic level (TL), and have been demonstrated in previous work for a range of organ-isms, including bivalves (Vokhshoori & McCarthy, 2014), corals (Prouty et al., 2014; Sher-wood et al., 2014), and top ocean predators (e.g., Vokhshoori et al., 2019). Together, the unique systematics of $\delta^{15}N_{AA}$ allows CSI-AA to be used in under- standing N sources and trophic dynamics in greater detail. However, $\delta^{15}N_{AA}$ patterns and systematics associated with chemosynthetic production have never been previously investigated. In part, this is due to the difficulty of obtaining environmentally relevant endmember samples.

In this study, we explore the application of amino acid nitrogen isotope analysis to better address the sources and mechanisms of N utilization in one of the most ecologically important species within methane seep environments, with a particular focus on $\delta^{15}N_{AA}$ patterns as a promising tracer of chemosymbiotic AA synthesis. *B. childressi* is widely doc-umented at methane seeps and hydro- thermal vents in the Pacific and Atlantic Ocean basins (Duperron et al., 2013), often co-occurring with its close relative *Bathymodiolus heckerae*. However, while its close relative has dual symbiont sup- port from methanotrophic and thiotrophic bacteria, *B. childressi* was recently found to only host methanotrophic symbionts (Coykendall et al., 2019).

Together, these aspects make *B. childressi* an ideal species in which to characterize the CSI-AA patterns of methane chemosymbiosis.

Our overarching goal is to explore new geochemical proxies for seep faunal energy nitrogen sources, which may potentially be applied in the future to interpret fossil seep archives where proteins are preserved (e.g., shells, carbonates), in addition to environmental gradients and temporal changes in seep activity. Our central hypothesis is that chemo-autotroph CSI-AA signatures would be unique from photoautotrophs, based on the differ-ences in metabolic pathways, and that the CSI-AA values from gill tissue where the endo-symbionts reside can be used to identify these patterns. We address the following specific questions: (a) Are there unique $\delta^{15}N_{AA}$ fingerprints associated with chemosynthesis in *B. childressi* tissue, and specifically can the gill tissue in seep mussels where the endosym-bionts are housed, be used as a diagnostic methanotroph chemosynthetic endmember? and (b) Can $\delta^{15}N_{AA}$ values be used to both distinguish and quantify reliance on chemo-symbiosis and heterotrophy in a seep mussel? To address these main questions, we compare $\delta^{15}N_{AA}$ patterns from filter-feeding littoral mussels (a closely related photosynthetic microalgae consumer endmember), phytoplankton, and adjacent surface sediment to those in methanotrophic-hosted seep mussel tissues. We also examine the main inorganic N sources and bulk $\delta^{13}C$ and $\delta^{15}N$ values in seep mussels from across a range of environments with widely varying mussel patch size and finally use our proposed parameters to estimate the degree of chemosynthesis in relation to mussel bed size at three distinct seep locations along the USAM.

1.2 Methods

1.2.1 Study location and site description

Baltimore (390 m), Chincoteague (930 m), and Norfolk (1,490 m) methane seep fields are located along the USAM about 100km off- shore (Fig. 1.1a). *Bathymodiolus childressi*

occurs at all seep sites and range in mussel bed sizes from small, patchy (Fig. 1.1b) to massive fields (Fig. 1.1c) that cover several hundred square meters (CSA Ocean Sciences Inc et al., 2017; Coykendall et al., 2019; Ruppel et al., 2017). Baltimore seep field is the northernmost site and is located on the southern flank of Baltimore Canyon, at the canyon mouth. Chincoteague seep field is ~115 km east of Chincoteague Island on the Virginia margin and is the largest of the three sites in this study (Ruppel et al., 2017). Chincoteague is further down-slope than the other two sites and is not in proximity of a canyon system. Norfolk seep field is the most southern site, located outside of Norfolk Canyon. The surrounding sediments at these seeps also contain living and dead mussel patches, microbial mats, and carbonate rocks (Bourque et al., 2017; Demopoulos et al., 2019; Prouty et al., 2016)

1.2.2 Sample collection and processing

Collections were conducted on the University of Delaware's R/V Hugh R. Sharp (HRS1704 cruise) using the remotely operated vehicle (ROV) Global Explorer managed by Oceaneering Inc. in May of 2017 (Ruppel et al., 2017). Multiple gear types were used to collect

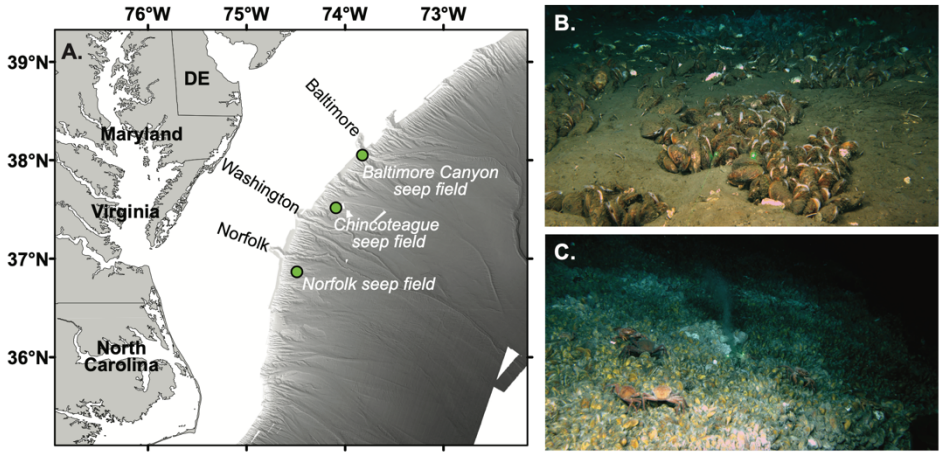

Figure 1. 1 Sampling locations and mussel bed photographs. (a) Map showing the Baltimore Canyon, Chincoteague, and Norfolk seep fields (green circles) sites, relative to the major shelf break canyons (Baltimore, Washington, and Norfolk) along the United States Atlantic margin. In situ photographs show examples of deep-sea mussel (Bathymodiolus childressi) bed environment from (b) Norfolk seep field, a small “sparsely patched” mussel bed, and (c) Chincoteague mussel field, a dense mussel bed with very active methane seeping. Photographs from IMMERS expedition (Interagency Mission for Methane Research on Seafloor Seeps) on the R/V Hugh R. Sharp with ROV Global Explorer in April 2017

samples including scoop and push cores operated by the ROV manipulator arm and Niskin bottles attached to the ROV. Seep mussels were collected from within large mussel beds at three different seep sites (Norfolk, Baltimore and Chincoteague) with the scoop. At Norfolk seep field, we collected specimens from varying sized mussel beds (small, medium, large) to evaluate the potential impact of patch size on seep-defined energy use. Mussel bed sizes represent relative size difference where “small” was defined as areas with only a hand-ful of mussels, “medium” was approximately 3–4 times bigger, and “large” was extensive fields that spanned several video frames. Pushcores (31.65 cm2 × 30 cm) were used to sample sediment from mussel bed and bacterial mat habitats, as well as from background (e.g., non-seep) sediments. From the pushcores, sediment surface water was collected along with porefluids from the upper two fractions (0–2 and 2–4 cm) using Rhizon samplers (0.15-μm pore size). Niskin bottles attached to the ROV were tripped 10 m above the seafloor to collect bottom water from areas where pushcores were taken. Seawater collected for dissolved nutrient analysis was stored in acid- cleaned high-density polyethylene 20-ml scintillation vials and triple- washed with extra filtrate before storage of samples. Littoral mussels were collected from two sites along the California coast: Pacifica in 2010 (37°39′N, 122°29′W) and Santa Cruz in 2016 (36°57′2 N, 122°2′39 W), and stored frozen at −20°C until further processing.

1.2.3 Nutrient and stable isotope analysis

Porewater, sediment surface water, and bottom water were analyzed for dissolved nutrients (NH_4^+ and [NO_3^- + NO_2^-] at the University of California at Santa Barbara's Marine Science Institute Analytical Laboratory via flow injection analysis for NH_4^+ and [NO_3^- + NO_2^-], with precisions of 0.6%–3.0%, 0.6%–0.8%, 0.9%–1.3%, and 0.3%– 1.0% relative standard deviations, respectively. Select samples were collected and analyzed for nitrate isotope ($\delta^{15}N$ and $\delta^{18}O$) analyses at the University of California at Davis’ Stable Isotope Facilities using the denitrifier method (Sigman et al., 2001).

1.2.4 Bulk stable isotope analysis

In the laboratory, mussels were first dissected to separate the adductor muscle and gill tissue, rinsed with deionized water, stored frozen, and then freeze-dried for 24–48 hr along with sediment material. Mussel tissues were then homogenized, and ~0.5 mg was weighed into tin capsules. Sediment samples were acidified with 0.5N hydrochloric acid (HCl) to remove inorganic carbon, dried, and ~500 mg of dry sediment weighed into tin capsules. Stable carbon and nitrogen iso- topes of the organic fraction were measured either at the University of California, Santa Cruz Light Stable Isotope Lab (sil.ucsc.edu), on a Thermo Delta V Advantage Isotope Ratio Mass Spectrometer (IRMS), or at the Washington State University using a Costech elemental analyzer interfaced with a GV instruments Isoprime IRMS. Within-run analytical error was assessed via repeated analysis of internal protein-aceous reference materials (Pugel and Acetanilide). Isotope values are reported using delta (δ) notation in parts per thousand (‰): $\delta^{13}C$ or $\delta^{15}N = [(R_{sample}/R_{standard}) - 1] \times 1{,}000$, where R is the ratio of heavy- to-light isotope of the sample (R_{sample}) and standard ($R_{standard}$), respec-tively, referenced to that of atmospheric N2 (air) for $\delta^{15}N$ and Vienna PeeDee Belemnite (VPDB) for $\delta^{13}C$.

1.2.5 Amino acid stable isotope analysis

A subset of dissected mussel tissue types (gill and muscle), and sediment samples, were analyzed for individual amino acid $\delta^{15}N$ values following established McCarthy Lab protocols (e.g., Batista et al., 2014). Briefly, ~5 mg of mussel tissue and ~500–1,000 mg of sediment were weighed into 8 ml hydrolysis vials, submerged in 1–2 ml of 6N HCl, purged with N2 gas to remove oxygen, and hydrolyzed for 20 hr at 110°C. After hydrolysis, samples were cooled to room temperature until further processing. Sediments were centrifuged at 377 RCF three times for 5 min. Between spins, supernatant was carefully pipetted and transferred into a clean 4-ml dram vial and then rinsed with 1 ml 0.5N HCl. Samples were then dried down under N2 gas at 80°C and resuspended in 1 ml of 0.1N HCl. Sediment samples were

filtered through a 0.22-μm polyethersulfone disk filter. Samples were then purified using cation-exchange chromatography with the DOWEX 50WX8-400 resin. Before dry down, the purified filtrate was spiked with the internal standard Norleucine.

Amino acids were analyzed as trifluoroacetyl isopropyl ester (TFA-IP) derivatives after Silfer et al. (1991) protocol. After drying at 60°C under N2, amino acid isopropyl esters were prepared with a 1:4 mixture of acetyl chloride:isopropanol at 110°C for 60 min and then acetylated using a 1:1 mixture of dichloromethane (DCM) and trifluoroacetic anhydride (TFAA) at 110°C for 10 min. Samples were dried and re-dissolved in ethyl acetate for amino acid analysis. Derivatized sediment samples were further purified using a liquid–liquid ex- traction method with chloroform and P-buffer (1 M $KH_2PO_4^+$ + 1 M Na_2HPO_4). Purified samples were gently dried under N_2 gas, re-acetylated with TFAA, dried again, and re-solubilized in ethyl acetate for final injection. $\delta^{15}N_{AA}$ values were measured using a Varian gas chromatograph coupled to a Finnegan Delta-Plus IRMS at the UCSC-SIL. Using this method, we measured $\delta^{15}N$ values of the following AAs: alanine (Ala), glycine (Gly), threonine (Thr), serine (Ser), valine (Val), leucine (Leu), isoleucine (Ile), proline (Pro), aspartic acid + asparagine (Asx), glutamic acid + glutamine (Glx), phenylalanine (Phe), tyrosine (Tyr), and lysine (Lys). All samples were analyzed in triplicate for nitrogen and corrected to an external AA mix standard. Value verification and reproducibility to monitor consistency of wet chemistry and instrument analysis was checked in two ways: first, the internal Norleucine standard with known value, and second, an ongoing external cyano-bacteria laboratory standard that is analyzed with every sample set according to McCarthy Lab protocols. Reproducibility as estimated with standard deviation for samples and cyanobacteria external standard was typically less than <0.5‰ (range: 0.1‰–1.3‰).

$\delta^{15}N_{AA}$ values are classified into specific AA groupings based on their fractionation behavior and biochemistry. One group of amino acids, known as “trophic AAs,” become

strongly enriched in ^{15}N with trophic transfer (e.g., glutamic acid, proline), while other amino acids tend to show little to no fractionation with trophic transfer (e.g., phenylalanine, lysine, methionine) and are called “source AAs” (McClelland & Montoya, 2002). Molar percentages (Mol%) for each sample were also determined from GC/IRMS data based on peak areas for each AA. Calibration curves were created for each run using a dilution series bracketing all measured peak sizes, created from the same external AA standard used for $\delta^{15}N$ measurements. The average analytical error for Mol% values across all AAs analyzed was ±10 Mol%.

1.2.6 $\delta^{15}N_{AA}$ parameter definitions and statistics

We calculated compound-specific amino acid-derived trophic level (TLCSIA) using the most common single trophic discrimination fac- tor (TDF), which is based on N isotope fractionation between glutamic acid (Glu) and phenylalanine (Phe) in algal-based food webs (Chikaraishi et al., 2009). Multiple TL calculations have been proposed for various food webs (see McMahon & McCarthy, 2016); however, there are no data to evaluate an equation for chemosynthetic-based systems. The chemosynthetic methanotrophs hosted by *B. childressi* likely synthesize AAs *de novo* from inorganic nitrogen sources and therefore should exhibit CSIA patterns similar to other unicellular primary producers, including algae or fee-living bacteria grown on organic-free media (Chikaraishi et al., 2009; Yamaguchi et al., 2017). Importantly, as is well established in CSI-AA literature, the pattern of individual AA relative fractionation is independent of N source $\delta^{15}N$ value. Therefore, the standard TL formulation established for marine food webs seems most representative for the purpose of this study:

$$TL_{CSIA} = 1 + [\ \delta^{15}N_{Glu} - \delta^{15}N_{Phe} - \beta\ /TDF_{Glu\text{-}Phe}\ ], \qquad (1)$$

where $\delta^{15}N_{Glu}$ and $\delta^{15}N_{Phe}$ represent the stable nitrogen isotope values of mussel Glu and Phe, respectively, β represents the difference in $\delta^{15}N$ values between Glu and Phe of primary producers (3.4‰ ± 0.9 for aquatic cyanobacteria and algae; Chikaraishi et al., 2009), and

$TDF_{Glu\text{-}Phe}$ is the literature value of 7.6‰ (McClelland & Montoya, 2002). We note that we use this equation with the caveat that the average β value might not exactly reflect that in chemo-synthetic production. However, while such uncertainty might slightly change absolute TL values (0–0.1 increase), it would not change our interpretation of the relative results between sites, since we are comparing TL between the same species with the same symbionts.

In order to evaluate $\delta^{15}N_{AA}$ metabolic patterns, we normalized measured $\delta^{15}N_{AA}$ values by subtraction from either average $\delta^{15}N$ values of trophic AA ($\delta^{15}N_{TrAA}$) or source AA ($\delta^{15}N_{SrcAA}$) values. This adjustment removes the impact of shifting baseline values or trophic discrimination effects, respectively, allowing $\delta^{15}N_{AA}$ pattern to be directly compared to data from other locations:

$$\text{Normalized } \delta^{15}N_{AA} = \text{Raw } \delta^{15}N_{AA} - \delta^{15}N_{TrAA} \text{ (or } \delta^{15}N_{SrAA}), \quad (2)$$

where the average δ15NTrAA is subtracted from the raw δ15N value of each trophic AA (Glu, Asp, Ala, Ile, Leu, Pro, and Val) and the average δ15NSrcAA is subtracted from each source AA (Gly, Ser, Phe, and Lys) and Thr for each sample, where:

$$\delta^{15}N_{TrAA} = \text{average } \delta^{15}N \text{ values of Glu, Asp, Ala, Ile, Leu, Pro, and Val} \quad (3)$$

$$\delta^{15}N_{SrcAA} = \text{average } \delta^{15}N \text{ values of Gly, Ser, Phe, and Lys} \quad (4)$$

Accumulating studies have indicated that Gly and Ser should not be categorized as source AA, but as “transitional” since they exhibit patterns of both trophic and source AAs depending on quality of diet, however mainly for higher trophic level organisms (reviewed by McMahon & McCarthy, 2016). However, given our data are for primary marine consumers, and results (reported below) suggesting that Gly and Ser behave like source AAs (non-fractionating with trophic transfer), we have reported them in the traditional grouping for the purposes of this study.

The ΣV parameter is a $\delta^{15}N_{AA}$-based proxy for total microbial AA resynthesis, originally proposed by McCarthy et al. (2007), and is based on the average deviation of individual $\delta^{15}N$

values of trophic amino acids from the mean $\delta^{15}N$ value of trophic amino acids. We calculated ΣV values here using seven trophic amino acids (Glu, Asp, Ala, Val, Leu, Ile, and Pro):

$$\Sigma V = 1/n \, \Sigma \, Abs(\chi i) \qquad (5)$$

where χ is the deviation of each trophic AA = $\delta^{15}N_{AA}$ – Avg. $\delta^{15}N$ (Glu, Asp, Ala, Val, Leu, Ile, and Pro), and n is the number of amino acids used in the calculation.

For statistical analyses, t tests, ANOVAs, and mixing models were performed in R (v.3.3.1) with Rstudio interface (v.0.98.1028). Normality (Q–Q plots) and homoscedasticity (Bartlett's test) of the data were verified before statistical analyses. We calculated standard ellipse areas corrected for small sample sizes (SEAc; n < 10) for each site population using the stable isotope Bayesian ellipses in R package (SIBER; Jackson et al., 2011) and used the stable isotope analysis in R package (MixSIAR; Stock & Semmens, 2016) to run mixing models in order to estimate source contribution to mussel diet. The sources were divided into two categories based on feeding mode: chemoautotrophy (symbiont) and heterotrophy (host filter-feeding). The endmember sources for these two modes were inferred from the $\delta^{15}N_{AA}$ values measured in the gill tissue between littoral mussel (complete heterotrophy) and the most active seep site (Chincoteague), based on observations from ROV Global Explorer dive footage showing it as the most actively venting site (Ruppel et al., 2017). The gill tissue was chosen to represent the most appropriate chemosynthetic endmember because symbionts are located entirely in the gills of the mussel host (Childress et al., 1986).

1.3 Results

1.3.1 Nutrient concentrations in mussel beds and surrounding

Ammonium and nitrate concentrations and nitrate δ15N values were measured from three different water types: porewater, sediment sur- face water, and bottom water within our three study sites (Baltimore Canyon, Chincoteague, and Norfolk seep fields; Table 1.1; Fig.

S1). Measurements were taken within various sized mussel beds and from non-seep environments (e.g., background). [NO_3^-] ranged from 1.17μM to 23.59μM, where the highest concentrations were measured in bottom water and the lowest in porewater, irrespective of bed size. The $\delta^{15}N\text{-}NO_3^-$ values ranged from −13.7‰ to 5.6‰; how- ever, $\delta^{15}N\text{-}NO_3^-$ values did not correlate ($p > .05$) with either water type or [NO_3^-]. [NH_4^+] varied widely: 0.67μM to 242μM, with the highest concentrations measured in porewater. Bottom water [NO3−] was consistently ~19μM at all sites. Concentrations of both NH_4^+ and NO_3^- ranged between 0 and 25 μM in sediment surface water. There was also no significant trend in [NO_3^-] versus [NH_4^+] ($p > .05$). Between mussel bed sizes and seep sites, [NO_3^-] was consistent within each water type, but porewater [NH_4^+] was the highest at the large mussel beds at Chincoteague and Baltimore Canyon.

1.3.2 Bulk isotope data

Bulk $\delta^{15}N$ values ranged between −1.9‰ and 4.4‰, and $\delta^{13}C$ values ranged from −84.0 to −54.0‰ among both muscle and gill tissues (Fig. 1.2 and Fig. S2). Muscle $\delta^{15}N$ and $\delta^{13}C$ values were significantly higher than those in gill tissue (1.8 ± 1.2‰ vs. 0.5 ± 1.2‰, $p < .0001$ for $\delta^{15}N$; and −64.2 ± 5.8 vs. −67.3 ± 7.6 for $\delta^{13}C$, $p < .027$). *Bathymodiolus childressi* $\delta^{13}C$ and $\delta^{15}N$ muscle isotope values also varied between the three seep sites (Fig. 1.2a). In

Table 1. 1 Descriptive information, nutrient concentrations (ammonium and nitrate), and nitrogen isotope value of nitrate measured in bottom water, sediment surface water, and porewater in areas within and surrounding mussel beds from seep fields of Chincoteague, Norfolk, and Baltimore Canyon

Seep	Sample ID	Water type	NH_4^+ (μM)	NO_3^- (μM)	$\delta^{15}N\text{-}NO_3^-$	Patch size	Site Description
Baltimore	HRS1704-GEX-06-076	bottom water	2.17	23.59	4.73	Medium	Baltimore Canyon; mussel field (somewhat patchy)
	HRS1704-GEX-06-072-2	porewater	162.57	2.61	0.29	Medium	Baltimore Canyon; mussel field (somewhat patchy)
	HRS1704-GEX-06-089-1	sediment surface water	0.70	23.34	4.64	Background	Baltimore Canyon; background at "50" m
	HRS1704-GEX-06-072-1	sediment surface water	3.56	22.50	4.81	Large	Baltimore; mussel field
Chincoteague	HRS1704-GEX-05-051	bottom water	0.72	18.41	4.92	Large	Chincoteague SW; very active vent site
	HRS1704-GEX-05-052	bottom water	0.06	18.50	4.78	Large	Chincoteague SW; very active vent site
	HRS1704-GEX-05-065	bottom water	0.72	19.34	4.67	Background	Chincoteague SW; background over soft sediment
	HRS1704-GEX-05-068	bottom water	0.77	19.54	4.84	Large	Chincoteague SW; over "vent hole," no active bubbles
	HRS1704-GEX-05-055-2	porewater	241.82	N/A	–13.67	Large	Chincoteague SW; black anoxic sed. In dense mussel field
	HRS1704-GEX-05-061-2	porewater	17.49	N/A	N/A	Background	Chincoteague SW; bacterial mat sediment
	HRS1704-GEX-05-064-2	porewater	3.60	12.98	2.73	Background	Chincoteague SW; background soft sediment
	HRS1704-GEX-05-055-1	sediment surface water	20.17	N/A	5.11	Large	Chincoteague SW; black anoxic sed. In dense mussel field
	HRS1704-GEX-05-061-1	sediment surface water	2.59	13.04	4.61	Background	Chincoteague SW; bacterial mat sediment
	HRS1704-GEX-05-064-1	sediment surface water	10.62	18.20	4.76	Background	Chincoteague SW; background soft sediment
Norfolk	HRS1704-GEX-03-015	bottom water	0.68	19.14	5.02	Background	Norfolk Canyon; background
	HRS1704-GEX-03-021	bottom water	0.60	19.21	4.98	Large	Norfolk Canyon; above dense mussel bed
	HRS1704-GEX-03-019-2	porewater	31.03	1.43	N/A	Large	Norfolk; middle of large mussel patch
	HRS1704-GEX-03-010-2	porewater	26.19	1.17	1.17	Medium	Norfolk; medium mussel patch
	HRS1704-GEX-03-008-2	porewater	117.46	7.48	N/A	Small	Norfolk; small mussel patch
	HRS1704-GEX-03-014-1	sediment surface water	1.53	7.45	3.49	Background	Norfolk ~50 cm from mussel edge; background
	HRS1704-GEX-03-019-1	sediment surface water	2.46	19.74	5.21	Large	Norfolk; middle of large mussel patch
	HRS1704-GEX-03-010-1	sediment surface water	5.50	8.85	5.58	Medium	Norfolk; medium mussel patch
	HRS1704-GEX-03-008-1	sediment surface water	1.62	20.56	4.64	Small	Norfolk; small mussel patch

particular, Chincoteague seep field (HRS1704-GEX05-053; 925 m) had the lowest $\delta^{13}C$ values (−74.6 ± 1.5‰ for muscle and −81.6 ± 2.2‰ for gill) and highest $\delta^{15}N$ values (3.5 ± 0.4‰ for muscle and 2.4 ± 0.3‰ for gill) (Fig. 1.2). The other two sites, Baltimore Canyon (HRS1704-GEX06-075; 325 m) and Norfolk (HRS1704-GEX03-023; 1,494 m), had overlapping bulk tissue values for both $\delta^{15}N$ and $\delta^{13}C$. Baltimore Canyon mussel isotope values were as follows: Bulk $\delta^{13}C$ values were −62.5 ± 1.1‰ for muscle and −64.1 ± 0.5‰ for gill; $\delta^{15}N$ values were 1.0 ± 0.5‰ for muscle and −0.2 ± 0.4‰ for gill. Norfolk $\delta^{13}C$ values were −63.1 ± 1.5‰ for muscle and −65.4 ± 1.8‰ for gill; $\delta^{15}N$ values were 1.5 ± 0.5‰ for muscle and 0.1 ± 0.5‰ for gill. Chincoteague $\delta^{13}C$ and $\delta^{15}N$ values in gill and muscle dif- fered significantly from Norfolk and Baltimore Canyon (muscle: $F_{2,26} = 225.5$, $p < .0001$ for $\delta^{13}C$, $F_{2,26} = 68.24$, $p < .0001$ for $\delta^{15}N$; gill: $F_{2,26} = 294.3$, $p < .0001$ for $\delta^{13}C$, $F_{2,26} = 94.73$, $p < .0001$ for $\delta^{15}N$), but Norfolk and Baltimore did not statistically differ in either tissue type for carbon or nitrogen isotopes.

At the Norfolk seep field muscle and gill tissue, $\delta^{15}N$ values were not statistically different between mussel patch sizes (muscle: $F_{2,29} = 0.361$, $p = .7$; gill: $F_{2,29} = 0.405$, $p = .67$ for $\delta^{15}N$). Average $\delta^{15}N$ values ranged from 1.2 to 1.5‰ and −0.1 to 0.3‰ for muscle and gill tissue, respectively (Fig. S2). However, $\delta^{13}C$ values at the large mussel bed (HRS1704-GEX03-023) were significantly lower (−63.1‰ and −65.4‰) than both the medium (HRS1704-GEX03-011; −60.2‰ and −62.1‰) and small (HRS1704- GEX03-009; −60.0‰ and −67.3‰) mussel beds in muscle and gill tissue (muscle: $F_{2,29} = 8.63$, $p < .0011$; gill: $F_{2,29} = 10.37$, $p < .0004$).

Standard ellipse areas corrected for small sample size (SEAc, $n \leq 10$) represent the isotopic niche width (units: $‰^2$) of bulk $\delta^{13}C$ and $\delta^{15}N$ biplots for seep sites and mussel bed size measured in muscle (Fig. 1.2a,b) and gill (Fig. S2) tissue, which can be used as a proxy for trophic plasticity in a group (Jackson et al., 2011). Sample size (i.e., number of individual specimens) between groups was kept relatively similar (±3) to control for potentially larger

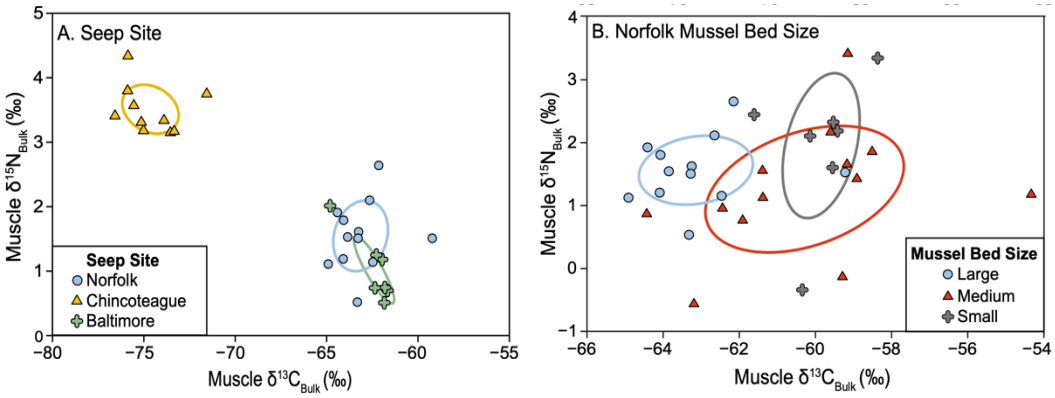

igure 1. 2 Biplot of *Bathymodiolus childressi* muscle tissue $\delta^{13}C$ and $\delta^{15}N$ values organized by (a) eep sites: Baltimore (HRS1704- GEX06-075, green crosses), Chincoteague (HRS1704-GEX05-053, ellow triangles), and Norfolk (HRS1704-GEX03-023, blue circles), and (b) by mussel bed size for the orfolk seep field site only: small bed (HRS1704-GEX03-009, gray crosses), medium bed (HRS1704-EX03-011, red triangles), and large bed (HRS1704-GEX03-023, blue circles), n = 10 for each group. he colored ellipses represent the standard ellipse areas (SEA) for each of the groups

variability with larger sample sizes. Among sites, niche widths were 1.96‰^{2} at Chinco-teague (n = 10), 0.98‰^{2} at Baltimore Canyon (n = 7), and 2.73‰^{2} at Norfolk's large mussel bed (HRS1704-GEX03-023, n = 12). Niche widths among mussel bed sizes at Norfolk were 2.73‰^{2} for large mussel bed (HRS1704-GEX03-023, n = 12), 8.20‰^{2} for medium (HRS1704- GEX03-011, n = 13), and 3.15‰^{2} for small (HRS1704-GEX03-009, n = 7). At Norfolk, the largest niche width was observed at the medium mussel bed, whereas small and large mussel bed size had similar SEAc sizes, but they did not overlap in isotopic space.

1.3.3 Amino acid nitrogen isotope data

Compound-specific amino acid nitrogen isotope patterns from both muscle (Fig. 1.3a) and gill (Fig. 1.3b) tissues separate into the typical AA groupings: trophic AAs, source AAs, and metabolic threonine (McClelland & Montoya, 2002). Overall, the range of $\delta^{15}N_{AA}$ values was −10‰ to 18‰ across all sites, with Baltimore seep field samples yielding uniformly the lowest $\delta^{15}N_{AA}$ values in both tissues. Across all sites, muscle $\delta^{15}N_{AA}$ values were always higher than gill $\delta^{15}N_{AA}$ values, consistent with the pattern observed in the bulk data for muscle and gill (Fig. S3). The mean trophic AAs values (4.4 ± 2.4‰) were about 4‰ higher than mean source AAs (−0.1 ± 1.1‰), and threonine uniformly had the lowest $\delta^{15}N$ values (−6.3 ± 2.6‰) (Fig. 1.3a,b).

This amino acid isotopic pat- tern between metabolic groups is similar to that observed in multiple other metazoan consumers (see McMahon & McCarthy, 2016 review). However, in contrast to patterns previously observed in consumers of non-chemosynthetic production, three amino acids exhibited distinctly unique signatures (Fig. 1.3): $\delta^{15}N_{Pro}$ values had the highest values in both tissue types, substantially elevated relative to $\delta^{15}N_{Glu}$ (4‰–10‰ higher). In addition, $\delta^{15}N_{Ile}$ and $\delta^{15}N_{Leu}$ values were much lower, especially in the gill tissue, than is expected for typical consumers (−2‰ to −8‰ depleted; see discussion). These excursions from typical metazoan heterotrophic patterns are even more apparent when chemosynthetic

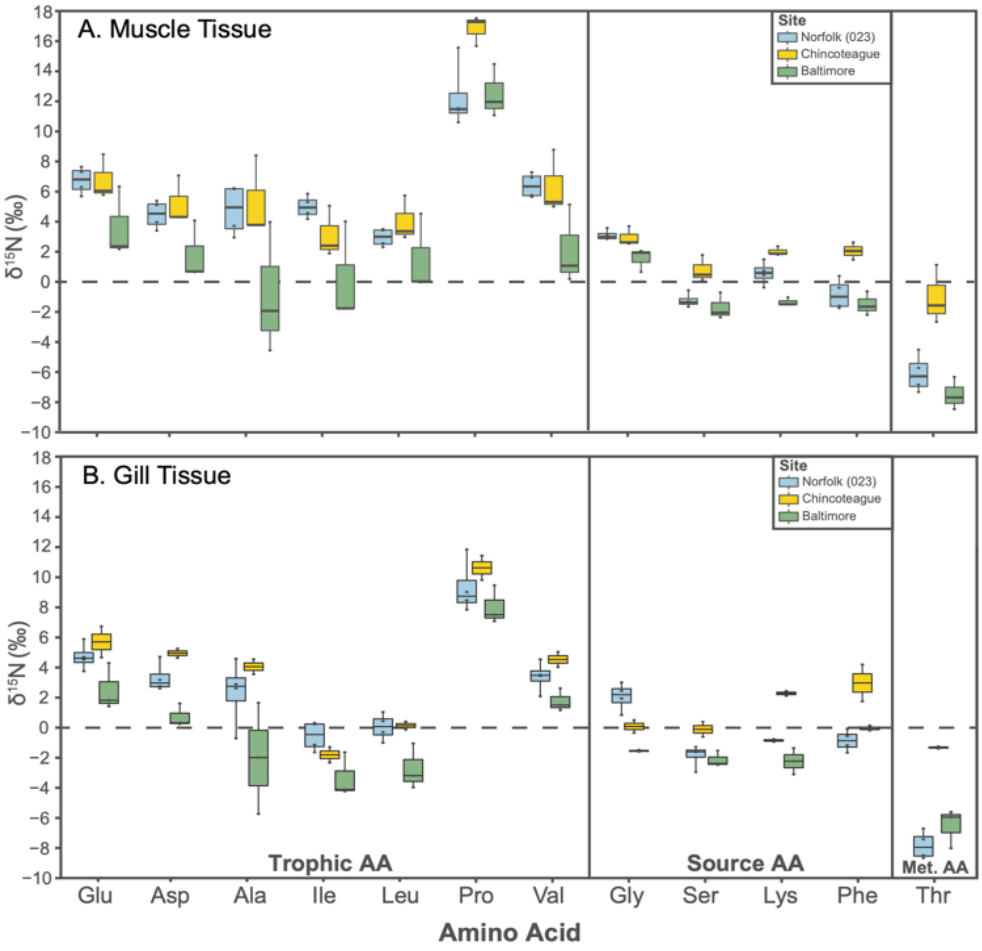

Figure 1. 3 Individual amino acid nitrogen isotope values of *Bathymodiolus childressi* (a) muscle and (b) gill tissue from Norfolk (HRS1704-GEX03-023, light blue), Chincoteague (HRS1704-GEX05-053, yellow), and Baltimore Canyon (HRS1704-GEX06-075, green) seep fields for three individual specimens at each site. Amino acid abbreviations are as defined in text: Glu, glutamic acid; Asp, aspartic acid; Ala, alanine; Ile, isoleucine; Leu, leucine; Pro, proline; Val, valine; Gly, glycine; Ser, serine; Tyr, tyrosine; Lys, lysine; Phe, phenylalanine; and Thr, threonine

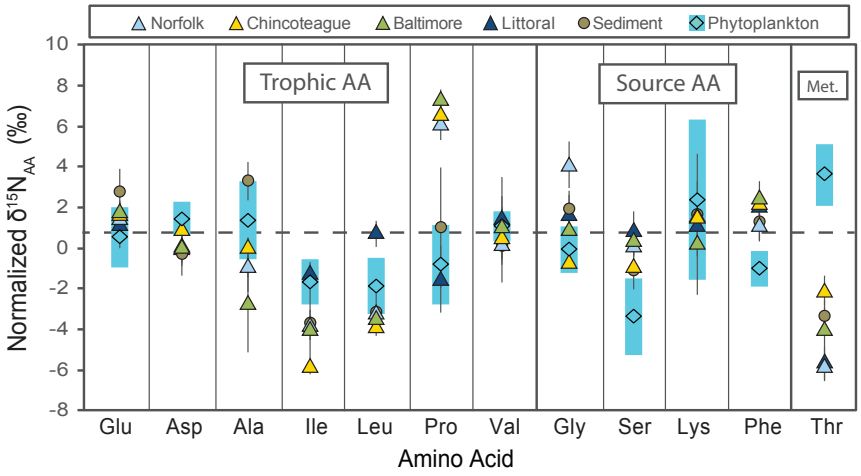

Figure 1. 4 Comparison of AA $\delta^{15}N$ CSIA patterns of seep mussel gills to those of photosynthetic primary producers, littoral marine mussels, and pushcore sediment from Norfolk seep. Normalized nitrogen isotope values of individual amino acids, where the "trophic AA" group is normalized to the average TrAA (Glu, Asp, Ala, Ile, Leu, Pro, Val) of each individual, and the "source AA" and "Met." (metabolic AA) groups are normalized to the average source AA (Gly, Ser, Lys, Phe) in order to remove trophic discrimination effects due to trophic transfer (see methods). Shape of symbol indicates sample type (triangle: mussel gill; diamond: phytoplankton, circle: sediment) Abbreviations are as follows: Glu, glutamic acid; Asp, aspartic acid; Ala, alanine; Ile, isoleucine; Leu, leucine; Pro, proline; Val, valine; Gly, glycine; Ser, serine; Lys, lysine; Phe, phenylalanine; and Thr, threonine. Raw amino acid data are given in supplemental material, Data Repository

mussel data are compared to phytoplankton and littoral mussel $\delta^{15}N_{AA}$ patterns, as well as the surrounding seep sediments (Fig. 1.4 and Fig. S7).

Relative amino acid molar abundance (Mol%) was also measured and compared between littoral mussel and chemosynthetic gill and muscle tissue (Fig. S5), to explore potential influence of chemo- synthetic production on AA composition. Most notably, the Mol% Gly in *B. childressi* was both more variable in chemosynthetic muscle tissue (17%–25%) and universally far higher compared with the Mol% Gly in littoral mussels (~12%). Mol% Glu was also uniformly lower in seep mussels than littoral mussels in both tissue types (~3% or greater). Principal component analysis (PCA) of the Mol% measurements for the 12 measured amino acids found that Gly and Glu, followed by Pro, were the most important amino acids separating littoral and chemosynthetic muscle tissue (Fig. S6).

1.3.4 CSI-AA $\delta^{15}N$ baseline and trophic level proxies

We used established $\delta^{15}N_{AA}$ ecological proxies to decouple trophic transfer effects from "baseline" nitrogen source isotope values, which are typically indistinguishable in $\delta^{15}N_{Bulk}$ data. Of the source AAs, $\delta^{15}N_{Phe}$ is widely considered the best proxy for baseline nitrogen isotope values (McMahon & McCarthy, 2016; Ohkouchi et al., 2017). While gill $\delta^{15}N_{Bulk}$ values were consistently more depleted in ^{15}N than muscle tissue, the $\delta^{15}N_{Phe}$ values did not consistently exhibit this same trend between tissue types (Fig. 1.5a). At the three Norfolk sites, gill $\delta^{15}N_{Phe}$ was lower or the same as muscle $\delta^{15}N_{Phe}$. However, at Chincoteague and Baltimore, gill $\delta^{15}N_{Phe}$ was higher than muscle. At Norfolk (1,495 m, moderate seeping) and Baltimore (393 m, moderate seeping), baseline $\delta^{15}N_{Phe}$ values center between −2‰ and 0‰, whereas at Chincoteague (925 m, vigorous seeping), they are substantially higher (2‰–4‰).

The CSIA-based trophic level (TL_{CSIA}) of seep mussels ranged between 0.7 and 2.2 ± 0.5. Norfolk medium mussel bed had the highest TL_{CSIA}, whereas Chincoteague and Baltimore

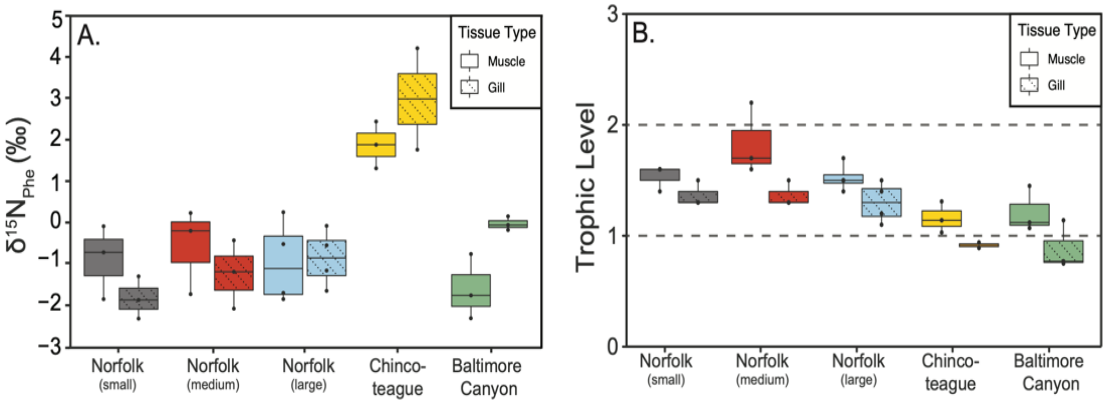

Figure 1. 5 Trophic level and baseline $\delta^{15}N$ proxies for *Bathymodiolus childressi* muscle (open symbols) and gill (cross-hatch symbols) tissues. (a) $\delta^{15}N_{Phe}$ values, proxy for $\delta^{15}N$ baseline and (b) CSI-AA derived trophic level. Colors indicate site: Baltimore (HRS1704-GEX06-075, green), Chincoteague (HRS1704- GEX05-053, yellow), and Norfolk seep field by mussel bed size: small bed (HRS1704-GEX03-009, gray), medium bed (HRS1704- GEX03-011, red), and large bed (HRS1704-GEX03-023, blue)

had the lowest TL_{CSIA}. TL_{CSIA} in muscle tissue was always higher than in gill tissue at all sites (Fig. 1.5b).

1.3.5. Mixing model results

We conducted several statistical tests to explore how trophic $\delta^{15}N_{AA}$ patterns varied between chemosynthetic mussels and other organism and sample types (e.g., phytoplankton, littoral mussels, sediment). A PCA of all trophic AAs and threonine in the gill tissue revealed clear separation in particular between chemosynthetic and non-chemosynthetic CSI-AA patterns, but also some separation between seep sites (Fig. 1.6). As captured in the PCA, proline, leucine, isoleucine, and threonine were the most informative AAs for separating chemo-synthetic mussels from littoral mussels and seep sediment, as well as separating mussels from different seep sites; together, these four amino acids were the most important in explaining 77.5% of variance. The $\delta^{15}N$ value of proline was most important in separating littoral

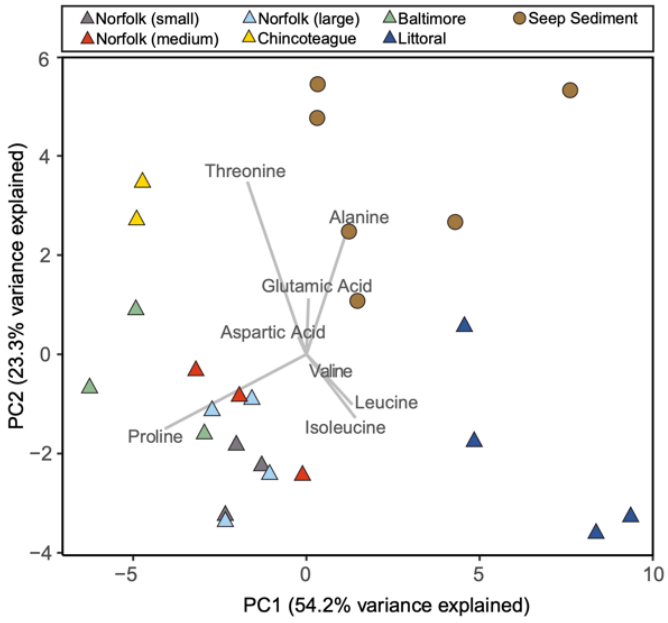

Figure 1. 6 Principal component analysis of normalized $\delta^{15}N$ for gill tissue in seep and littoral mussels (triangles) and pushcore seep sediment (circles) samples. Values in parentheses are the percentage variation accounted by the first and second principal components. The first principal component (PC1) separates the seep mussels from littoral and sediment, and the second principal component (PC2) separates chemosynthetic mussels between seep sites. The vector lengths show that proline, hreonine, isoleucine, and leucine were the most important AAs for explaining variations in the first two PCs. See Figure S4 for PCA results in muscle tissue and scores for each PCA

mussels from seep mussels, while Leu, Ile, and Thr were important in separating seep mussels by site.

Based on TL_{CSIA} and PCA results, we assumed that the $\delta^{15}N$ value of the littoral mussel gill tissue was 100% heterotrophic (filter-feeding), and Chincoteague mussel gill samples (which had the lowest TL values) were the best chemosynthetic endmember. We used these two endmembers in a multivariate mixing model (MixSIAR). Based on the CSI-AA $\delta^{15}N$ values of the four amino acids with the most predictive power noted above (Pro, Leu, Ile, and Thr), we estimated resource contribution (heterotrophy vs. chemoautotrophy) to seep mussels for all our collection sites. MixSIAR output indicated that while seep mussels appear to uniformly obtain most of their nitro- gen from their chemosymbionts, the amount of heterotrophy was significant, and also varied substantially between sites (ranging 3%– 20% ± 2%–10%; Fig. 1.10).

1.4 Discussion

1.4.1 Bulk stable carbon and nitrogen isotope values in seep mussels

Seep mussel gill tissue $\delta^{13}C$ values were uniformly lower than muscle tissue (Fig. S2) indicating high carbon flow from symbionts to host (Riekenberg et al., 2016; Rodrigues et al., 2013). Similar low $\delta^{13}C$ values have previously been observed in Bathymodiolin species with methanotrophic and thiotrophic chemosymbionts from hydrothermal vent systems (Trask & Van Dover, 1999). Interestingly, we found the opposite pattern in particle filter-feeding littoral mussels, where both bulk $\delta^{13}C$ and $\delta^{15}N$ values in gills were higher than in muscle tis- sue. We hypothesize that this could be due to differences in isotopic routing involved with nutrient flow between tissues with or without symbionts.

The larger variation in $\delta^{13}C$ values between seep sites compared to $\delta^{15}N$ variability suggests that *B. childressi* can take up carbon and nitrogen sources independently, as has

previously been suggested (Lee & Childress, 1995). Our isotope data also suggest that the different mussel beds appear to be utilizing different combinations of nitrogen sources. For example, the standard ellipse areas (SEAc; Fig. 1.2 a,b) showed the ecological isotopic niche width of the medium mussel bed at Norfolk was the largest of any site, while Baltimore and Chincoteague had the smallest niche widths. This suggests that either the Norfolk site has more heterogeneous microhabitats or mussels are utilizing a greater proportion of mixed nitrogen sources. Such variation could be a function of mussel bed size, in addition to environmental differences between sites related to depth and seep activity. We note that between large mussel beds from the different seep sites, SEAc niche widths were more similar to each other (Fig. 1.2a).

The variation in $\delta^{13}C$ values between sites and mussel bed sizes suggests different carbon sources to mussels and/or different isotopic value of methane-derived carbon between seep sites (Demopoulos et al., 2019). Based on the $\delta^{13}C$ values of methane- derived authigenic carbonates collected at Norfolk and Baltimore seep sites, Prouty et al. (2016) suggest that microbial methane is the dominant carbon source supporting chemo-synthetic communities, and very low mussel $\delta^{13}C$ values (~ −63‰) are consistent with a dependence on microbial methane (Demopoulos et al., 2019). Chincoteague had by far the lowest $\delta^{13}C$ values of all seep sites. Based on ROV observations, Chincoteague was the most actively venting site, continuously venting bubbles into the water column (Fig. 1.1b; Ruppel et al., 2017), whereas venting at Baltimore and Norfolk seep sites was less vigorous and more diffuse.

Bulk $\delta^{15}N$ values in all mussel samples were low (−2‰ to 4‰), consistent with previously reported ranges for chemosynthetic mussels from the USAM (Demopoulos et al., 2017, 2019), and Gulf of Mexico (Becker et al., 2010, 2014). At the same time, different sites appear to have distinct $\delta^{15}N$ values, with Chincoteague mussels ^{15}N-enriched compared to $\delta^{15}N$ at Norfolk and Baltimore sites (Fig. 1.2). There are multiple mechanisms that could be

driving $\delta^{15}N$ differences between sites, including the influence of diazotrophy, different concentrations and $\delta^{15}N$ values of "baseline" DIN pools (e.g., NO_3^- vs. NH_4^+), biomolecular uptake mechanisms for DIN (Lee & Childress, 1994) and heterotrophy.

Given the high concentrations of ammonia present in porewaters at all beds sampled (Table 1.1; Fig. S1), $\delta^{15}N$ values in chemosynthetic production might be expected to be tied strongly to the $\delta^{15}N$ value of the available ammonium pool at each location. Unfortunately, we were not able to measure ammonia $\delta^{15}N$ values from samples conducted for this study; moreover, there are no directly comparable values from sediments in this region. However, ammonium measured from pore water fluids in sediments from sites nearby our study sites along the NE Atlantic Margin would suggest similarly depleted $\delta^{15}N$ values (Borowski & Paull, 2000). Ammonia $\delta^{15}N$ values at these sulfate-reducing zones (Blake Ridge and Carolina Rise) were 3‰–5‰, their source originating primarily from microbial fermentation reactions at depth in the sediments. At the same time, low $\delta^{15}N$ values in other chemosynthetic macro-invertebrates in methane seep sites have also been attributed to diazotrophy (Kennicutt et al., 1992), an idea supported by the presence of nif genes, a tracer for diazotrophic N_2 fixation, which have been found in anaerobic methane seep sediments (Dekas et al., 2013). While high [NH4+] in porewater at the seep sites in this study (30–250 μM; Table 1.1; Fig. S1) would seem to obviate the need to expend energy to fix additional nitrogen, past work has suggested that N_2 fixation may be controlled in some environments by the availability of carbon and electrons from methane, rather than a function of NH_4^+ levels (Dekas et al., 2013 and refs therein).

$\delta^{15}N$ values at any specific site would also depend strongly on the degree of N utilization of DIN substrates. Given the high ammonia concentrations in porewater, incomplete utilization of the NH4+ pool would be expected, leading to strong discrimination against ^{15}N and therefore low $\delta^{15}N$ values (Sigman et al., 2001). The exact N isotope fractionation for chemosynthetic bacteria is unknown; however, fractionation due to incomplete NH_4^+ uptake by marine bacteria can range from −4‰ to −26‰ (extracellular [NH_4^+] between10 and 100 μM;

Hoch et al., 1992). Such extremely large potential isotopic fractionations suggest that the main control on bulk $\delta^{15}N$ values between specific locations may be linked to local inorganic N concentrations and gradients, and thus the degree of utilization, as opposed to endmember NH_4^+ or NO_3^- $\delta^{15}N$ values.

Overall, our current data set clearly cannot distinguish between the multiple possible sources, endmember $\delta^{15}N$ values, and possible degrees of fractionation linked to partial utilization that would be required to fully characterize bulk $\delta^{15}N$ values at each site. Further, it is important to stress that none of these mechanisms are mutually exclusive; and without site-specific measurement of all DIN $\delta^{15}N$ values, together with their concentrations and some way to address possible N fixation, different mechanisms leading to specific $\delta^{15}N$ values cannot be determined. However, what is most important for this study is that no matter what mixture of DIN sources may contribute to chemosynthetic $\delta^{15}N$ values, together these ultimately constitute the "baseline" $\delta^{15}N$ value for each site, which we are able to directly quantify using CSI-AA proxies described below. Finally, differences in baseline $\delta^{15}N$ values do not alter diagnostic chemosynthetic CSI-AA patterns (Ohkouchi et al., 2015), allowing us to use CSI-AA data to investigate signatures of chemosynthesis.

1.4.2 CSI-AA ecosystem proxies

This is the first study to use nitrogen amino acid isotopes in a deep-sea chemosynthetic environment. CSI-AA parameters allow decoupling of potentially shifting baseline $\delta^{15}N$ values from trophic level, while comparison of normalized data with well-established CSI-AA patterns for marine photoautotrophs can reveal diagnostic CSI-AA signatures of chemosynthesis. Methane seep environments are physically and biologically heterogeneous, and our $\delta^{15}N_{AA}$ results highlight differences between sites that were not revealed from the bulk isotope results alone. For example, whereas $\delta^{15}N_{Bulk}$ values were generally overlapping and not statistically different ($P > .05$) at Norfolk seep field, TLCSIA calculation revealed higher TL at the medium

mussel bed (HRS1704-GEX003-011) followed by the small mussel bed (HRS1704-GEX003-009). Seep mussels inhabit a wide range of venting activity, from vigorous fluid flow to transitional sediments with diffuse flow. This adapt-ability is due in large part to mixotrophy, which allows seep mussels to endure variations in fluid flow in time or space. Further, while lower $\delta^{15}N$ values have been associated with higher density mussel beds (Demopoulos et al., 2019), we found the highest $\delta^{15}N_{Bulk}$ and $\delta^{15}N_{Phe}$ ($\delta^{15}N_{Baseline}$) values at the Chincoteague seep field, which we consider to be the chemo-synthetic endmember based on the low TL value of mussels and high observed methane bubbling rates. This decoupling of $\delta^{15}N_{Baseline}$ values from TL indicates that bulk $\delta^{15}N$ values are largely tracking $\delta^{15}N_{Baseline}$ values of the DIN source value or recycling and TL to a lesser degree. For mixotrophic organisms such as *B. childressi* however, this decoupling is a more complex consideration than in other commonly studied marine heterotrophic organisms, since both $\delta^{15}N_{Baseline}$ and degree of heterotrophy can change between sites.

1.4.3 New CSI-AA proxies for chemosynthetic production

Results from the unique application of CSI-AA on chemosynthetic biomass yield unique signatures for microbial chemosynthetic pro- duction preserved in $\delta^{15}N_{AA}$ and molar abundance patterns, representing novel tracers for chemosynthesis. One important underlying assumption, however, is that the $\delta^{15}N_{AA}$ patterns we observe in gill tissue of *B. childressi* largely represent the $\delta^{15}N_{AA}$ patterns of the chemosymbiont primary producers. This assumption is supported by direct observation of symbionts located in specialized epithelial cells in the gills of chemosymbiotic bivalves (Childress et al., 1986; Ponnudurai et al., 2017). To our knowledge, no direct estimates exist on percent of gill biomass represented by symbionts, but the low TL_{CSIA} for gill tissue (representing our inferred “primary producer” endmember) TL_{CSIA} (Fig. 1.5b) strongly supports their residence in this tissue. Therefore, differences in $\delta^{15}N_{AA}$ and $Mol\%_{AA}$ patterns between chemosynthetic mussels and similar tissues in hetero- trophic littoral mussels are likely related to the presence (or absence) of symbionts.

The overall pattern of ^{15}N-enriched trophic AAs observed in the seep mussels is similar to that expected in all heterotrophs (Fig. 1.3). However, three amino acids (Pro, Leu, and Ile) fractionate very differently from those previously observed in any primary producers or

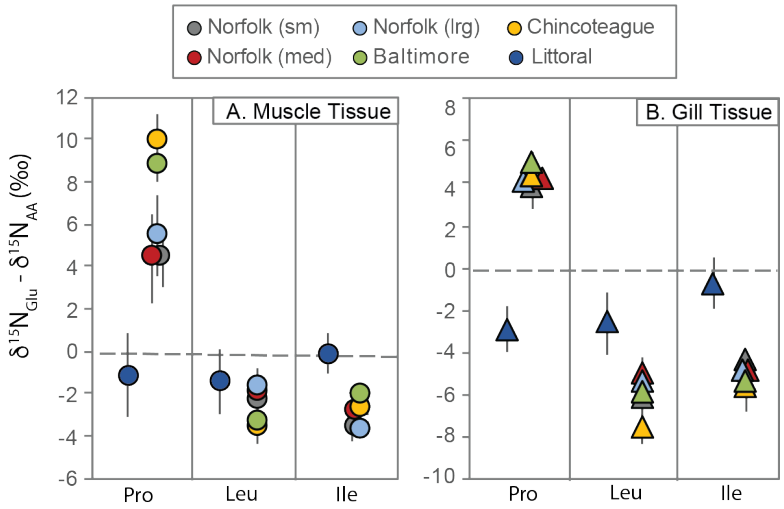

Figure 1. 7 Isotopic offset of three trophic AAs (Pro, Ile, and Leu) from $\delta^{15}N_{Glu}$, the AA central to nitrogen metabolism in (a) muscle (circle) and (b) gill (triangle) tissue of seep mussels from the three seep sites in this study: Norfolk seep field by mussel bed size: small bed (HRS1704-GEX03-009, gray), medium bed (HRS1704-GEX03-011, red), and large bed (HRS1704-GEX03-023, blue), Baltimore (HRS1704-GEX06-075, green), and Chincoteague (HRS1704-GEX05-053, yellow), compared to littoral mussels (dark blue**).**

consumers. Pro in particular has a relative $\delta^{15}N$ value far higher than previously observed thus far in any organism. In a typical marine primary consumer (e.g., herbivorous zooplank-ton, littoral mussels, etc.), trophic AAs are ~6‰ to 7‰ enriched in ^{15}N relative to source AAs (McClelland & Montoya, 2002; Vokhshoori & McCarthy, 2014). However, the $\delta^{15}N_{Pro}$ in both gill and muscle tis- sue of *B. childressi* was ~15‰ higher than the average source AAs (Fig. 1.3a,b) and 4‰ – 10‰ higher than $\delta^{15}N_{Glu}$ (Fig. 1.7). When compared to littoral mussels, the $\delta^{15}N_{Pro}$ values in *B. childressi* values were consistently 6‰–10‰ higher than $\delta^{15}N_{Glu}$, a pattern that to our knowledge has never previously been observed (Fig. 1.7). Seep mussel $\delta^{15}N_{Pro}$ enrichment relative to $\delta^{15}N_{Glu}$ is particularly significant, as Glu is directly linked to glutamate pool in central N metabolism, and is the main source of N for transamination for all other AA; Glu therefore typically has the highest, or near highest, $\delta^{15}N$ value of any AA (McCarthy et al., 2013;

McMahon & McCarthy, 2016). Trophic AAs are enriched in 15N as a result of a kinetic isotope fractionation during metabolic transamination (Chikaraishi et al., 2007). Therefore, we speculate that Pro's extremely high $\delta^{15}N$ value in chemosynthetic symbiont tissue could be linked to the unique bio- synthetic pathway of Pro relative to other trophic AAs. While determining the exact biochemical pathway is beyond the scope of these data, it is possible that instead of the typical transamination of Glu to the corresponding keto acids, Pro is biosynthesized from Glu via the formation of L-Glu-5-semialdehyde and then to L-1-pyrroline-5-carboxylate (Yamaguchi et al., 2017). The unique biosynthetic pathway from the other trophic AAs could help to explain the high $\delta^{15}N$ values observed.

In contrast, the $\delta^{15}N_{Ile}$ and $\delta^{15}N_{Leu}$ values had unexpectedly low relative $\delta^{15}N$ values in the seep mussels, particularly in the gill tissue (Fig. 1.3 and Fig. 1.4). The relative offset from $\delta^{15}N_{Glu}$ was −6‰ to −8‰ in the gill tissue, compared to that of littoral mussels, which was ~ −2‰ to 0‰ (Fig. 1.7). While these offsets are not as dramatic as those observed for Pro, they

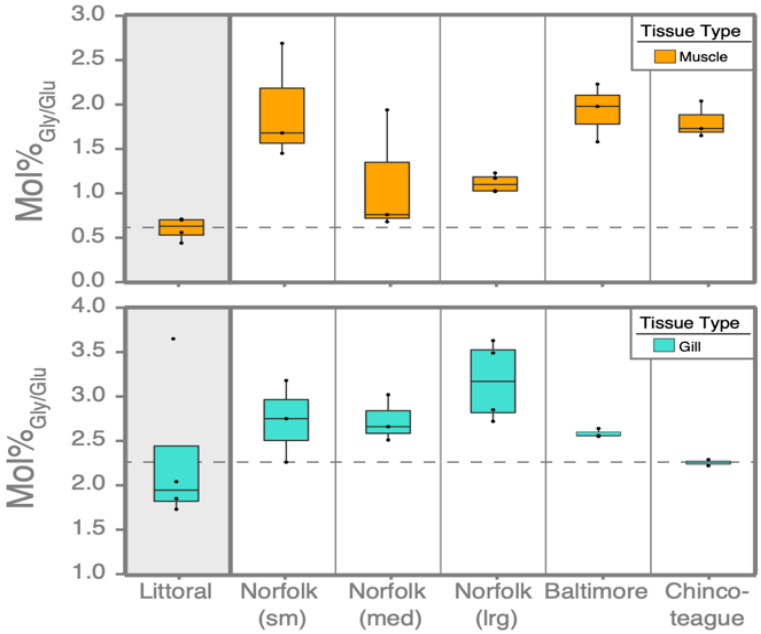

Figure 1. 8 Ratio of Gly mol% to Glu Mol% in muscle (orange) and gill (turquoise) tissues from seep mussels in this study compared to littoral mussels (shaded gray box). Dashed line represents the mean littoral Gly/Glu mol% (*n* = 4).

are nevertheless outside the previously observed ranges in both plankton and littoral heterotrophic mussels. Yamaguchi et al. (2017) found similar patterns in cultured bacteria and archaea, although to a lesser degree, suggesting that the high energetic costs of Ile and Leu synthesis (Akashi & Gojobori, 2002) could reduce the metabolic flux associated with the degradation of Ile and Leu in organisms to save energy, thus preserving ^{15}N depletion during biosynthetic transamination from Glu.

Finally, the relative molar abundance of Gly and Glu data suggests an additional potential AA geochemical tracer for chemosynthesis (Fig. 1.8). For example, we hypothesize that higher Gly/Glu Mol% in chemosynthetic mussels relative to littoral mussels could be a direct indicator for the amount of *de novo* AA synthesis from bacterial endosymbionts versus catabolism of macromolecules by the host. However, this pattern was only observed in the muscle tissue. Regardless of the presence of endosymbionts, Gly Mol% in gill tissue is relatively high in marine bivalves (this study), and differences in molar abundance found in the muscle tissue may be a function of the metabolic demands of the host. However, we recognize that additional data such as ^{15}N and ^{13}C nutrient tracers combined with molecular-based measurements are needed to explain differences in molar abundances.

1.4.4 Microbial resynthesis index in chemosynthetic environments

The microbial resynthesis index, ΣV, is a measure of relative heterotrophic resynthesis (McCarthy et al., 2007) and typically increases with trophic transfer as the contribution of bacterial AA biomass in- creases with trophic level (Calleja et al., 2013; Ohkouchi et al., 2017), illustrated here in the littoral mussel data (Fig. 1.9). In contrast, the strong inverse relationship of ΣV and TL_{CSIA} in chemosynthetic mussels is opposite from what would be expected in heterotrophic organisms. This relationship may actually be character-istic of chemosynthetic environments where the majority of bacterial production is auto-trophic. For example, in the gill and muscle tissue of *B. childressi* ΣV decreases with increasing TL (Fig. 1.9), consistent with

autotrophic production (low TL) that is also purely bacterial (high ΣV). In contrast, an increase in TL in a chemosynthetic system indicates increasing heterotrophy/filter feeding. Instead of indicating ex- tensive bacterial degradation as in most systems, the seep data in Fig. 1.9 suggest that in a chemoautotrophic organism, elevated ΣV primarily indicates increased degree of microbial chemoautotrophy. We suggest that the trend exhibited in seep mussels represents a mixing line between two different metabolic modes (e.g., heterotrophy and autotrophy) and/or relative nutrient source between mussel host and bacterial endosymbionts.

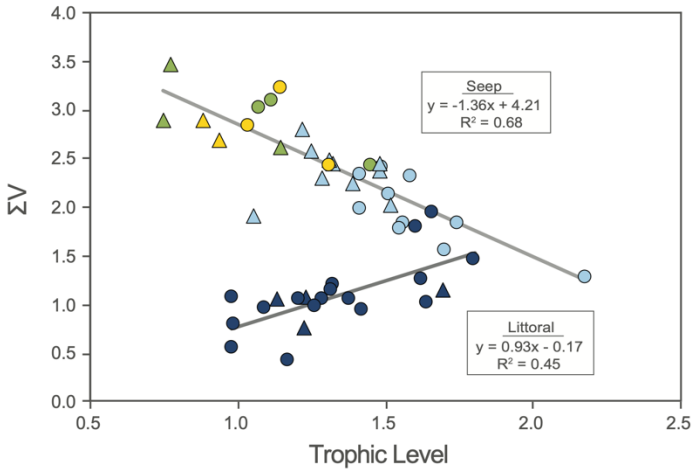

Figure 1. 9 Relationship between trophic level and Σ*V* parameter in gill (triangle) and muscle (circle) tissue of seep mussels from the three seep sites in this study: Norfolk, HRS1704-GEX03-009, 011 and 023, light blue), Baltimore (HRS1704-GEX06-075, green), and Chincoteague (HRS1704-GEX05-053, yellow), compared to the same relationship in littoral mussels (dark blue).

The high ΣV values implied for chemoautotrophic bacteria are a novel observation; however, this would not necessarily be expected based on photoautotrophic bacteria, which do not have elevated ΣV values (McCarthy et al., 2013). We speculate that the high ΣV in chemoautotrophic gill tissue may be indicative of the different possible pathways for synthesizing AAs between bacterial endosymbionts and host. Bathymodiolin species, as heterotrophic consumers, must synthesize AAs via catabolism of dietary sources, for example, suspended and sinking particles (Page et al., 1990), free amino acids (Lee & Childress, 1995), or digestion of symbionts (Ponnudurai et al., 2017). In contrast, bacteria have a broader flexibility in obtaining amino acids: de novo synthesis of AAs from inorganic nitrogen, direct or

"salvage" incorporation of unaltered AAs into new proteins, or strict catabolism (e.g., McCarthy et al., 2007; McMahon & McCarthy, 2016 and references therein). Since endosymbionts synthesize AAs *de novo* from DIN, the observed high values of ΣV, here particularly driven by relative high values of $\delta^{15}N_{Pro}$ and low values of $\delta^{15}N_{Ile}$ and $\delta^{15}N_{Leu}$, may be characteristic of AA synthesis by methane-oxidizing bacteria.

In contrast to the mussel data, ΣV and TL values from pushcore sediments from Norfolk chemosynthetic habitats show no correlation at all, nor do the values fall on either the littoral or seep field mussel mixing line (Fig. S8 and Fig. 1.9). This suggests that most organic matter in these sediments is composed of surface-derived production. If sedimentary organic matter is predominantly surface- derived production, ΣV and TL are not necessarily expected to have any direct relationship since TL predominantly indicates the surface planktonic ecosystem structure, while ΣV indicates mainly bacterial heterotrophy occurring after deposition (e.g., Batista et al., 2014). Finally, we note that while these data do not suggest significant chemosynthetic OM contribution to nearby sediments, these push cores are only from one site and the "patchy" nature of seeps may not reflect the full pattern of such heterogeneous environments.

1.4.5 Resource contribution to chemosymbiotic mussels among seep sites

In environments with chemosynthetic production, it is difficult to assess the relative degree of mixotrophy in symbiont-bearing organisms using traditional bulk isotope techniques. Bulk isotope work can provide information on endmember C source mixing; however, it does not directly trace organic chemoautotroph biochemistry. While *B. childressi* has a very high weight:volume gill tissue index relative to littoral mussels (Riou et al., 2010), indicative of adaptation for endosymbionts, the bivalve still has a functional gut and actively filter-feeds on particles from the water column (Pile & Young, 1999). Bathymodiolin species

have been shown to filter-feed both sinking (70–300 μm) and suspended (1–70 μm) particles (Page et al., 1990), and diatom tests found in the guts of Bathymodiolin mussels confirm the ability to consume surface-derived particles (Riou et al., 2010). However, the suspended particle size fraction is more efficiently taken up by deep-sea mussels than large sinking particles and is likely composed of mixture of organic matter from locally derived material from bacterial mats as well as highly degraded POM (Pile & Young, 1999), further complicating any interpretation based on assumed endmembers. It has been posited that the amount of heterotrophy could vary seasonally, linked to seep mussel spawning events during phytoplankton blooms and when energetic requirements are higher (Riou et al., 2010). For example, in Baltimore Canyon there is a strong seasonality in phytodetritus flux to the seafloor (Prouty et al., 2017); seep mussels at this site could be changing their feeding mode with seasonal pulses of increased surface production. Geochemical tools specific for the biochemical signatures of chemosynthetic OM could be valuable in assessing increased heterotrophy with seasonal phytoplankton bloom pulses.

We synoptically applied our proposed new geochemical parameters to quantify relative contribution of heterotrophy versus chemoautotrophy, to both test our conclusions about resource differences among seep fields and to investigate environmental controls on them (Riekenberg et al., 2016). All of our proposed molecular proxies (TL_{CSIA}, $Mol\%_{Gly/Glu}$, and MixSIAR model output) consistently indicated that Norfolk small and medium mussel beds (HRS1704- GEX03-009, 011) have the highest degree of heterotrophy (e.g., filter-feeding). First, the average TL_{CSIA} for mussels at these sites were highest, indicating minimum contribution from endosymbionts. Second, many of the seep mussel's comparative molar abundance of Gly ($Mol\%_{Gly/Glu}$) were similar to the purely heterotrophic, filter-feeding littoral mussels. Finally, our MixSIAR model, based on the four most informative amino acids (as indicated by PCA, Fig. 1.5), quantified the highest degree of heterotrophy (~15% to 20%) for these Norfolk mussel beds. This result represents the first CSI- AA-based approach to directly

quantify relative chemoautotrophy in a symbiont-bearing organism using δ15NAA-based estimates. In addition, our nitrogen data also suggest that Norfolk mussels from this site might supplement their nitrogen demands at least in part through heterotrophy given the lower concentration of DIN sources, NH4+ and NO3− in porewater and sediment surface water (bottom water data not available) (Table 1.1).

In contrast, based on our new CSI-AA geochemical proxies mussels from the Chincoteague (HRS1704-GEX05-053) and Baltimore (HRS1704-GEX06-075) sites uniformly indicated the highest degree of reliance on chemoautotrophy-derived nutrition: highest $\delta^{15}N_{Pro}$ values (Fig. 1.3) lowest TL (Fig. 1.5), highest ΣV values (Fig. 1.9), and similar $Mol\%_{Gly/Glu}$ to the littoral mussels (Fig. 1.8). MixSIAR results from these sites indicate essentially complete chemoautotrophy (~98%; Fig. 1.10). Together, the combined evidence from our multiple AA-based parameters and geochemical environmental data shows that seep mussel heterotrophy in fact varies quite substantially in different seep environments.

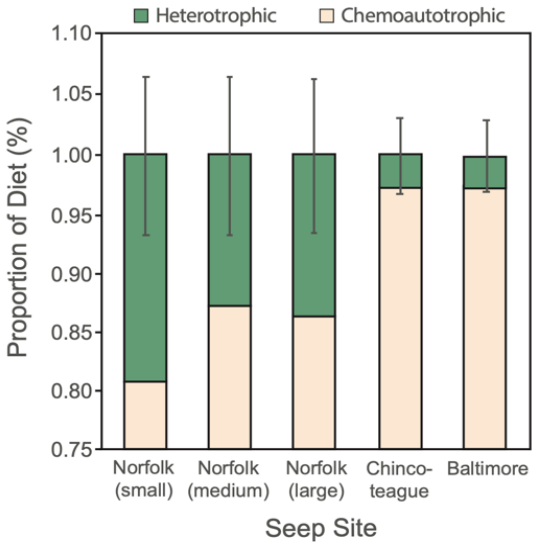

Figure 1. 10 MixSIAR results based on *Bathymodiolus childressi* gill $\delta^{15}N_{AA}$ values ($\delta^{15}N_{Pro}$, $\delta^{15}N_{Leu}$, $\delta^{15}N_{I;e}$, $\delta^{15}N_{Thr}$) illustrating relative contribution (median ± 95% credible intervals) of heterotrophic versus chemoautotrophic food resources at each site. See Table S1 for detailed input variable and output.

Finally, we should note that MixSIAR models with CSI-AA have previously been applied using $\delta^{13}C$ values of essential amino acids ($\delta^{13}C_{EAA}$), as they are highly diagnostic for

classifying different pri- mary producer groups (Larsen et al., 2013), and these $\delta^{13}C_{EAA}$ values are conserved up food chains (McMahon et al., 2010). McCarthy et al. (2013) found that relative $\delta^{15}N_{AA}$ values can also be diagnostic of prokaryotic and eukaryotic primary producers, but since $\delta^{15}N_{AA}$ values shift with trophic transfer, it has not been previously used to estimate relative source contribution in purely heterotrophic systems. However, in a symbiont /host system $\delta^{15}N_{AA}$ values are more akin to a mix of resource contribution, suggesting that $\delta^{15}N_{AA}$ Bayesian models can be adapted for this system.

1.5 Conclusion

New production via chemosynthetic endosymbionts is the primary mechanism for organic nitrogen production; however, our CSI-AA data revealed that heterotrophic filter feeding also contributed to total mussel biomass, with magnitude varying between sites and mussel bed size. Despite Norfolk being the deepest site (1,495 m), heterotrophic filter feeding was greatest. Mussel bed size appearing to be the most important environmental variable, our smaller mussel bed sizes at Norfolk had higher TL, suggesting more nitrogen derived from heterotrophy than mussels within dense, large mussel beds. At the shallowest site (Baltimore, 390 m), we anticipated that sinking POM would be more important to seep mussel diet, given POM concentrations declines with depth. On the contrary, the $\delta^{15}N_{AA}$ results revealed this was not the case; nitrogen was almost entirely chemo- autotrophic in seep mussels from large beds at Baltimore.

We propose that a suite of new isotopic and molecular AA-based proxies (highly elevated relative $\delta^{15}N_{Pro}$; $\delta^{15}N_{Glu\text{-}Pro}$ parameter, $Mol\%_{Gly/Glu}$ parameter) are unique indicators for chemosynthetic production based on symbionts present in *B. childressi*. The TLCSIA helps to indicate relative degree of heterotrophy, while additional proxies (e.g., $\delta^{15}N$ of Ile, Leu, and ΣV) are indicative of chemoautotrophic AA production. Finally, we propose that our Bayesian mixing model (MixSIAR) based on most diagnostic $\delta^{15}N$-AAs can return environmentally consistent

quantitative estimates of the relative amounts of chemoautotrophy vs. heterotrophy in a mixotrophic organism. These geochemical proxies can be now used with any tissue from any living organism or with any archive that has well-preserved protein. As such, they could be applied to mixotrophic organisms from deep-sea chemosynthetic environments (e.g., hydrothermal vents, brine pools) or other chemosynthetic organisms to help shed light on nitrogen systematics in deep-sea food webs that have otherwise been confounded with using bulk $\delta^{15}N$. Finally, because protein in fossil shell has been shown to be an excellent archive for CSI-AA data in both the shell matrix (Misarti et al., 2017) and shell periostracum (Whitney et al., 2019), mussel shell recovered from sediment cores or sedimentary deposits could allow the creation of extended CSI-AA geologic records of seep ecosystems, aiding in understanding the extent to which chemosynthesis contributes to benthic marine food webs and biogeochemical cycles.

Acknowledgements

This work was sponsored by the National Oceanographic Partnerships Program. Funding was provided by the U.S. Geological Survey and the Bureau of Ocean Energy Management (BOEM). Ship and ROV costs for IMMeRSS were sponsored by the NOAA Office of Exploration and Research through interagency agreement 16-01118 with the USGS. Additional support for the project is provided by the U.S. Department of Energy National Energy Technology Laboratory under interagency agreement DE- FE0023495 with the USGS Gas Hydrates Project. We are grateful to Stephanie Christensen, Dyke Andreasen and Colin Carney (UCSC-SIL) for assisting with isotopic analyses; the captain, crew and science party of the UNOLS ships Hugh R. Sharp for shipboard support provided by the NOAA Office of Ocean Exploration and Research, and Oceaneering for the ROV Global Explorer. Any use of trade, product, or firm names is for descriptive purposes only and does not imply endorsement by the US Government.

References

Aharon, P. (1994). Geology and biology of modern and ancient submarine hydrocarbon seeps and vents: An introduction. *Geo-Marine Letters*, *14*, 69–73. https://doi.org/10.1007/BF01203716

Akashi, H., & Gojobori, T. (2002). Metabolic efficiency and amino acid composition in the proteomes of *Escherichia coli* and *Bacillus subtilis*. *Proceedings of the National Academy of Sciences of the United States of America*, *99*(6), 3695–3700. https://doi.org/10.1073/pnas.06252 6999

Batista, F. C., Ravelo, A. C., Crusius, J., Casso, M. A., & McCarthy, M. D. (2014). Compound specific amino acid $\delta^{15}N$ in marine sediments: A new approach for studies of the marine nitrogen cycle. *Geochimica Et Cosmochimica Acta*, *142*, 553–569. https://doi.org/10.1016/j. gca.2014.08.002

Becker, E. L., Cordes, E. E., Macko, S. A., Lee, R. W., & Fisher, C. R. (2014). Spatial patterns of tissue stable isotope contents give insight into the nutritional sources for seep communities on the Gulf of Mexico lower slope. *Marine Ecology Progress Series*, *498*, 133–145. https://doi. org/10.3354/meps10598

Becker, E. L., Lee, R. W., Macko, S. A., Faure, B. M., & Fisher, C. R. (2010). Stable carbon and nitrogen isotope compositions of hydrocarbon- seep bivalves on the Gulf of Mexico lower continental slope. *Deep Sea Research Part II: Topical Studies in Oceanography*, *57*, 1957–1964. https://doi.org/10.1016/j.dsr2.2010.05.002

Borowski, W. S., & Paull, C. K. (2000). Data report: Nitrogen isotopic composition of pore-water ammonium, Blake Ridge, site 997. In C. K. Paull, R. Matsumoto, P. J. Wallace, & W. P. Dillon(Eds.), *Proceedings ODP, Sci. Results* (pp. 171–172). College Station, TX: TAMU. https:// doi.org/10.2973/odp.proc.sr.164.213.2000

Bourque, J. R., Robertson, C. M., Brooke, S., & Demopoulos, A. W. J. (2017). Macrofaunal communities associated with chemosynthetic habitats from the U.S. Atlantic margin: A comparison among depth and hab- itat types. *Deep Sea Research Part II: Topical Studies in Oceanography*, *137*, 42–55. https://doi.org/10.1016/j.dsr2.2016.04.012

Calleja, M. L., Batista, F., Peacock, M., Kudela, R., & McCarthy, M. D. (2013). Changes in compound specific $\delta^{15}N$ amino acid signatures and D/L ratios in marine dissolved organic matter induced by hetero- trophic bacterial reworking. *Marine Chemistry*, *149*, 32–44.

Chikaraishi, Y., Kashiyama, Y., Ogawa, N. O., Kitazato, H., & Ohkouchi, N. (2007). Metabolic controls of nitrogen isotope composition of amino acids in marine macroalgae and gastropods: Implications for aquatic food web studies. *Marine Ecology Progress Series*, *342*, 85–90.

Chikaraishi, Y., Ogawa, N. O., Kashiyama, Y., Takano, Y., Suga, H., Tomitani, A., Miyashita, H., Kitazato, H., & Ohkouchi, N. (2009). Elucidation of aquatic food-web structure based on compound-specific nitrogen isotopic composition of amino acids. *Limnology & Oceanography: Methods*, *7*, 740–750.

Childress, J. J., Fisher, C. R., Brooks, J. M., Kennicutt, M., Bidigare, R., & Anderson, A. E. (1986). A methanotrophic marine molluscan (Bivalvia, Mytilidae) symbiosis: Mussels fueled by gas. *Science*, *233*(4770), 1306–1308.

Coykendall, D. K., Cornman, R. S., Prouty, N. G., Brooke, S., Demopoulos, A. W. J., & Morrison, C. L. (2019). Molecular characterization of Bathymodiolus mussels and gill symbionts associated with chemo- synthetic habitats from the U.S. Atlantic margin. *PLoS One*, *14*(3), e0211616. https://doi.org/10.1371/journal.pone.0211616

CSA Ocean Sciences Inc, Ross, S. W., Brooke, S., Baird, E., Coykendall, D. K., Davies, A. J., Demopoulos, A. W. J., France, S. C., Kellogg, C. A., Mather, R., Mienis, F., Morrison, C., Prouty, N., Roark, B., & Robertson, C. M. (2017). *Exploration and research of mid-Atlantic Deepwater hard bottom habitats and shipwrecks with emphasis on canyons and coral communities: Atlantic Deepwater Canyons Study*. Vol I. Final Technical Rept., Vol. II: Final Appendices. OCS Study BOEM 2017-060 (Vol. I) & 061 (Vol. II) U.S. Dept. of the Interior, Bureau of Ocean Energy Management, Atlantic OCS Region, pp. 1000 (p + appendices).

Dekas, A. E., Chadwick, G. L., Bowles, M. W., Joye, S. B., & Orphan, V. J. (2013). Spatial distribution of nitrogen fixation in methane seep sed- iment and the role of the ANME archaea. *Environmental Microbiology*, *16*(10), 3012–3029. https://doi.org/10.1111/1462-2920.12247

Demopoulos, A. W. J., McClain-Counts, J. P., Bourque, J. R., Prouty, N. G., Smith, B. J., Brooke, S., Ross, S. W., & Ruppel, C. D. (2019). Examination of *Bathymodiolus childressi* nutritional sources, isoto- pic niches, and food-web linkages at two seeps in the US Atlantic margin using stable isotope analysis and mixing models. *Deep Sea Research Part I: Oceanographic Research Papers*, *148*, 53–66. https:// doi.org/10.1016/j.dsr.2019.04.002

Demopoulos, A. W. J., McClain-Counts, J., Ross, S. W., Brooke, S., & Mienis, F. (2017). Food-web dynamics and isotopic niches in deep- sea communities residing in a submarine canyon and on the adjacent open slopes. *Marine Ecology Progress Series*, *578*, 19–33. https://doi. org/10.3354/meps12231

Duperron, S., Gaudron, S. M., Rodrigues, C. F., Chuna, M. R., Decker, C., & Olu, K. (2013). An overview of chemosynthetic symbioses in bivalves from the North Atlantic and Mediterranean Sea. *Biogeosciences*, *10*, 3241–3267. https://doi.org/10.5194/bg-10-3241-2013

Graham, B. S., Koch, P. L., Newsome, S. D., McMahon, K. W., & Aurioles, D.(2010). Using isoscapes to trace the movements and foraging behavior of top predators in oceanic ecosystems. In J. West, G. J. Bowen, T. E. Dawson, & K. P. Tu (Eds.), *Isoscapes: Understanding move- ment, pattern, and process on Earth through isotope mapping* (pp. 299– 318). Springer-Verlag.

Grupe, B. M., Krach, M. L., Pasulka, A. L., Maloney, J. M., Levin, L. A., & Frieder, C. A. (2015). Methane seep ecosystem functions and ser- vices from a recently discovered southern California seep. *Marine Ecology*, *36*, 91–108. https://doi.org/10.1111/maec.12243

Hoch, M. P., Fogel, M. F., & Kirchman, D. L. (1992). Isotope fractionation associated with ammonium uptake by a marine bacterium. *Limnology and Oceanography*, *37*(7), 1447–1459.

Hoch, M. P., Snyder, R. A., Cifuentes, C. A., & Coffin, R. B. (1996). Stable isotope dynamics of nitrogen recycled during interactions among marine bacteria and protists. *Marine Ecology Progress Series*, *132*, 229–239. https://doi.org/10.3354/meps132229

Jackson, A. L., Inger, R., Parnell, A. C., & Bearhop, S. (2011). Comparing isotopic niche widths among and within communities: SIBER – Stable Isotope Bayesian Ellipses in R. *Journal of Animal Ecology*, *80*(3), 595– 602. https://doi.org/10.1111/j.1365-2656.2011.01806.x

Kennicutt, M. C. II, Burke, R. A., Macdonald, I. R., Brooks, J. M., Denoux, G. J., & Macko, S. A. (1992). Stable isotope partitioning in seep and vent organisms: Chemical and ecological significance. *Chemical Geology*, *101*, 293–310.

Kiel, S. (Ed.) (2010). *The vent and seep biota, topics in Geobiology 33*. © Springer Science+Business Media B.V.

Larsen, T., Ventura, M., Andersen, N., O'Brien, D. M., Piatkowski, U., & McCarthy, M. D. (2013). Tracing carbon sources through aquatic and terrestrial food webs using amino acid stable isotope fingerprinting. *PLoS One*, *8*, e73441. https://doi.org/10.1371/journal.pone.0073441

Lee, R. W., & Childress, J. J. (1994). Assimilation of inorganic nitrogen by marine invertebrates and their chemoautotrophic and methanotrophic symbionts. *Applied and Environmental Microbiology*, *60*, 1852–1858.

Lee, R. W., & Childress, J. J. (1995). Assimilation of inorganic nitrogen by seep mytilid Ia, an undescribed deep-sea mussel containing methanotrophic endosymbionts: Fate of assimilated nitrogen and the relation between methane and nitrogen assimilation. *Marine Ecology Progress Series*, *123*, 137–148. https://doi.org/10.3354/meps123137

Lee, R. W., & Childress, J. J. (1996). Inorganic N assimilation and ammonium pools in a deep-sea mussel containing methanotrophic endosymbionts. *Biology Bulletin*, *190*, 373–384. https://doi. org/10.2307/1543030

Levin, L. A. (2005). Ecology of cold seep sediments: Interactions of fauna with flow, chemistry and microbes. In R. N. Gibson, R. J. A. Atkinson, & J. D. M. Gordon (Eds.), *Oceanography and marine biology: An annual review* (Vol. *43*, pp. 1–46). Taylor and Francis.

Levin, L. A., Baco, A. R., Bowden, D., Colaço, A., Cordes, E., Cunha, M. R., Demopoulos, A., Gobin, J., Grupe, B., Le, J., Metaxas, A., Netburn, A., Rouse, G. W., Thurber, A. R., Tunnicliffe, V., Van Dover, C., Vanreusel, A., & Watling, L. (2016). Hydrothermal vents and methane seeps: Rethinking the sphere of influence. *Frontiers in Marine Science*, *3*(72). https://doi.org/10.3389/fmars.2016.00072

Levy, E. M., & Lee, K. (1988). Potential contribution of natural hydro- carbon seepage to benthic productivity and the fisheries of Atlantic Canada. *Canadian Journal of Fisheries Aquatic Science*, *35*, 349–352. https://doi.org/10.1139/f88-041

MacAvoy, S. E., Carney, R. S., Morgan, E., & Macko, S. A. (2008). Stable isotope variation among the mussel *Bathymodiolus childressi* and as- sociated heterotrophic fauna at four cold-seep communities in the Gulf of Mexico. *Journal of Shellfish Research*, *27*, 147–151. https://doi. org/10.2983/0730-8000(2008)27[147:SIVATM]2.0.CO;2

McCarthy, M. D., Benner, R., Lee, C., & Fogel, M. L. (2007). Amino acid nitrogen isotopic fractionation patterns as indicators of heterotrophy in plankton, particulate, and dissolved

organic matter. *Geochimica Et Cosmochimica Acta*, *71*, 4727–4744. https://doi.org/10.1016/j. gca.2007.06.061

McCarthy, M. D., Lehman, J., & Kudela, R. (2013). Compound-specific amino acid δ15N patterns in marine algae: Tracer potential for cyanobacterial vs. eukaryotic organic nitrogen sources in the ocean. *Geochimica Et Cosmochimica Acta*, *103*, 104–120.

McClelland, J. W., & Montoya, J. P. (2002). Trophic relationships and the nitrogen isotopic composition of amino acids in plankton. *Ecology*, *83*, 2173–2180.

McMahon, K. W., Fogel, M. L., Elsdon, T. S., & Thorrold, S. R. (2010). Carbon isotope fractionation of amino acids in fish muscle reflects biosynthesis and isotopic routing from dietary protein. *Journal of Animal Ecology*, *79*, 1132–1141.

McMahon, K. W., & McCarthy, M. D. (2016). Embracing variability in amino acid $\delta^{15}N$ fractionation: Mechanisms, implications, and applications for trophic ecology. *Ecosphere*, *7*(12), 1–26.

Misarti, N., Gier, E., Finney, B., Barnes, K., & McCarthy, M. (2017). Compound-specific amino acid δ15N values in archaeological shell: assessing diagenetic integrity and potential for isotopic baseline reconstruction. *Rapid Communications in Mass Spectrometry*, *31*, 1881–1891.

Ohkouchi, N., Chikaraishi, Y., Close, H. G., Fry, B., Larsen, T., Madigan, D. J., McCarthy, M. D., McMahon, K. W., Nagata, T., Naito, Y. I., Ogawa, N. O., Popp, B. N., Steffan, S., Takano, Y., Tayasu, I., Wyatt, A. S. J., Yamaguchi, Y. T., & Yokoyama, Y. (2017). Advances in the application of amino acid nitrogen isotopic analysis in ecological and biogeochemical studies. *Organic Geochemistry*, *113*, 150–174. https://doi. org/10.1016/j.orggeochem.2017.07.009

Ohkouchi, N., Ogawa, N. O., Chikaraishi, Y., Tanaka, H., & Wada, E. (2015). Biochemical and physiological bases for the use of carbon and ni- trogen isotopes in environmental and ecological studies. *Progress in Earth and Planetary Science*, *2*, 1–17.

Paerl, H. W., & Pinckney, J. L. (1996). A mini-review of microbial consortia: Their roles in aquatic production and biogeochemical cycling. *Microbial Ecology*, *31*, 225–247.

Page, H. M., Fisher, C. R., & Childress, J. J. (1990). Role of filter-feeding in the nutritional biology of a deep-sea mussel with methanotrophic symbionts. *Marine Biology*, *104*(2), 251–257. https://doi.org/10.1007/ BF01313266

Pile, A. J., & Young, C. M. (1999). Plankton availability and retention efficiencies of cold-seep symbiotic mussels. *Limnology & Oceanography*, *44*(7), 1833–1839.

Ponnudurai, R., Kleiner, M., Sayavedra, L., Petersen, J. M., Moche, M., Otto, A., Becher, D., Takeuchi, T., Satoh, N., Dubilier, N., Schweder, T., & Markert, S. (2017). Metabolic and physiological interdependencies in the Bathymodiolus azoricus symbiosis. *ISME Journal*, *11*, 463–477.

Prouty, N. G., Mienis, F., Campbell-Swarzenski, P., Roark, E. B., Davies, A. J., Robertson, C. M., Duineveld, G., Ross, S. W., Rhode, M., & Demopoulos, A. W. J. (2017). Seasonal variability in the source and composition of particulate matter in the depositional zone of

Baltimore Canyon, U.S. Mid-Atlantic Bight. *Deep Sea Research Part I: Oceanographic Research Papers*, *127*, 77–89. https://doi. org/10.1016/j.dsr.2017.08.004

Prouty, N. G., Roark, E. B., Koenig, A. E., Demopoulos, A. W. J., Batista, F. C., Kocar, B. D., Selby, D., McCarthy, M. D., Mienis, F., & Ross, S. W. (2014). Deep-sea coral record of human impact on watershed quality in the Mississippi River Basin. *Global Biogeochemical Cycles*, *28*, 2013GB004754. https://doi.org/10.1002/2013GB004754

Prouty, N. G., Sahy, D., Ruppel, C. D., Roark, E. B., Condon, D., Brooke, S., Ross, S. W., & Demopoulos, A. W. J. (2016). Insights into methane dynamics from analysis of authigenic carbonates and chemo- synthetic mussels at newly-discovered Atlantic Margin seeps. *Earth Planetary Science Letters*, *449*, 332. https://doi.org/10.1016/j. epsl.2016.05.023

Riekenberg, P. M., Carney, R. S., & Fry, B. (2016). Trophic plasticity of the methanotrophic mussel *Bathymodiolus childressi* in the Gulf of Mexico. *Marine Ecology Progress Series*, *547*, 91–106. https://doi. org/10.3354/meps11645

Riou, V., Colaco, A., Bouillon, S., Khripounoff, A., Dando, P., Mangion, P., Chevalier, E., Korntheuer, M., Santos, R. S., & Dehairs, F. (2010). Mixotrophy in the deep sea: A dual–endosymbiotic hydrothermal mytilid assimilates dissolved and particulate organic matter. *Marine Ecology Progress Series*, *405*, 187–201. https://doi.org/10.3354/ meps08515

Rodrigues, C. F., Hilario, A., & Cunha, M. R. (2013). Chemosymbiotic species from the Gulf of Cadiz (NE Atlantic): Distribution, life styles and nutritional patterns. *Biogeosciences*, *10*(4), 2569–2581.

Ruppel, C., Demopoulos, A. W. J., Prouty, N. G., Sahy, D., & Condon, D. (2017). *Exploring U.S. Atlantic margin seeps with a remotely-operated vehicle. U.S.* (Vol. *17*, 2nd ed., pp. 12–15). Department of Energy National Energy Technology Laboratory's Fire in the Ice.

Seabrook, S., Cabrera De Leo, F., & Thurber, A. R. (2019). Flipping for Food: The use of a methane seep by Tanner Crabs (*Chionoecetes tanneri*). *Frontiers in Marine Science*, *6*, 43. https://doi.org/10.3389/ fmars.2019.00043

Sherwood, O. A., Guilderson, T. P., Batista, F. C., Schiff, J. T., & McCarthy, M. D. (2014). Increasing sub-tropical North Pacific ocean nitrogen fixation since the Little Ice Age. *Nature*, *505*, 78–81. https://doi. org/10.1038/nature12784

Sigman, D. M., Casciotti, K. L., Andreani, M., Barford, C., Galanter, M., & Böhlke, J. K. (2001). A bacterial method for the nitrogen isotopic analysis of nitrate in seawater and freshwater. *Analytical Chemistry*, *73*, 4145–4153. http://dx.doi.org/10.1021/ac010088e

Silfer, J. A., Engel, M. H., Macko, S. A., & Jumeau, E. J. (1991). Stable carbon isotope analysis of amino-acid enantiomers by conventional isotope ratio mass spectrometry and combined gas-chromatography isotope ratio mass-spectrometry. *Analytical Chemistry*, *63*, 370–374.

Stock, B. C., & Semmens, B. X. (2016). *MixSIAR GUI User Manual v3.1*. UC San Diego, San Diego, CA: Scripps Institution of Oceanography. https://doi.org/10.5281/zenodo.47719. https://github.com/brian stock/MixSIAR/, Version 3.1.

Trask, J. L., & Van Dover, C. L. (1999). Site-specific and ontogenetic variations in nutrition of mussels (*Bathymodiolus* sp.) from the Lucky Strike hydrothermal vent field, Mid-Atlantic Ridge. *Limnology & Oceanography*, *44*(2), 334–343.

Vokhshoori, N. L., & McCarthy, M. D. (2014). Compound-specific $\delta^{15}N$ amino acid measurements in littoral mussels in the California upwelling ecosystem: A new approach to generating baseline $\delta^{15}N$ isoscapes for coastal ecosystems. *PLoS One*, *9*, e98087.

Vokhshoori, N. L., McCarthy, M. D., Collins, P. W., Etnier, M. A., Rick, T., Eda, M., Beck, J., & Newsome, S. D. (2019). Broader foraging range of ancient short-tailed albatross populations into California coastal waters based on bulk tissue and amino acid isotope analysis. *Marine Ecology Progress Series*, *610*, 1–13. https://doi.org/10.3354/meps1 2839

Whitney, N. M., Johnson, B. J., Dostie, P. T., Luzier, K., & Wanamaker, A. D. Jr (2019). Paired bulk organic and individual amino acid δ15N anal- yses of bivalve shell periostracum: A paleoceanographic proxy for water source variability and nitrogen cycling processes. *Geochimica Et Cosmochimica Acta*, *254*, 67–85. https://doi.org/10.1016/j. gca.2019.03.019

Yamaguchi, Y. T., Chikaraishi, Y., Takano, Y., Ogawa, N. O., Imachi, H., Yokoyama, Y., & Ohkouchi, N. (2017). Fractionation of nitrogen iso- topes during amino acid metabolism in heterotrophic and chemolitho- autotrophic microbes across Eukarya, Bacteria, and Archaea: Effects of nitrogen sources and metabolic pathways. *Organic Geochemistry*, *111*, 101–112. https://doi.org/10.1016/j.orggeochem.2017.04.004

Supplemental Materials

Figure S1. Nutrient concentrations (NO_3^-, blue; NH_4^+, yellow) measured in three water types (bottom water, sediment surface water, porewater) sampled within varying sized mussel beds from Baltimore Canyon, Chincoteague and Norfolk Canyon. Sediment surface water and porewater were collected from pushcores, and bottom water was sampled from 10L Niskin bottles mounted to the ROV *Global Explorer.*

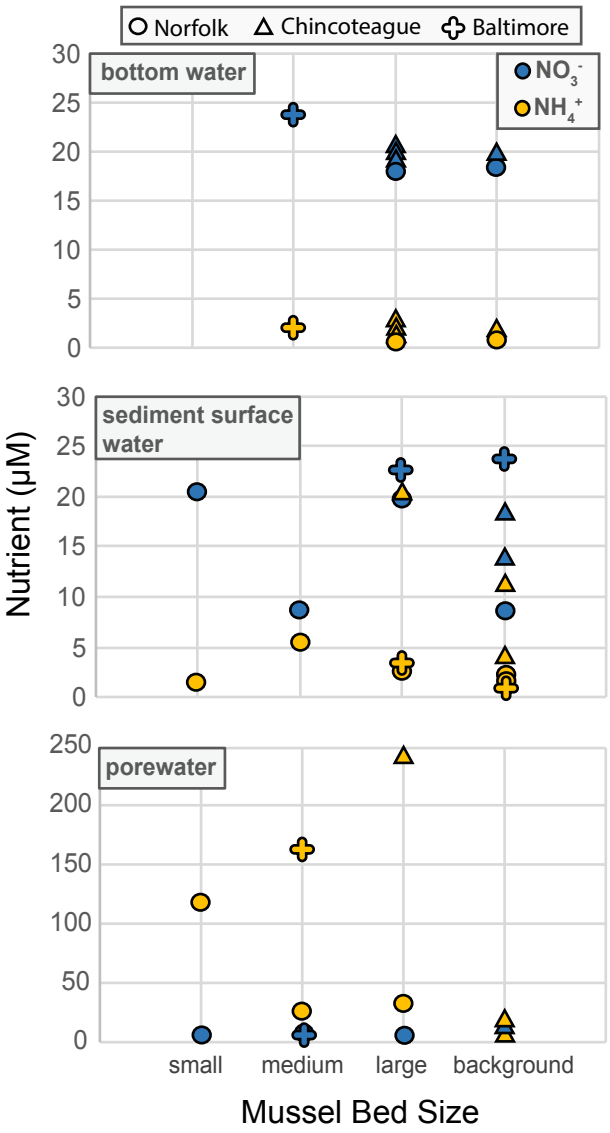

Figure S2. Bulk biplot and SIBER ellipse areas of muscle (black) and gill (red) by (A) seep site (Chincoteague- triangle; Norfolk, large- circle; Baltimore- cross) and (B) mussel bed density (Large- cross; Medium- triangle; Small- circle). The colored ellipses represent the standard ellipse areas (SEAc) for each of the groups.

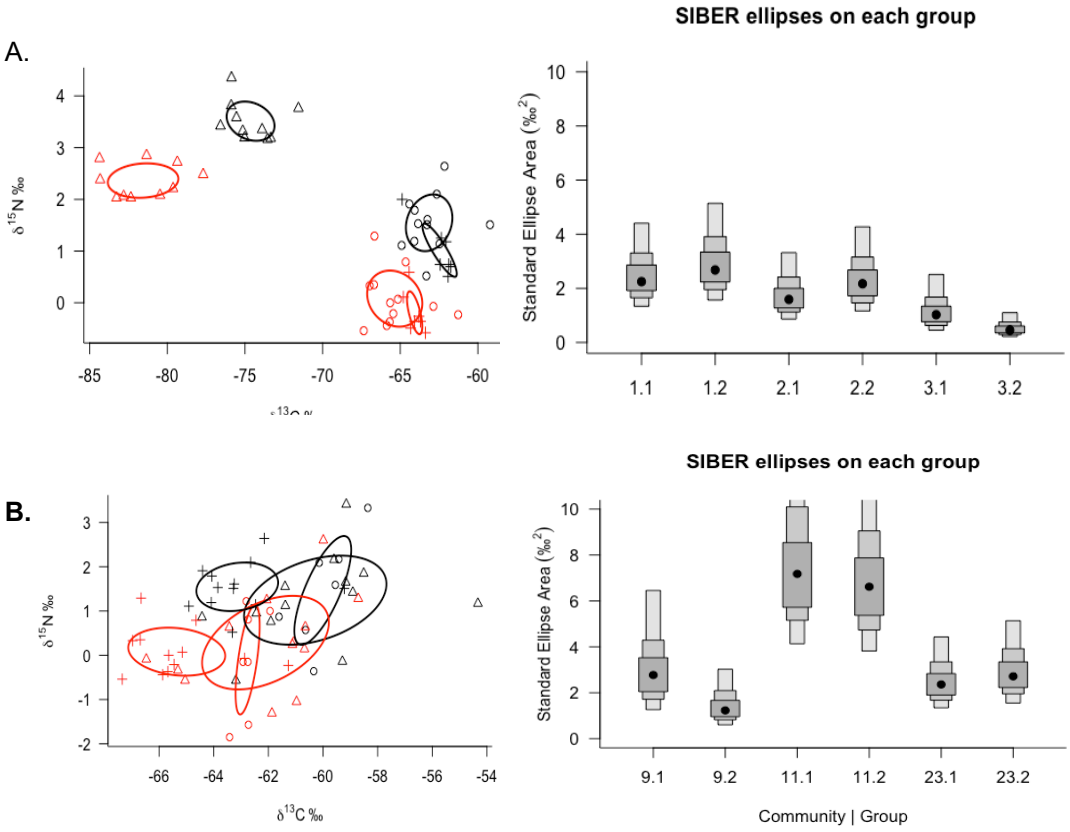

Figure S3. Measured $\delta^{15}N$ isotope results of *B. childressi* (A) muscle tissue and (B) gill tissue organized by seep sites: Baltimore (HRS1704-GEX06-075, green triangles), Chincoteague (HRS1704-GEX05-053, orange diamonds) and Norfolk sites: small bed (HRS1704-GEX03-009, red circles), medium bed (HRS1704-GEX03-011, blue circles), and large bed (HRS1704-GEX03-023, yellow circles)

A) Muscle Tissue

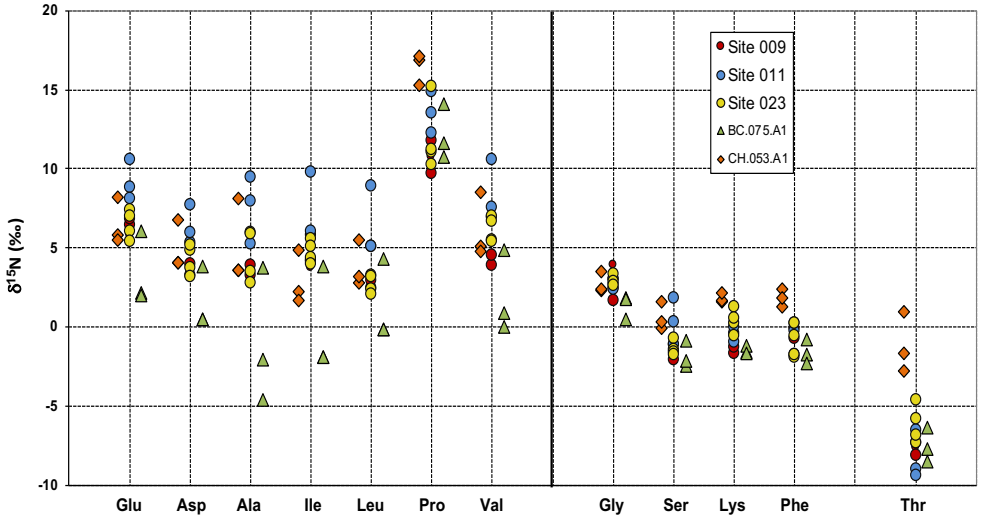

B) Gill Tissue

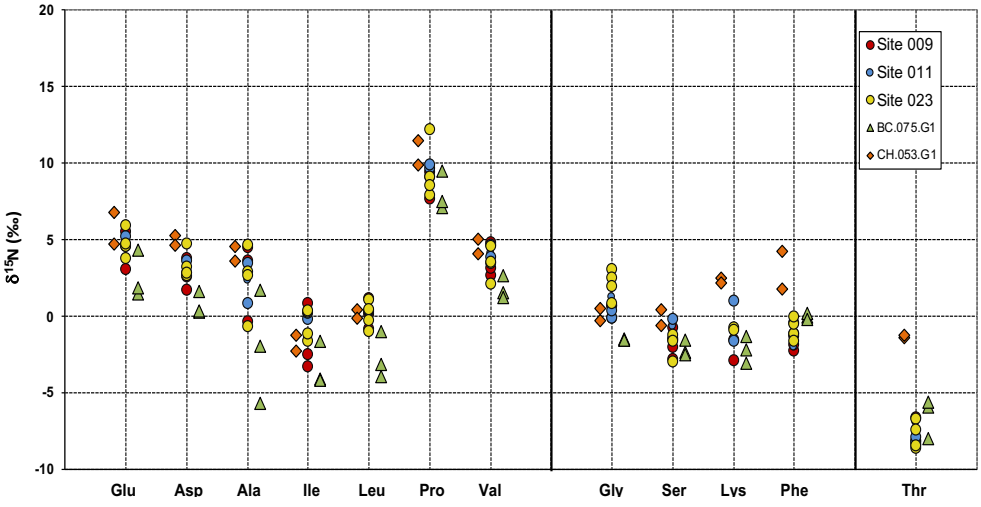

Figure S4. Principal component analysis of Trophic AAs and Thr Normalized to Avg. TrAA of (A) Muscle and (B) Gill Tissue in littoral mussels (purple), pushcore seep sediment (pink), and seep mussels: Baltimore (HRS1704-GEX06-075, teal), Chincoteague (HRS1704-GEX05-053, green) and Norfolk sites: small bed (HRS1704-GEX03-009, blue), medium bed (HRS1704-GEX03-011, red), and large bed (HRS1704-GEX03-023, yellow). Values in parentheses are the percentage variation accounted by the first and second principal components.

A. Muscle Tissue

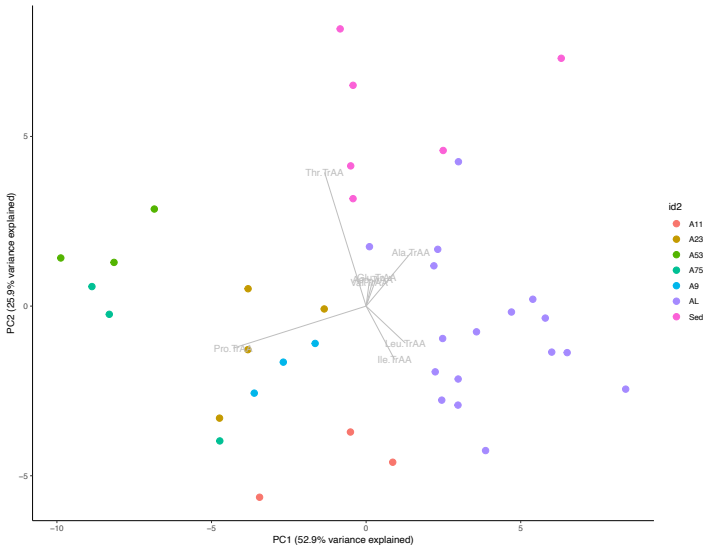

Importance of components:

	PC1	PC2	PC3	PC4	PC5	PC6	PC7	PC8
Standard deviation	4.6812	3.2771	2.00412	1.66363	1.04071	0.88596	0.39546	0.002634
Proportion of Variance	0.5285	0.2590	0.09687	0.06675	0.02612	0.01893	0.00377	0.000000
Cumulative Proportion	0.5285	0.7875	0.88442	0.95117	0.97730	0.99623	1.00000	1.000000

	PC1	PC2	PC3	PC4
Ala.TrAA	0.29017173	0.3147904	-0.30560107	-0.50775949
Val.TrAA	0.01969132	0.1405693	-0.58357741	0.50570208
Leu.TrAA	0.25370026	-0.2180253	0.62164035	0.07534609
Ile.TrAA	0.18418800	-0.3147503	0.01611145	0.49032273
Pro.TrAA	-0.85926007	-0.2474425	-0.02241533	-0.17144853
Asp.TrAA	0.04285969	0.1543881	0.24517097	-0.13840425
Glu.TrAA	0.06856586	0.1703370	0.02934382	-0.25305381
Thr.TrAA	-0.26880751	0.7876968	0.34333188	0.35744331

B. Gill Tissue

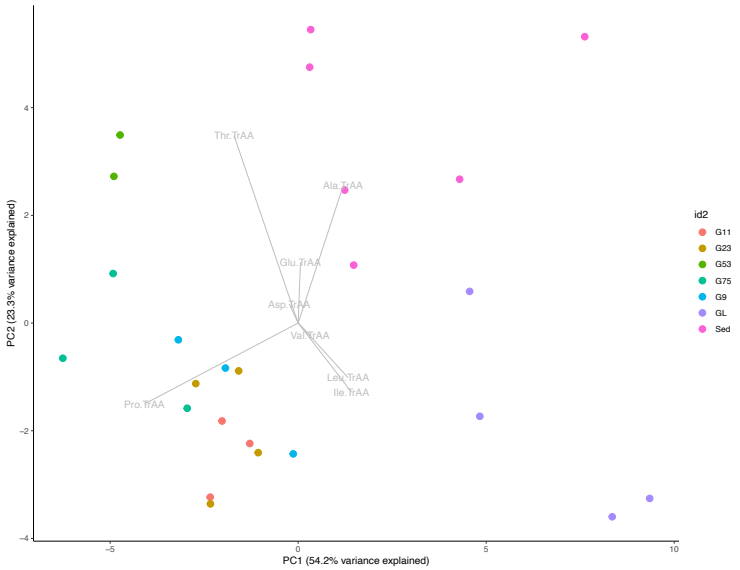

Importance of components:

	PC1	PC2	PC3	PC4	PC5	PC6	PC7	PC8
Standard deviation	4.2908	2.8122	2.1624	1.30332	0.9579	0.52825	0.31740	0.002787
Proportion of Variance	0.5416	0.2327	0.1376	0.04997	0.0270	0.00821	0.00296	0.000000
Cumulative Proportion	0.5416	0.7743	0.9119	0.96183	0.9888	0.99704	1.00000	1.000000

	PC1	PC2	PC3	PC4
Ala.TrAA	0.23949287	0.50984084	-0.65603311	0.120965618
Val.TrAA	0.06349067	-0.04614757	0.36024978	0.211950307
Leu.TrAA	0.26590285	-0.20299583	0.19759033	-0.609958970
Ile.TrAA	0.28369535	-0.25642342	0.23669400	0.622774653
Pro.TrAA	-0.81773263	-0.30045165	-0.24238534	0.072104896
Asp.TrAA	-0.04698247	0.07085887	0.08028137	-0.415601963
Glu.TrAA	0.01216620	0.22540000	0.02488657	-0.002323955
Thr.TrAA	-0.34114909	0.69632974	0.52816624	0.051153346

Figure S5. Relative molar abundance of 12 amino acids measured in littoral and seep mussels. (A) muscle and (B) gill tissue of seep mussels from the three seep sites in this study: Norfolk seep field by mussel bed size: small bed (HRS1704-GEX03-009, grey), medium bed (HRS1704-GEX03-011, red), and large bed (HRS1704-GEX03-023, blue), Baltimore (HRS1704-GEX06-075, green), and Chincoteague (HRS1704-GEX05-053, yellow), compared to littoral mussels (dark blue).

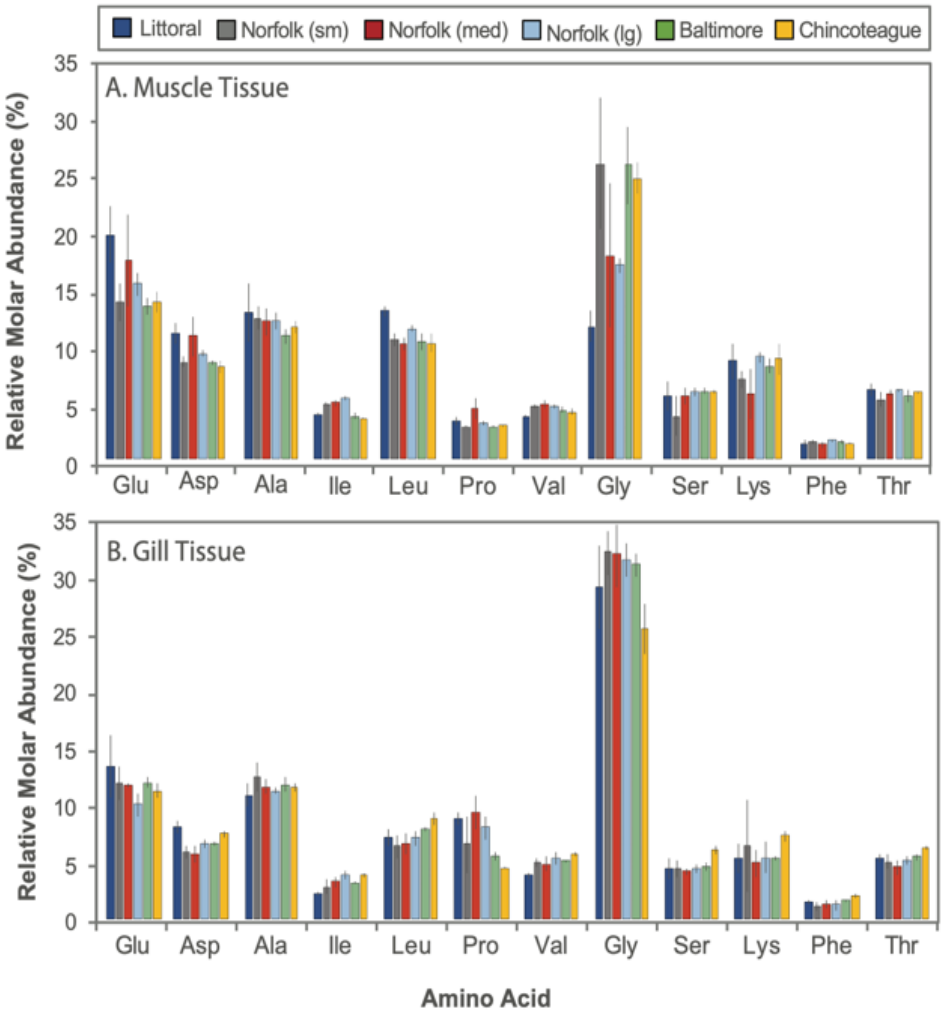

Figure S6. PCA of relative molar abundance of 12 amino acids in (A) muscle and (B) gill tissue of seep and littoral mussels. littoral mussels (pink), and seep mussels: Baltimore (HRS1704-GEX06-075, teal), Chincoteague (HRS1704-GEX05-053, green) and Norfolk sites: small bed (HRS1704-GEX03-009, blue), medium bed (HRS1704-GEX03-011, red), and large bed (HRS1704-GEX03-023, yellow)

A. Muscle Tissue

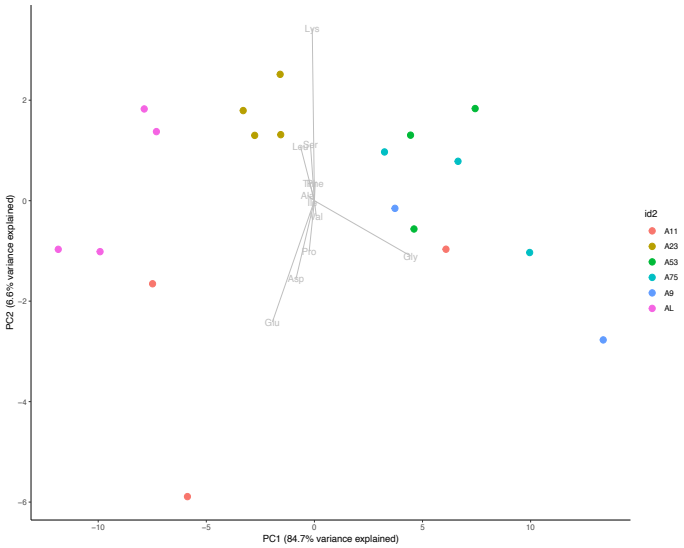

Importance of components:

	PC1	PC2	PC3	PC4	PC5	PC6	PC7	PC8	PC9	PC10	PC11	PC12
Standard deviation	7.2546	2.03073	1.73794	1.03152	0.94720	0.4859	0.25864	0.24332	0.14916	0.10070	0.04034	9.132e-10
Proportion of Variance	0.8471	0.06637	0.04861	0.01713	0.01444	0.0038	0.00108	0.00095	0.00036	0.00016	0.00003	0.000e+00
Cumulative Proportion	0.8471	0.91344	0.96206	0.97918	0.99362	0.9974	0.99850	0.99945	0.99981	0.99997	1.00000	1.000e+00

	PC1	PC2	PC3	PC4
Ala	-0.062329104	0.020895483	-0.713299314	-0.385265656
Gly	**0.890423779**	-0.220248507	0.146805632	-0.124493952
Thr	-0.042216192	0.068505374	-0.094207276	0.117992603
Ser	-0.036798334	0.223434273	-0.190925101	0.640659364
Val	0.017402580	-0.062122687	-0.119821082	0.149030516
Leu	**-0.128843087**	**0.216068479**	-0.008100107	-0.528407282
Ile	-0.016947458	-0.006232758	-0.086946467	0.116722819
Pro	-0.048531328	-0.201423293	0.027161109	0.254912393
Asp	-0.170484614	**-0.311226210**	0.086857794	0.006986037
Glu	**-0.388671149**	**-0.483004547**	0.416046734	-0.150198381
Phe	0.006979367	0.069579944	0.071887818	-0.002753809
Lys	-0.019984460	**0.685774447**	0.464540260	-0.09518465

B. Gill Tissue

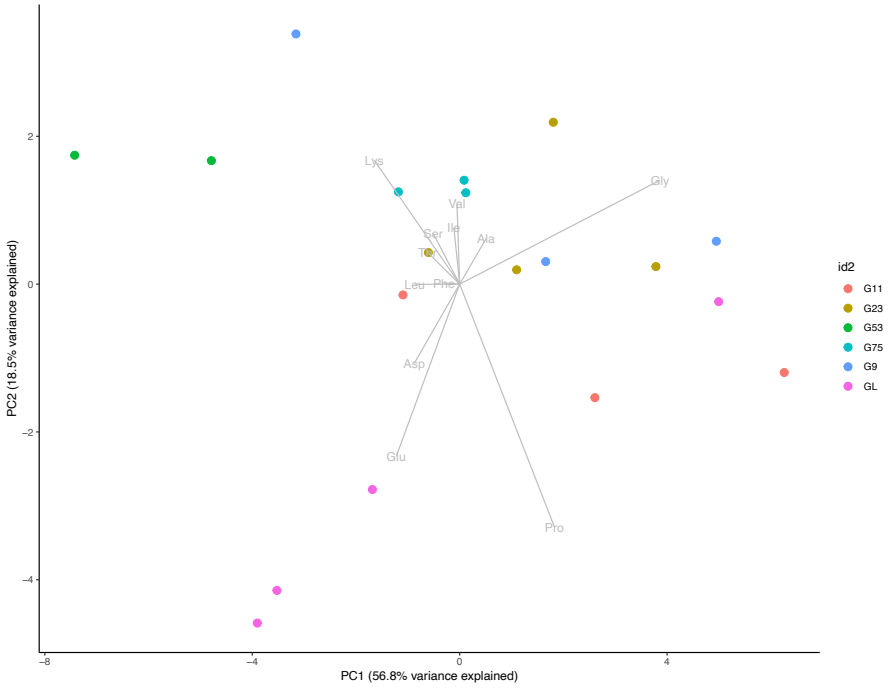

Importance of components:

	PC1	PC2	PC3	PC4	PC5	PC6	PC7	PC8	PC9	PC10	PC11	PC12
Standard deviation	3.6394	2.0773	1.7250	1.08835	0.83586	0.69298	0.44899	0.41920	0.16058	0.13815	0.05148	1.026e-09
Proportion of Variance	0.5679	0.1850	0.1276	0.05078	0.02995	0.02059	0.00864	0.00753	0.00111	0.00082	0.00011	0.000e+00
Cumulative Proportion	0.5679	0.7529	0.8805	0.93124	0.96120	0.98179	0.99043	0.99796	0.99907	0.99989	1.00000	1.000e+00

	PC1	PC2	PC3	PC4
Ala	0.10227274	0.1236035506	-0.10129699	-0.42560823
Gly	0.77272135	0.2813147846	0.34957613	-0.08272947
Thr	-0.12399718	0.0859194086	-0.07989819	0.05004455
Ser	-0.10190616	0.1366750498	-0.15038180	0.11041238
Val	-0.01047327	0.2192516650	-0.23126541	-0.03815674
Leu	-0.17301613	-0.0006284707	-0.33311852	-0.25952242
Ile	-0.02266052	0.1538193815	-0.23883664	0.07106190
Pro	0.36579021	-0.6577574172	-0.15460382	0.43929210
Asp	-0.17489836	-0.2142698102	-0.05064231	0.21239110
Glu	-0.24446429	-0.4656983287	0.55585128	-0.47451263
Phe	-0.06021211	0.0025808595	-0.08859969	-0.10239789
Lys	-0.32915629	0.3351893269	0.52321596	0.49972533

Figure S7. Amino acid $\delta^{15}N$ of pushcore sediments (0-2 and 2-4 cm intervals) from Norfolk Seep field

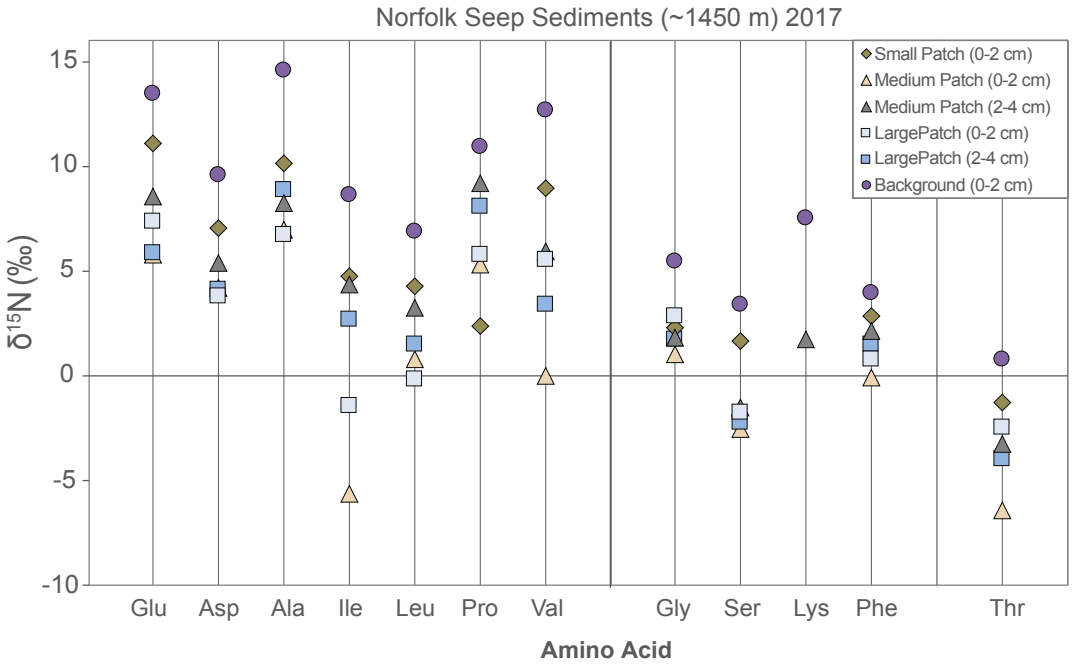

Figure S8. Microbial resynthesis index, ΣV (McCarthy et al. 2007) versus Trophic Level (Chikaraishi et al. 2007) of pushcore surface sediment from Norfolk seep field (HRS1704-GEX03) overlaid by seep mussel (shaded gray) and littoral mussel (shaded blue) gill and muscle tissue combined.

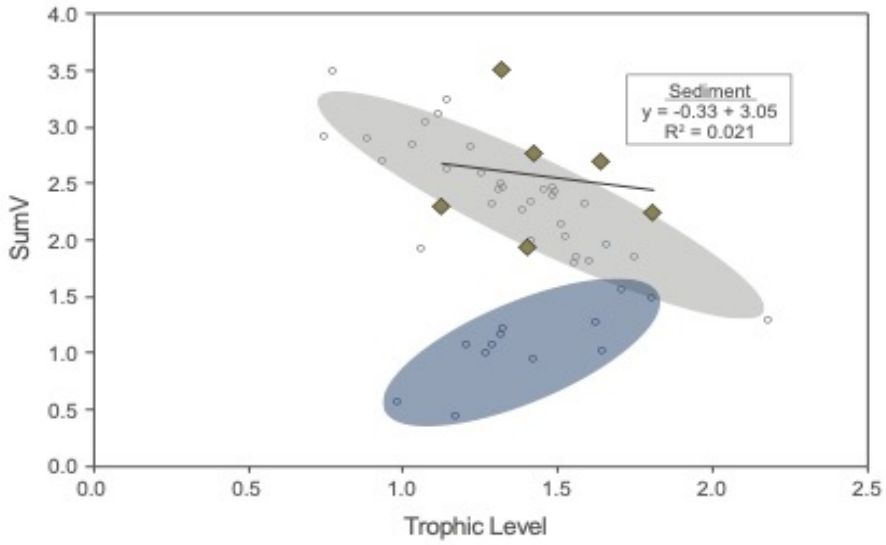

Table S1. Summary Statistics for MixSIAR output

# Summary Statistics - 4 amino acids (Pro, Leu, Iso, Thr)									
	Mean	SD	2.50%	5%	25%	50%	75%	95%	97.50%
Station.SD	2.856	3.423	0.315	0.398	0.867	1.589	3.176	10.793	14.142
p.global.Chemoauto	0.814	0.185	0.245	0.399	0.777	0.88	0.93	0.976	0.985
p.global.Littoral	0.186	0.185	0.015	0.024	0.07	0.12	0.223	0.601	0.755
p.Station 9.Chemoauto	0.807	0.065	0.697	0.714	0.765	0.8	0.841	0.932	0.978
p.Station 11.Chemoauto	0.872	0.066	0.747	0.767	0.828	0.866	0.913	0.999	1
p.Station 23.Chemoauto	0.863	0.063	0.75	0.77	0.822	0.857	0.901	0.995	1
p.Station 53.Chemoauto	0.972	0.031	0.893	0.91	0.956	0.983	0.997	1	1
p.Station 75.Chemoauto	0.974	0.03	0.896	0.914	0.959	0.984	0.998	1	1
p.Station 9.Littoral	0.193	0.065	0.022	0.068	0.159	0.2	0.235	0.286	0.303
p.Station 11.Littoral	0.128	0.066	0	0.001	0.087	0.134	0.172	0.233	0.253
p.Station 23.Littoral	0.137	0.063	0	0.005	0.099	0.143	0.178	0.23	0.25
p.Station 53.Littoral	0.028	0.031	0	0	0.003	0.017	0.044	0.09	0.107
p.Station 75.Littoral	0.026	0.03	0	0	0.002	0.016	0.041	0.086	0.104

Input data:

Source Endmembers									
Source	MeanLeu.TrAA	MeanIle.TrAA	MeanPro.TrAA	MeanThr.TrAA	SDLeu.TrAA	SDIle.TrAA	SDPro.TrAA	SDThr.TrAA	n
Littoral	0.69110799	-1.2510974	-1.5404813	-12.483437	0.49602207	0.41688669	1.40917851	2.52006528	4
Chemoauto	-3.894419	-5.8328524	6.60091429	-5.350419	0.66760982	0.36052344	0.34964747	0.89674609	2

Trophic Discrimination Factor								
Source	MeanLeu.TrAA	MeanIle.TrAA	MeanPro.TrAA	MeanThr.TrAA	SDLeu.TrAA	SDIle.TrAA	SDPro.TrAA	SDThr.TrAA
Littoral	0	0	0	0	0	0	0	0
Chemoauto	0	0	0	0	0	0	0	0

Consumer values				
Station	Leu.TrAA	Ile.TrAA	Pro.TrAA	Thr.TrAA
9	-2.3711667	-4.7990833	6.13608333	-8.0885
9	-3.1272143	-3.4154643	5.13370238	-12.658881
9	-2.8084643	-5.4527143	6.17328571	-11.071214
11	-3.236756	-3.365881	6.13057738	-10.457506
11	-3.5160714	-4.0046548	5.82417857	-12.067071
11	-2.8939464	-2.9810714	6.65438691	-11.08403
23	-3.684551	-4.5075034	7.39254422	-13.398503
23	-3.161932	-3.7918844	5.6984966	-8.8582177
23	-2.6551224	-2.7810748	5.92330612	-11.587742
23	-3.2413605	-4.0893129	5.52106803	-10.367313
53	-4.1898476	-5.8784476	6.84815238	-5.9845143

53	-3.5989905	-5.7872571	6.35367619	-4.7163238
75	-3.9913929	-4.1427262	7.05569048	-5.9755595
75	-2.8583452	-3.8916786	7.84607143	-5.2798452
75	-3.476869	-4.058869	7.04188095	-10.446036

Chapter 2

Ecological isotope proxies in bivalve shell for paleoecological reconstructions

"It is advisable to look from the tide pool to the stars and then back to the tide pool again."

- John Steinbeck, *The Log from the Sea of Cortez*

The following contains material that was submitted to *Palaeogeography, Palaeoclimatology, Palaeoecology* on 15 October 2021:

Calibrating bulk and amino acid $\delta^{13}C$ and $\delta^{15}N$ isotope ratios between bivalve soft tissue and shell for reconstructing paleoecological archives

Natasha L. Vokhshoori, Brett J. Tipple, Laurel Teague, Alex Bailess, Matthew D. McCarthy

Abstract: Ecological isotope proxies measured in ancient bivalve shell matrix protein have great promise for paleoecological reconstruction. Compound-specific isotopes of amino acids (CSI-AA) may be an ideal tool for developing paleoecological proxies as initial research shows CSI-AA is less subject to alteration under geologic conditions relative to bulk isotope values. While CSI-AA proxies have been developed and applied in modern bivalve soft tissues, they have yet to be systematically investigated in shell matrix protein. Here, we measured stable isotope values of carbon ($\delta^{13}C$) and nitrogen ($\delta^{15}N$) in both bulk and individual AAs, comparing soft tissue and shell organic fractions to test the fidelity of a suite of ecological isotope proxies in shell. We sampled three ubiquitous bivalve species seasonally for one year from two common coastal environments: littoral rocky intertidal and estuarine delta ecosystems. Particulate organic matter (POM) was simultaneously collected to investigate relationships between tissue types and local POM isotope signatures. The ecological proxies tested include trophic niche breadth from bulk isotopes as well as baseline $\delta^{13}C$ and $\delta^{15}N$ values, resource contribution, and trophic level from CSI-AA. We found niche breadth corresponded well between tissue types, but that bulk isotope values were significantly higher in shell compared to soft tissue. In the CSI-AA record, there were no differences in baseline $\delta^{13}C$ and $\delta^{15}N$ proxies between tissue types. While no consistent seasonal trends were observed in the $\delta^{13}C$ record, summer bulk and baseline $\delta^{15}N$ values were least positive in both ecosystems in both tissues. Food resource contribution estimates from shell also closely matched soft tissue, however trophic level estimates were consistently higher in shell, attributed to a systematic offset in Glutamic acid $\delta^{15}N$ values. We therefore propose a mollusk-specific trophic discrimination

factor, and corresponding shell isotope enrichment factor to correct for isotopic routing, both required for accurate paleoecological reconstructions.

2.1 Introduction

Bivalves and their shells are in many respects ideal bioarchives for developing detailed paleoecological records of nearshore marine primary productivity, as they feed at the base of the food chain, are abundant in coastal environments with precisely known source locations, and shell material is well preserved in both archeologic and geologic archives. Stable isotopes of carbon ($\delta^{13}C$) and nitrogen ($\delta^{15}N$) from whole tissue (bulk) and amino acids (AA) measured in the shells of bivalves therefore represent a largely unexplored source of highly detailed information into past coastal primary productivity and ecosystem trophic structure. While bulk $\delta^{13}C$ and $\delta^{15}N$ values are useful for reflecting the trophic niche of a community (Jackson et al. 2011, Newsome et al. 2007), $\delta^{13}C$ and $\delta^{15}N$ of individual AAs carry for more detailed information, recording both trophic level (Chikaraishi et al. 2009) and food resource contribution (Stock and Semmens 2016), as well as the isotopic values at the base of its food chain (Vokhshoori et al. 2014, Shen et al. 2021), commonly referred to as the isotopic “baseline.” New analytical tools and reliable paleoarchives are therefore key for understanding how natural and anthropogenic environmental changes have influenced marine ecosystems in the past, in order to understand future change and potential mitigation.

CSI-AA ecological proxies are based on the differences in fractionation of specific AAs between diet and consumer. For C, primary producers synthesize essential AAs (EAA) with a unique $\delta^{13}C$ “fingerprint” based on evolutionary divergence (Larsen et al. 2009, 2013). Since animals must acquire EAAs from their diet, $\delta^{13}C_{EAA}$ fingerprints are passed up the food chain unaltered, and thus preserve the signature of the primary producer assemblage through trophic transfers (Hare et al. 1991, Howland et al. 2003, McMahon et al. 2010). Libraries of the EAA

$\delta^{13}C$ values for potential primary producer types for a given ecosystem (e.g. Larsen et al.2009, 2013; Tipple et al. submitted) combined with Bayesian mixing models (e.g. MixSIAR; Stock & Semmens 2016) can therefore be used for quantifying shifting baseline resource contribution to consumers within that system. For N, the "trophic AA" group (e.g., Glutamic Acid: Glu) undergo significant transamination/deamination which predictably increases the $\delta^{15}N$ values with each trophic transfer. A second group now called "Transitional AA" (e.g. Gly and Ser) can undergo major de novo synthesis in a consumer (McMahon and McCarthy, 2016). And a third group collectively known "source AAs" (e.g. Phenylalanine: Phe) show little to no fractionation with trophic transfer, and thus reflect baseline nitrogen values.

However, for any potential bioarchive of isotopic information, both precise trophic levels and isotope systematics must be well characterized, typically by conducting field or captive feedings studies. For example, if there are tissue-specific bulk or compound specific isotope offsets, due to isotopic routing or other factors, calibrations will be required to reconstruct original ecosystem values. While it is generally assumed AAs from different tissue types (e.g., muscle, shell, bone, etc.) reflect common trophic enrichment patterns linked to central metabolism, specific tissues can also have characteristic isotope offsets (Wolf et al. 2015). Specifically, for paleo-bioarchives, for example, McMahon and co-authors (2018) showed differences in deep-sea coral polyp tissues and its structural gorgonian proteins.

This study aims to address the fundamental methodological questions required before bulk and CSI-AA data in ancient bivalve shell can be used to reconstruct past coastal ocean changes. We present the first paired $\delta^{13}C$ and $\delta^{15}N$ data in bulk and individual AAs in both shell matrix protein and soft tissue of three species of marine bivalves. Bivalves were collected live from two well-characterized coastal environments – Monterey Bay littoral upwelling system and northern San Francisco Bay estuarine-delta system, sampled seasonally over one year. Olympia oysters (*Ostrea lurida*), and blue mussels (*Mytilus edulis*) were collected from the

estuarine site and California mussels (*Mytilus californianus*) from the littoral upwelling site, along with seawater particulate organic matter (POM) to directly assess the impacts of seasonal food source dynamics at the base of the food web on CSI-AA and bulk isotopic signals recorded in contrasted tissues of these bivalve species. For the ecological proxies investigated, we address two questions: 1.) can combined bulk and AA isotope techniques be used in bivalve shells to reconstruct detailed records of coastal primary productivity, and 2.), if yes, what calibrations are required?

2.2 Materials & Methods

2.2.1 Study location and site description

Sampling occurred at two ubiquitous, well-characterized coastal environments along California's coast: Littoral rocky intertidal zone of Monterey Bay (36°57'2 N, 122°2'39 W) and San Francisco Bay estuary (37°56'29 N, 122°28'56 W, spring sampling site- 37°39'50 N, 122°23'21 W) (Fig. 2.1).

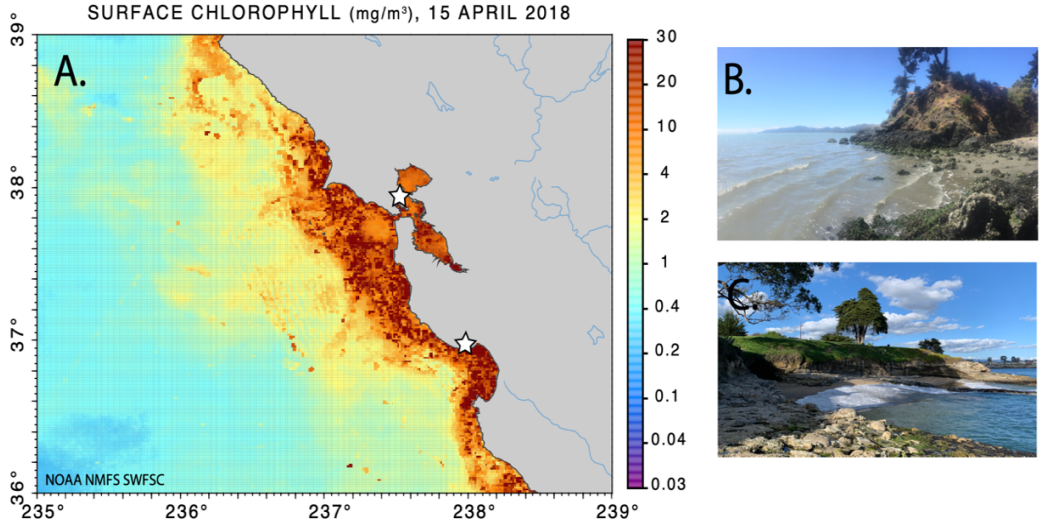

Figure 2. 1 Sampling locations and photographs of sampling sites. (A) Surface chlorophyll a (mg/m^3) for a day in the year of sampling (15 April 2018), typical production for this region, where sampling locations* denoted on map by star. Photographs of sampling sites: (B) Northern San Francisco Bay estuary (37°56'29 N, 122°28'56 W) and (C) Monterey Bay littoral upwelling system (36°57'2 N, 122°2'39 W). * SF Bay samples were from two locations indistinguishable from this map view.

The Monterey Bay is characterized by strong seasonal upwelling that occurs in spring and early summer which supplies cold, nutrient rich waters to the surface stimulating high primary production, predominantly composed of diatoms and dinoflagellates. Interannual and decadal oceanic variability due to ENSO and PDO can strongly affect average sea surface temperature (SST) and upwelling intensity on the coast, where the strongest El Niño events (i.e. above average SST and weakened upwelling) coincide with positive phases of the PDO (Jacox et al. 2015).

In contrast, Northern San Francisco (SF) Bay is characterized as a partially mixed estuary (Cloern 1996), where nutrients are supplied from both marine inflow through a narrow deep channel (via the Golden Gate) and freshwater runoff from the Sacramento-San Joaquin River Delta system (Jassby et al. 1993). The confluence of marine and freshwater sources produces spatial gradients of salinity, suspended sediments, nutrients and biological communities (Cloern 1996). This dynamic estuary is regulated by seasonal winter storm events and also diurnal tidal currents through the Golden Gate channel, both mechanisms stimulating mixing and supplying different organic carbon sources. Together, these hydrodynamics supply a mixture of marine and terrestrial primary producers, including various phytoplankton species (marine and freshwater), vascular plants (woody terrestrial and submerged), seagrasses and macroalgae (Cloern et al. 2002).

2.2.2 Sample collection and processing

Whole individuals 55-60 mm of California mussel (*Mytilus californianus*), Olympia oyster (*Ostrea lurida*) and Blue mussel (*Mytilus edulis*), as well as seawater particulate organic matter (POM) were collected from February 2018 to January 2019. Samples were collected seasonally: Spring (Apr./May), Summer (Jun./Jul.), Fall (Oct.) and Winter (Jan.), with *M. californianus* collected at the littoral site, and *O. lurida* and *M. edulis* at the estuarine site. 3-10 whole individual bivalves were collected in each season, with more frequent sampling at the

littoral site; simultaneously 5-10 L of seawater were collected in acid-washed 5-liter Nalgene bottles and remained chilled in a cooler until POM filtration in the lab.

Seawater was pre-filtered through a Nitex mesh (53µm) then filtered onto combusted 47mm 0.7µm GF/F filters. Typically, 3 L and 300 ml of littoral seawater and estuarine water was filtered onto a single filter, respectively. Sample yields were calculated using pre-weighed filters, a wedge of which was removed for bulk isotope analysis with the remaining filtrate and filter transferred to hydrolysis vials for CSI-AA.

Bivalves were dissected for the muscle adductor tissue, rinsed with deionized water, stored frozen, then lyophilized for 24 to 48 h; the remaining soft tissue parts were discarded. Mussel soft tissue was then homogenized and ~0.5mg was weighed into tin capsules for bulk isotope analysis. Bivalve shells were scrubbed clean using a wire brush and scalpel, then soaked in a dilute bath of bleach (NaOCl) for 1 h at room temperature, sonicated in nano-pure water, and dried overnight at 60ºC. Each shell was then crushed using a mortar and pestle, sieved through a 5 µm screen, and 1000 mg was weighed into a labelled 20x150mm borosilicate vial. To extract the organic matter (OM) fraction, samples were acidified with 1N HCl by pipetting 1mL increments until shell was completely dissolved (~35 mL); samples were stored 4 ºC overnight to complete the reaction. After acidification, OM fraction was isolated by filtration onto 22 mm 0.7 GF/F filters, rinsed thoroughly with nano-pure water, and dried overnight at 60ºC. Sample yields were calculated, a fraction was set aside for bulk $\delta^{13}C$ analysis, and the remaining amount was used for CSI-AA.

2.2.3 Bulk Stable Isotope Analysis

Stable isotopes of carbon ($\delta^{13}C_{bulk}$) and nitrogen ($\delta^{15}N_{bulk}$) were measured by the University of California Santa Cruz Stable Isotope Laboratory (UCSC-SIL) using a CE Instruments NC2500 elemental analyzer coupled to a Thermo Scientific DELTAplus XP isotope ratio mass spectrometer via a Thermo-Scientific Conflo III. For high C content samples,

automated in line CO_2 trapping is used to remove interference with N_2. Isotopes values are reported using delta (δ) notation: $\delta^{13}C$ or $\delta^{15}N = [(R_{sample}/R_{standard}) - 1]$, where R is the ratio of rare to common isotope of the sample (R_{sample}) and standard ($R_{standard}$), respectively, and corrected to VPDB (Vienna PeeDee Belemnite) for $\delta^{13}C$ and AIR for $\delta^{15}N$ against an in-house gelatin standard reference material (PUGel) which is extensively calibrated against international standard reference materials. Measurements are corrected for size effects, blank-mixing effects, and drift effects. An externally-calibrated Acetanilide standard reference material purchased from Dr. Arndt Schimmelmann of Indiana University is measured as a sample for independent quality control.

2.2.4 Amino Acid Stable Isotope Analysis

The stable carbon ($\delta^{13}C_{AA}$) and nitrogen ($\delta^{15}N_{AA}$) isotope values of amino acids from composites of bivalve soft tissue and demineralized shell OM, and seawater POM were analyzed following Batista *et al.*, 2014. Briefly, ~5 mg dry weight bivalve shell protein and soft tissue, and ~5-8 mg seawater POM sample on GF/F filters were weighed into 8 mL hydrolysis vials, submerged in 1-2 mL of 6N HCl, purged with N_2 gas to remove oxygen, and hydrolyzed for 20 h at 110°C. After hydrolysis, samples were cooled to room temperature and stored in a -4°C freezer until further processing. Samples were then purified using cation-exchange chromatography with the DOWEX 50WX8-400 resin. Before dry down, purified filtrate was spiked with Norleucine as an internal standard.

$\delta^{15}N$-AA and $\delta^{13}C$-AA values were measured as trifluoroacetyl isopropyl ester (TFA-IP) derivatives. After drying hydrolysates at 60°C under N_2, amino acid isopropyl esters were prepared with a 1:4 mixture of acetyl chloride:isopropanol at 110°C for 60 min and then aceytlated using a 1:1 mixture of dichloromethane (DCM) and trifluoroacetic anhydride (TFAA) at 110°C for 10 min (Silfer et al. 1991). Samples were again dried and finally re-dissolved in ethyl acetate for GC-IRMS analysis. AA isotopes values were measured using a Thermo Trace

gas chromatograph coupled to a Finnegan Delta-Plus IRMS and GCC III (isoLink) at the UCSC-SIL. Using this method, we measured $\delta^{15}N$ and $\delta^{13}C$ values of the following AAs: alanine (Ala), glycine (Gly), threonine (Thr), serine (Ser), valine (Val), leucine (Leu), isoleucine (Ile), proline (Pro), aspartic acid (Asp), glutamic acid (Glu), phenylalanine (Phe), tyrosine (Tyr), and lysine (Lys). All sample derivatives were injected/ quantified in triplicate. Measured $\delta^{13}C_{AA}$ values were corrected for the carbon atoms added during derivatization following the approach of Silfer et al. (1991) and Hare et al. (1991). Final isotope value accuracy and reproducibility was checked in two ways: first by comparison of the internal Norleucine standard with its known values, and second by assessing values of an in-house long-term McCarthy lab reference material (cyanobacteria), analyzed with every sample set according to McCarthy Lab protocols. Reproducibility, as estimated with standard deviation for samples, was on average less than < 0.3 ‰ (range: 0.0−0.6 ‰) for carbon and <0.5‰ (range: 0.1−1.3 ‰) for nitrogen.

2.2.5 Amino-acid ecological parameter definitions and statistics

We calculated trophic level (TL_{CSIA}) with two different equations: 1) TL_{CSIA} representing the algae data-based formulation (Chikaraishi and co-authors (2009),

$$TL_{CSIA} = 1 + [\ \delta^{15}N_{Glu} - \delta^{15}N_{Phe} - \beta\ /\ TDF_{Glu\text{-}Phe}\ ], \quad (1)$$

and 2) a proposed mollusk-specific formulation ($TL_{CSIA\text{-}mollusk}$), which includes a term for shell fractionation and uses empirically estimated trophic discrimination factor (TDF) values specific for mollusks:

$$TL_{CSIA\text{-}mollusk} = 1 + [\ (\delta^{15}N_{Glu} - \delta^{15}N_{Phe} - \beta)\ /\ (TDF_{Glu\text{-}Phe} - \varepsilon_{shell})\ ], \quad (2)$$

where $\delta^{15}N_{Glu}$ and $\delta^{15}N_{Phe}$ represent the stable nitrogen isotope values of bivalve Glu and Phe, respectively, β is a constant which represents the assumed difference in $\delta^{15}N$ between Glu and Phe of primary producers (3.4 ‰ for aquatic cyanobacteria and algae; McClelland and Montoya 2002; Chikaraishi et al. 2009), $TDF_{Glu\text{-}Phe}$ is defined as $\Delta^{15}N_{Glu} - \Delta^{15}N_{Phe}$, but reflects an assumed average change in ^{15}N of Glu and of Phe based on our

measured data corresponding to a single trophic transfer for filter-feeding molluscs (see section 3.5). The "classic" CSIA $TDF_{Glu\text{-}Phe}$ is 7.6 ‰ (Chikaraishi et al., 2009), while our newly proposed mollusk-specific $TDF_{Glu\text{-}Phe}$ is 3.4 ‰ ($TL_{CSIA\text{-}mollusk}$; this study). Finally, ε_{shell} is the new term proposed for the mollusk specific equation 2, representing the observed additional average fractionation in Glu (1.6 ‰) between tissue and shell, presumably due to isotopic routing to the shell protein biomineral fraction.

Baseline isotope values were estimated from common CSI-AA parameters. For $\delta^{15}N_{baseline}$ based on past work in mollusks (Vokhshoori & McCarthy 2014) we used the non-fractionating source AA Phenylalanine.

$$\delta^{15}N_{Baseline} = \delta^{15}N_{Phe}, \quad (3)$$

where $\delta^{15}N_{Phe}$ is the isotope value of Phenylalanine in a mollusk or seawater particulate organic matter.

For $\delta^{13}C_{baseline}$ we used the equation from Shen et al. (2021) for exported production in the nearshore California Current:

$$\delta^{13}C_{Baseline} = 0.75 \times \delta^{13}C_{EAA} - 5.9 \quad (4)$$

where $\delta^{13}C_{EAA}$ is the mol% adjusted measured average $\delta^{13}C$ of all EAAs (Ile, Leu, Lys, Phe, Thr and Val), 0.75 is the slope of a line between measured $\delta^{13}C_{bulk}$ and $\delta^{13}C_{EAA}$ values of suspended POM from the Monterey Bay and 5.9 is the associated y-intercept (Shen et al. 2021).

For statistical analyses, t-tests, ANOVAs and mixing models were performed in R (v.3.3.1) with RStudio interface (v.0.98.1028). Normality (Q-Q plots) and homoscedasticity (Bartlett's test) of the data were verified before statistical analyses. From bulk isotopes, we calculated total area (TA) and standard ellipse areas (SEA; n >10) for each site population using the stable isotope Bayesian ellipses in R package (SIBER; Jackson et al., 2011), and with normalized EAA $\delta^{13}C$ values we used the Bayesian mixing model stable isotope analysis in R package (MixSIAR; Stock & Semmens, 2016) to estimate resource contribution to bivalve diet using a "training set" of potential endmember sources from Larsen et al. 2009, 2013 and

Tipple et al. *submitted* (data repository). Endmembers sources we used for our mixing models were specific to each sampling location and are based the dominant primary producers in each ecosystem. For a complex system such as an estuary, there are many primary producer sources, therefore we combined primary producer groups based on broad phylogenetic associations, e.g. aquatic and terrestrial plants are in one group called 'plants' and micro- and macro- algae and in one group called 'algae'.

2.3 Results

2.3.1 Bulk isotope values and niche widths between species

M. californianus muscle tissue $\delta^{13}C$ values (-15.6 ± 0.3‰, n=54) were significantly different from estuarine species; *M. edulis* (-22.0 ± 0.9‰, n=15) and *O. lurida* (-23.2 ± 0.6‰, n=37) tissues (Tukey HSD t-test $P < 0.001$) (Table 2.1). Similarly, *M. californianus* muscle tissue $\delta^{15}N$ values (11.0 ± 0.4‰) were significantly different from estuarine species (*M. edulis*, 12.3 ± 1.0‰ and *O. lurida*, 12.7 ± 1.1‰) ($P < 0.001$). $\delta^{15}N$ values of the two estuarine species were not significantly different ($P = 0.14$), while *O. lurida* $\delta^{13}C$ values were ~1‰ more negative than *M. edulis* ($P < 0.0001$).

Isotope values of bulk shell matrix protein displayed similar patterns to those of the muscle tissues. *M. californianus* tissue $\delta^{13}C$ values (-14.5 ± 0.3‰, n = 22) were less negative and significantly different from both *M. edulis* (-20.0 ± 0.8‰, n = 15) and *O. lurida* (-21.3 ± 1.6‰, n = 15) (Tukey HSD t-test $P < 0.001$) (Table 2.1). Similarly, *M. californianus* shell $\delta^{15}N$ values (12.1 ± 0.3‰) were less positive and significantly different from both estuarine species (*M. edulis*, 12.9 ± 0.9‰ and *O. lurida*, 13.4 ± 1.1‰) ($P < 0.001$). $\delta^{15}N$ values of the two estuarine species were not significantly different ($P = 0.19$), while *O. lurida* $\delta^{13}C$ values were ~1‰ more negative than *M. edulis* ($P = 0.004$).

Table 2. 1 Mean bulk $\delta^{13}C$ and $\delta^{15}N$ values (‰) and standard deviation from muscle and shell organic matter by season and each bivalve species overall mean for littoral *M. californianus*, estuarine *O. Lurida* and estuarine *M. edulis*. Different superscript letters denote significant difference (ANOVA, $P<0.05$).

Littoral Mussel (*Mytilus californianus*)								
Season	$\delta^{13}C_{muscle}$	SD	$\delta^{13}C_{Shell}$	SD	$\delta^{15}N_{muscle}$	SD	$\delta^{15}N_{Shell}$	SD
spring	-15.57^{a}	0.29	-14.53^{a}	0.34	11.09^{a}	0.44	12.18^{a}	0.21
summer	-15.49^{a}	0.18	-14.76^{ab}	0.29	10.55^{b}	0.29	11.80^{a}	0.45
fall	-15.51^{a}	0.23	-14.19^{ac}	0.14	11.14^{a}	0.41	12.01^{a}	0.20
winter	-15.70^{a}	0.21	-14.46^{a}	0.29	11.14^{a}	0.28	12.20^{a}	0.32
Overall mean	-15.58	0.25	-14.48	0.32	11.01	0.42	12.10	0.34
Estuarine Oyster (*Ostrea lurida*)								
Season	$\delta^{13}C_{muscle}$	SD	$\delta^{13}C_{Shell}$	SD	$\delta^{15}N_{muscle}$	SD	$\delta^{15}N_{Shell}$	SD
spring	-23.60^{a}	0.46	-23.48^{a}	0.33	12.68^{a}	0.57	13.67^{ab*}	0.48
summer	-23.47^{a}	0.60	-21.19^{b}	0.39	11.06^{b}	0.30	12.22^{a}	1.07
fall	-23.04^{a}	0.52	-20.40^{b}	0.82	13.29^{a}	0.63	13.99^{b}	0.61
winter	-23.05^{a}	0.27	-20.46^{b}	0.52	13.00^{a}	0.74	14.15^{b}	0.17
Overall mean	-23.29	0.53	-21.25	1.35	12.46	1.07	13.44	1.11
Estuarine Mussel (*Mytilus edulis*)								
Season	$\delta^{13}C_{muscle}$	SD	$\delta^{13}C_{Shell}$	SD	$\delta^{15}N_{muscle}$	SD	$\delta^{15}N_{Shell}$	SD
spring	-20.17^{a}	0.04	-18.41^{a}	0.52	12.04^{a}	0.13	14.18^{ab}	0.49
summer	-22.80^{bd}	0.16	-20.34^{b}	0.44	11.32^{ab}	0.35	12.22^{ac}	0.48
fall	-22.74^{b}	0.46	-20.49^{b}	0.37	11.93^{a}	0.61	12.59^{a}	0.34
winter	-21.95^{bc}	0.30	-19.92^{b}	0.54	13.10^{ac}	0.98	13.38^{a}	0.98
Overall mean	-22.21	0.94	-20.01	0.80	12.05	0.92	12.89	0.90

Comparing shell to tissue, average shell stable isotope values were always more enriched in the heavy isotope (both $\delta^{13}C$ and $\delta^{15}N$) (Table 2.2). These isotopic offsets were significantly different in all cases (Tukey HSD t-test, $P < 0.01$). The average $\delta^{13}C$ offset in shell from tissue was 1.2‰ and ~2‰ in the littoral and estuarine ecosystem, respectively. The $\delta^{15}N$ shell and tissue offsets were on average 1‰ higher in shell OM for all species.

Table 2. 2 Mean bulk $\delta^{13}C$ and $\delta^{15}N$ offset (‰) between muscle tissue and shell organic matter in three bivalve species. Asterisk denotes degree of significant difference ($P > 0.05$, *$P < 0.05$, **$P < 0.01$, ***$P < 0.001$).

	n	shell - tissue mean offset	sd	min	max	range
$\delta^{13}C$						
Littoral Mussel	28	1.2***	0.4	0.2	1.8	1.6
Estuarine Mussel	18	2.1***	0.4	1.4	3.0	1.6
Estuarine Oyster	17	1.9***	1.2	0.9	3.3	4.3
$\delta^{15}N$						
Littoral Mussel	22	1.0***	0.4	0.0	1.7	1.6
Estuarine Mussel	18	0.9*	0.7	0.0	2.4	2.4
Estuarine Oyster	19	0.8**	0.8	0.5	3.1	3.5

Standard ellipse areas (SEA) represent the isotopic niche width (units: ‰^{2}) as reflected by bulk muscle or shell matrix protein $\delta^{13}C$ and $\delta^{15}N$ biplots for the three species of bivalves (Fig.2.2, Fig. S1). Among species, soft tissue *M. californianus* had the smallest niche width (0.32‰^{2}; $n = 54$) and total area (TA = 1.49‰^{2}). While soft tissue SEA of *M. edulis* (2.40‰^{2}; $n = 18$) was larger than *O. Lurida* (1.79‰^{2}; $n = 46$), the total area (TA) of isotope values for *O. Lurida* was larger (7.44‰^{2}) than *M. edulis* (5.03‰^{2}). Shell matrix protein SEA results were very

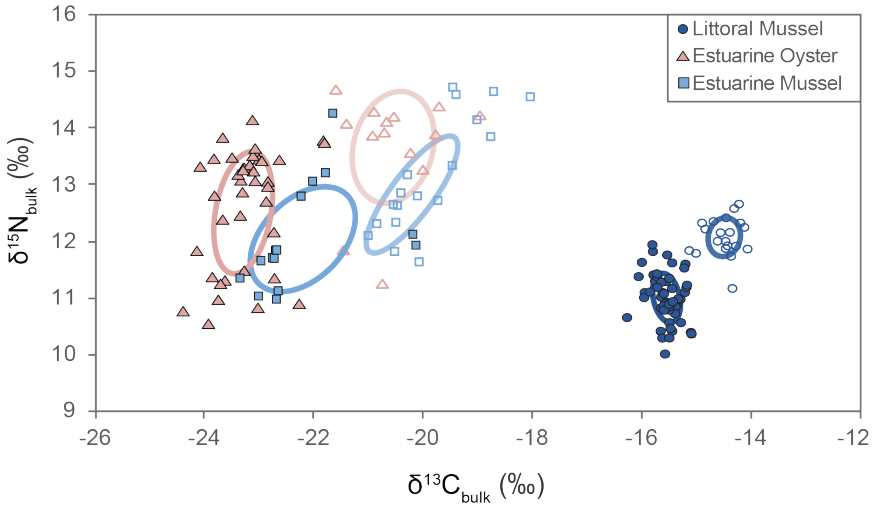

Figure 2. 2 Biplot of bivalve muscle tissue (filled symbols) and shell matrix protein (open symbols) bulk $\delta^{13}C$ and $\delta^{15}N$ values organized by species, littoral *M. californianus* (dark blue circle, $n = 54$), estuarine *O. Lurida* (pink triangle, $n = 37$) and estuarine *M. edulis* (light blue square, $n = 15$). The colored ellipses represent the standard ellipse areas (SEA) for each of the groups.

similar to soft tissue SEA, where *M. californianus* was 0.32‰^{2} (n = 22), *M. edulis* was 1.48‰^{2} (n = 15) and *O. Lurida* was 2.22‰^{2} (n = 15).

2.3.2 Bulk isotope values in particulate organic matter and offsets from bivalve tissue

Table 2.3 reports seawater particulate organic matter (POM) Nitex (>53μm) and GFF (<0.7μm) sample sizes, mean isotope values (±SD) and ranges (Table S1 additionally breaks out specific values by season). For both isotopes in both ecosystems, Nitex and GFF POM values were not statistically different (Tukey HSD t-test, P > 0.05), therefore data for both size fractions were combined, and reported as POM averages for each sampling period. At the littoral site, average seasonal $\delta^{13}C$ values of combined POM was -18.6 ± 1.7‰, ranging from -23.2 to -15.3‰; the corresponding average seasonal $\delta^{15}N$ value was 9.1 ± 2.2‰, ranging from 3.9 to 14.1‰. At the estuarine site, the average $\delta^{13}C$ value of combined POM was -22.4 ± 1.4‰, ranging from -23.7 to -19.7‰, and for $\delta^{15}N$ the average value was 9.9 ± 1.6‰, ranging from 7.7 to 12.7‰.

Table 2. 3 Seasonal to monthly ranges and average bulk $\delta^{13}C$ and $\delta^{15}N$ values (±1 SD) in two size fractions of seawater particulate organic matter: Nitex (>53μm) and GFF (0.7μm) from two coastal environments, Littoral (Santa Cruz, CA) and Estuary (Northern San Francisco Bay).

Littoral POM	n	max	min	range	seasonal mean	sd
$\delta^{13}C$ (‰)						
GFF	9	-18.1	-20.1	2.0	-19.0	0.7
Nitex	10	-15.3	-23.2	8.0	-18.3	2.2
Combined	19	-15.3	-23.2	8.0	-18.6	1.7
$\delta^{15}N$ (‰)						
GFF	10	14.1	3.9	10.3	10.3	2.9
Nitex	10	13.1	7.6	5.5	9.4	1.4
Combined	20	14.1	3.9	10.3	9.1	2.2

Estuarine POM	n	max	min	range	seasonal mean	sd
$\delta^{13}C$ (‰)						
GFF	4	-21.4	-23.7	2.3	-22.2	1.1
Nitex	5	-19.7	-23.7	4.0	-22.1	1.7
Combined	9	-19.7	-23.7	4.0	-22.2	1.4
$\delta^{15}N$ (‰)						
GFF	3	10.7	7.7	2.9	9.0	1.5
Nitex	5	12.7	9.4	3.3	10.5	1.4
Combined	8	12.7	7.7	5.0	9.9	1.6

Bulk isotopic offsets between bivalve tissue and seawater POM showed different patterns at the estuarine vs. littoral sites (Table S2). At the littoral site, *M. californianus* $\delta^{13}C_{bulk}$ values in soft tissue were 3.4 ± 0.3‰ greater than POM, and $\delta^{15}N$ values were 2.0 ± 1.4‰

greater. The shell matrix offsets were about 1‰ higher in both isotopes. At the estuarine environment, offsets were more variable. Soft tissue *O. Lurida* $\delta^{13}C$ values were 1.1 ± 1.2‰ *less* than POM, while *M. edulis* $\delta^{13}C$ values were 0.3 ± 1.4‰ greater. For $\delta^{15}N$ values, *O. Lurida* was 3.4 ± 1.8‰ greater than POM and *M. edulis* was 3.0 ± 1.1‰ greater. Shell matrix protein $\delta^{13}C$ offsets were more consistent, ~ 2‰ higher than the muscle tissue for both bivalve species, while $\delta^{15}N$ offsets were 1‰ greater in shell than muscle tissue.

2.3.3 Seasonal differences in bulk isotope records

Seasonal $\delta^{13}C$ and $\delta^{15}N$ dynamics present in the muscle soft tissue were generally also reflected in the shell matrix protein (Fig. 2.3, Table 2.1). Littoral summer (Jul.) $\delta^{15}N$ values were significantly lower in the muscle tissue (ANOVA, $F_{3,50} = 1.89$, $P > 0.05$), and lowest also in the shell protein, although not significant ($F_{3,25} = 3.565$, $P < 0.03$). In contrast, *M. californianus* $\delta^{13}C$ values in muscle were not significantly different between seasons ($F_{3,50} = 1.89$, $P > 0.05$), however summer and fall were significantly different from each other ($F_{3,25} = 3.565$, $P < 0.03$).

The estuarine environment also displayed low summer (Jun.) $\delta^{15}N$ values in both species. *O. Lurida* $\delta^{15}N$ values were significantly lower for summer in both muscle tissue ($F_{3,35} = 31.46$, $P < 0.0001$) and shell ($F_{3,14} = 7.97$, $P < 0.01$). In *M. edulis* summer $\delta^{15}N$ values were also lowest, but not significantly different, in both muscle ($F_{3,14} = 1.53$, $P = 0.25$) and shell ($F_{3,14} = 1.59$, $P = 0.24$). Similar to the littoral ecosystem, *O. Lurida* $\delta^{13}C$ values in muscle were not statistically different between seasons ($F_{3,19} = 2.935$, $P > 0.05$). Shell $\delta^{13}C$ values also generally showed no statistical differences, with the exception that spring $\delta^{13}C$ in shell was significantly more negative than the other seasons ($F_{3,10} = 20.34$, $P < 0.0001$). It should be noted however, that as discussed in the methods section, the estuarine site sampled for the spring season was at a slightly different location in Northern SF Bay, and this might contribute to some of the differences observed in Spring. For the *M. edulis*, muscle tissue $\delta^{13}C$ values were significantly different between seasons ($F_{3,11} = 41.71$, $P < 0.0001$), and in shell Spring was significantly

different from the rest of the seasons ($F_{3,11}$ = 10.47, P < 0.001) but also the sample size was much smaller (n = 3 to 5 per season versus 5 to 10) and could explain the higher variability in this group.

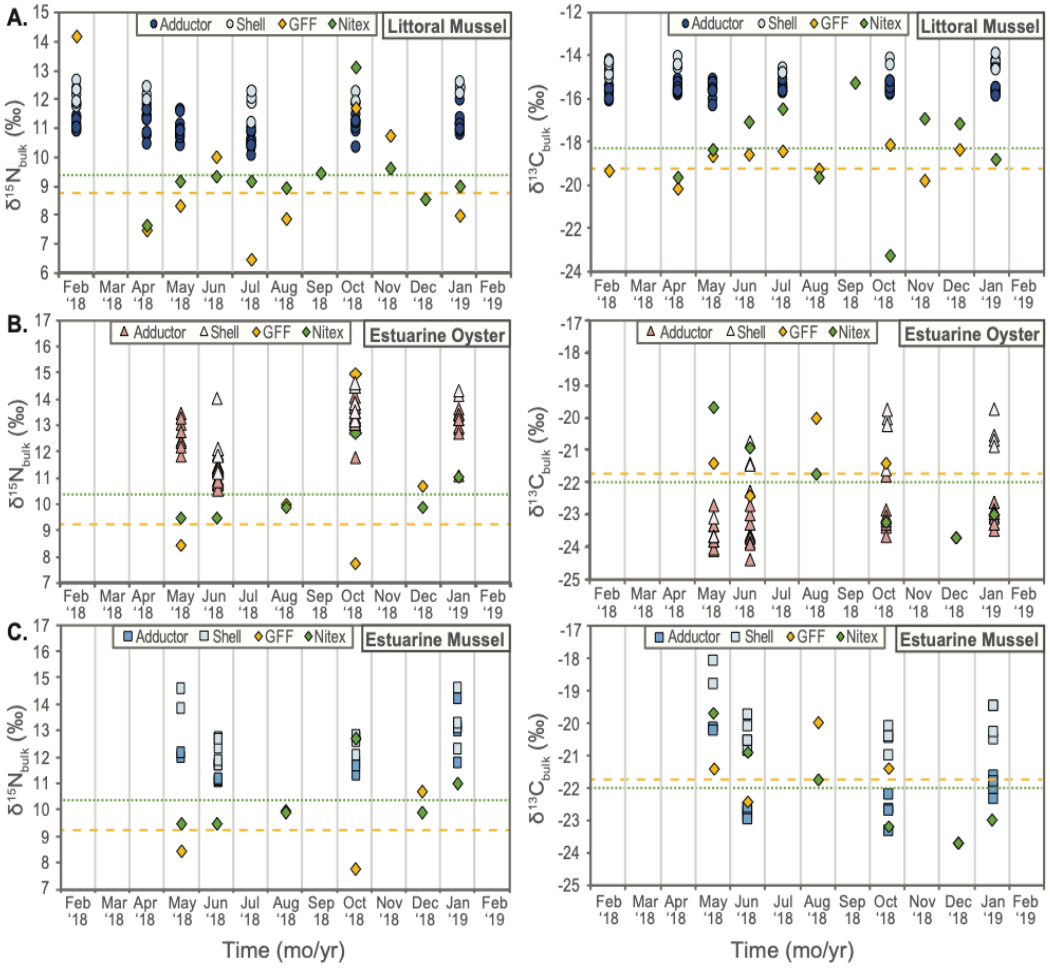

Figure 2. 3 Bulk $\delta^{13}C$ and $\delta^{15}N$ values of bivalve and seawater particulate organic matter organized by month of sampling. Bivalve muscle adductor tissue (dark shading) and shell matrix protein (light shading) for three bivalve species in this study: (A) littoral *M. californianus*, (B) estuarine *O. Lurida* and (C) estuarine *M. edulis*. Plotted with bivalve tissue isotope values are two size fractions of seawater POM: GFF (>0.7 µm, yellow diamond) and Nitex (>53 µm, green diamond). Mean of the two POM size fractions are shown for reference indicated by the colored dotted and hashed line (GFF, yellow dashed; Nitex, green dotted).

2.3.4 Amino acid molar abundance

Amino acid relative molar distributions (Mol%$_{AA}$) displayed major differences between tissue types (Fig. 2.4, Fig. S2), however as would be expected Mol%$_{AA}$ was similar within each

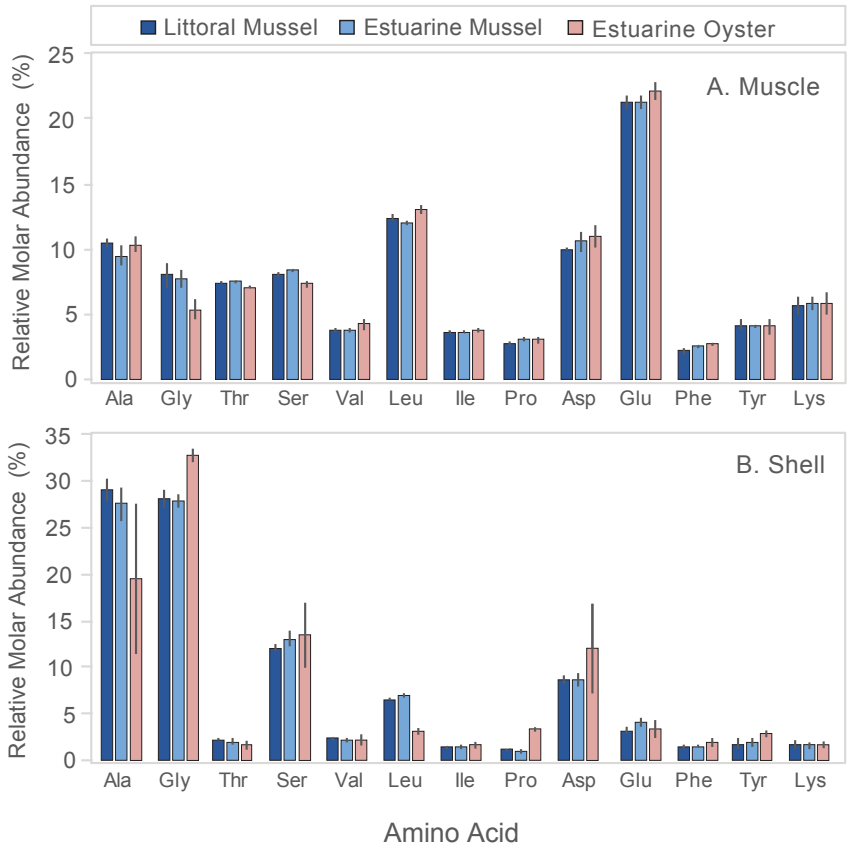

Figure 2. 4 Relative molar abundance of 12 amino acids measured in littoral *M. californianus* (dark blue), estuarine *M. edulis* (light blue) and estuarine *O. Lurida* (light pink) in (A) soft muscle tissue and (B) shell matrix protein. Error bars indicate ±1 SD

tissue. Soft muscle tissue overall Mol%$_{AA}$ was not significantly different between species: Glutamic acid was the most abundant (20%) followed by Leucine (15%) then Alanine and Aspartic acid (10%), with relatively minor (<5%) contributions by most other AA. However, there were nevertheless significant differences between *O. Lurida* and the two mussel species, *M. californianus* and *M. edulis*, most notably: Gly ($F_{2,9}$ = 12.51, P < 0.01), Ser ($F_{2,9}$ = 32.17, P < 0.0001), and Leu ($F_{2,9}$ = 17.32, P < 0.001). By contrast, in shell protein, Mol%$_{AA}$ distributions were distinct from muscle tissue. Glycine and Alanine were the most abundant (20-30 Mol%), followed by Serine (12-13%) and Aspartic Acid (8.5-10%), with again only small contributions by all other AA. Again, the *O. Lurida* Mol%$_{AA}$ in shell was significantly different from the two

mussel species for Gly ($F_{2,9}$ = 16.77, P < 0.001), Leu ($F_{2,9}$ = 61.39, P < 0.0001), and Pro ($F_{2,9}$ = 192.4, P < 0.0001).

2.3.5 Amino acid carbon and nitrogen isotope values, patterns, and tissue offsets

Measured amino acid $\delta^{13}C$ showed a remarkably similar patterns between species in both muscle tissue and shell protein (Fig. 2.4). Across all three species, $\delta^{13}C_{EAA}$ were very similar between shell and muscle tissue, with differences typically in the range of analytical error (<1‰; Fig. 2.5a). We note that littoral spring season data was not included in offset

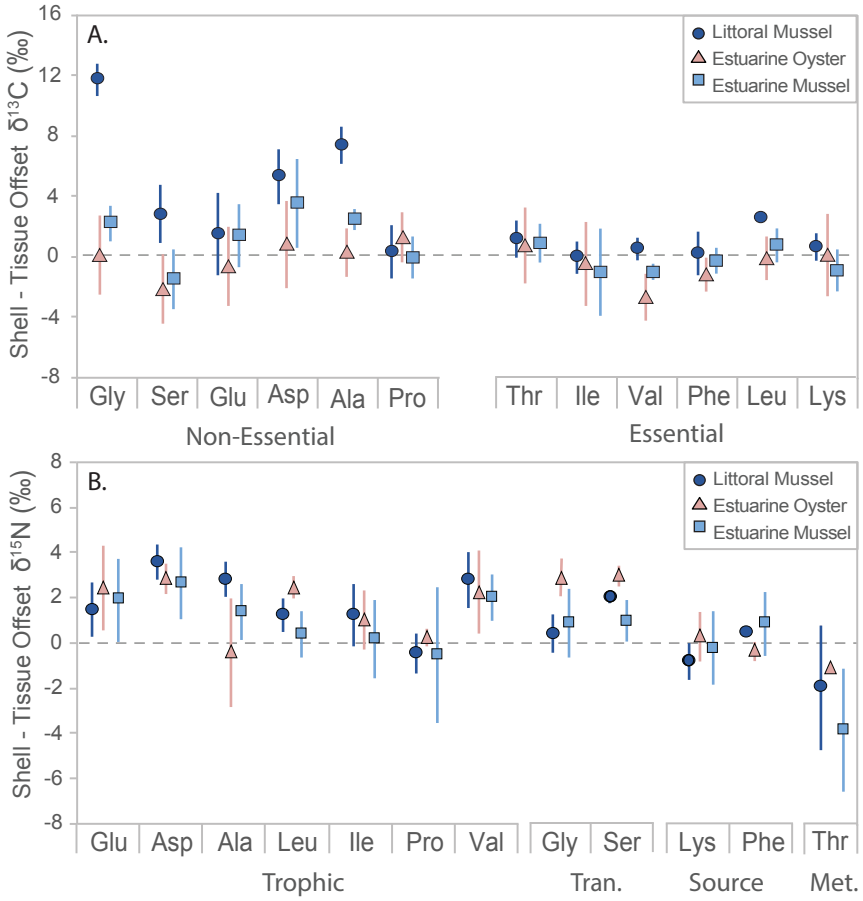

Figure 2. 5 Mean isotopic offset between shell and soft muscle tissue amino acid (A) $\delta^{13}C$ grouped by 'Essential' and 'Non-essential' amino acids, and (B) $\delta^{15}N$ grouped by 'Trophic', 'Transitional', 'Source' and 'Metabolic' amino acids, for three bivalve species, littoral *M. californianus* (dark blue circles), estuarine *O. Lurida* (pink triangle) and estuarine *M. edulis* (light blue square). Error bars indicate ±1 SD.

calculations because of the apparently anomalous values measured in the soft tissue for that season only (Fig. S3). The average $\delta^{13}C_{EAA}$ offset (shell – muscle tissue) was 0.4‰ in *M. californianus*, -0.6‰ in *O. Lurida* and -0.3‰ in *M. edulis*. In contrast, the offsets in the $\delta^{13}C_{NEAA}$ were larger and also showed much more variability, particularly in *M. californianus*.

The measured amino acid $\delta^{15}N$ value comparisons between species and tissue types showed the expected overall CSI-AA pattern, with Trophic AAs more enriched than the Transitional and Source AAs. However, there were also a few notable differences. In *O. Lurida* $\delta^{15}N_{Ile}$ and $\delta^{15}N_{Leu}$ values were consistently lower by ~4‰ relative to all other Trophic AAs in both tissue types, an offset which was not observed in two mussel species. Average offsets in $\delta^{15}N$ values (shell – soft tissue), excluding Thr, were between 3 and -1‰ (Fig. 2.5b). For specific AA groupings, the average $\delta^{15}N_{Tr\text{-}AA}$ offset was similar between species: 1.8‰ in *M. californianus*, 1.5‰ in *O. Lurida* and 1.1‰ in *M. edulis*. Specifically $\delta^{15}N_{Glu}$ (the canonical trophic-AA used in the TL_{CSIA} equation), the average offset among all species was 1.9 ± 1.6‰ (range -0.4 to 4.1‰). The two transitional AAs, Gly and Ser behaved differently between the bivalve genus; *O. Lurida* $\delta^{15}N$ offsets were 3‰ in shell, but 2‰ lower in *M. californianus* and *M. edulis*. Conversely, the average offset between tissue types in $\delta^{15}N_{Phe}$, the canonical source-AA used in the TL_{CSIA} equation and the proxy for $\delta^{15}N_{Baseline}$ value, was small 0.4±0.9‰ (range -0.9 to 1.5‰).

2.3.5 CSI-AA ecological proxies

Four CSI-AA ecological proxies were calculated and compared between tissue types: $\delta^{13}C_{baseline}$, $\delta^{15}N_{baseline}$ (Fig. 2.6), food resource contribution from Bayesian modeling output (Fig. 2.7), and trophic level (Fig. 2.8). Average $\delta^{13}C_{baseline}$ was essentially identical (less than 1‰ difference) between tissue types in all species. $\delta^{13}C_{baseline}$ values in muscle tissue and shell matrix protein in *M. californianus* was -19.1 ± 1.5‰ versus -20.7 ± 0.4‰, respectively; *M. edulis* was -24.8 ± 0.9‰ versus -25.7 ± 2.1‰, respectively; and *O. lurida* was -25.8 ± 1.1‰

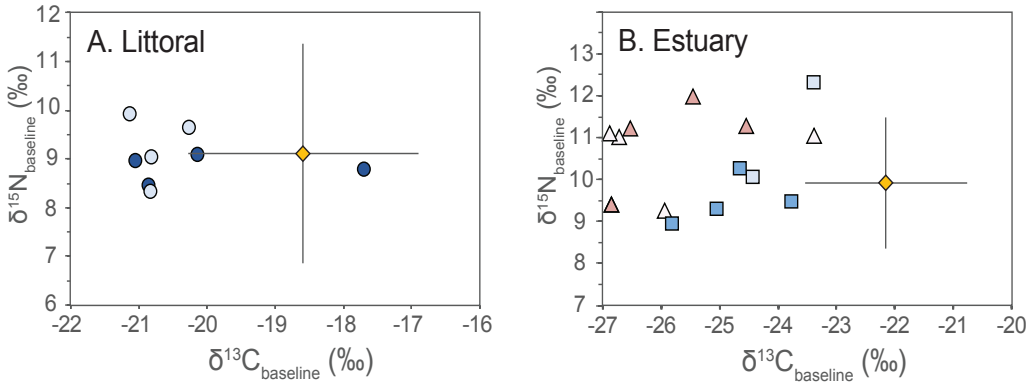

Figure 2. 6 Baseline production values estimated from mol% adjusted $\delta^{13}C$ essential amino acids and $\delta^{15}N$ phenylalanine values for (A) Littoral *M. californianus* (circles) and (B) Estuarine *O. Lurida* (triangles) and *M. edulis* (square) in muscle soft tissue (dark shade) and shell matrix protein (light shade). Yellow diamonds indicate mean bulk $\delta^{13}C$ and $\delta^{15}N$ and standard error bars for each ecosystem's seawater POM (Nitex and GFF combined). See methods for baseline isotope values calculations.

versus -25.7 ± 1.6‰, respectively. Similarly, $\delta^{15}N_{baseline}$ (defined here as the source AA $\delta^{15}N_{Phe}$; see methods) also showed little to no offset between muscle tissue and shell matrix protein across all species: *M. californianus* was 8.8 ± 0.7‰ versus 9.2 ± 0.3‰, respectively; *M. edulis* was 9.5 ± 0.6‰ versus 10.3 ± 1.4‰, respectively; and *O. lurida* was 11.0 ± 1.1‰ versus 10.6±0.9‰, respectively.

Resource contribution based on $\delta^{13}C_{EAA}$ using the Bayesian mixing model MixSIAR (Fig. 2.7) were also very similar between shell and muscle tissue in all bivalves. Model output indicated that the *M. californianus* diet was ~80% microalgae in both tissues followed by smaller amounts of macroalgae (10-15%) and bacteria (10-15%). Model estimates indicated similar relative resource proportions in *M. edulis* and *O. lurida* with 55-60% of algae (micro- and macro- combined), followed by ~20% bacteria and ~20-25% plants (terrestrial and aquatic combined).

Trophic level (TL) estimations (Fig. 2.8) using Equation 1 ranged from 1.3 to 1.5 in muscle tissue, and 1.5 to 1.9 in shell. However, using our newly proposed mollusk-specific (Methods, Eq. 2) TDF (3.4‰) combined with a fractionation factor based observed CSI-AA

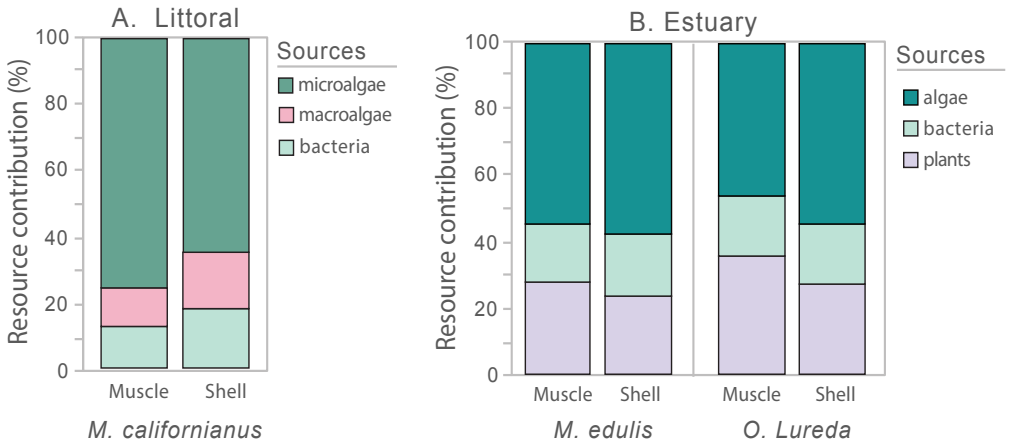

Figure 2. 7 Relative resource contribution of bivalve diet matches in soft tissue and shell. Estimations calculated using the Bayesian mixing model MixSIAR and is based on bivalve essential amino acid $\delta^{13}C$ values ($\delta^{13}C_{Val}$, $\delta^{13}C_{Leu}$, $\delta^{13}C_{Ile}$, $\delta^{13}C_{Thr}$, $\delta^{13}C_{Phe}$ and $\delta^{13}C_{Lys}$; median ± 95% credible intervals) and of 3 sources to the littoral environment (microalgae, macroalgae, bacteria; data from Larsen et al. 2013) and 3 sources to the estuarine environment (algae, bacteria and plants; data from Larsen et al. (2013) and Tipple et al. submitted). Note, these results are based on pre-determined input sources. The mixing model performs better with few sources, therefore, for the estuarine system, micro- and macro-algae were combined to represent algae, and aquatic- and terrestrial-plants were combined to represent plants (see data repository for training set).

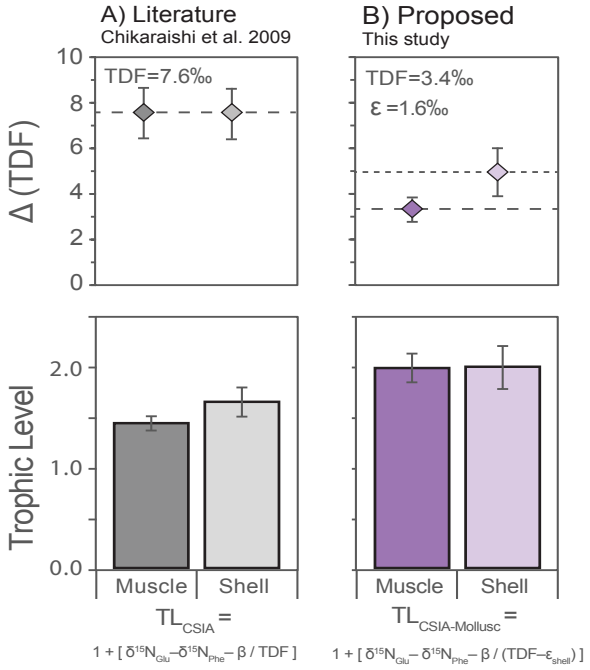

Figure 2. 8 Trophic level estimates calculated from the three bivalve species in this study based on amino acid $\delta^{15}N$ data from the equation proposed by Chikaraishi et al. (2009), where A) used the canonical trophic discrimination factor (TDF) Δ value = 7.6‰ in bivalve muscle (dark grey) and shell (light grey) and B) uses the newly proposed TDF value based on consistent TDFs measured in muscle (3.4‰; dark purple), and the additional hypothesized effect of 1.6‰ from isotopic routing to shell (light purple). Error bars are ± 1 standard deviation.

data offsets between soft tissue and shell (ε = 1.6‰), returned a very narrow range of TL values (TL = 2.0 ± 0.2) across both tissue types for all three species in both environments.

2.4 Discussion

2.4.1 Tissue offsets in bulk isotopes and AA composition

Shell matrix protein versus muscle tissue offsets were remarkably consistent in the bulk isotope record. As noted above, littoral and estuarine $\delta^{13}C_{bulk}$ values were about 1‰ and 2‰ greater in shell, respectively, and $\delta^{15}N_{bulk}$ values about 1‰ greater in both ecosystems (Table 2.2). These offsets were consistent irrespective of season (Table 2.3), suggesting they are a function of biochemical composition between the tissue types, and not shifts in diet. Bulk isotope enrichment in the biomineral fraction has previously been detected in mussel (Verteegh et al. 2011) and oyster (Ellis et al. 2014) shell. However, other studies investigating organics in bivalve shell, mostly clam species, have shown either the *opposite* or no difference in bulk isotope offsets (O'Donnell et al. 2003, Watanabe et al. 2009, Whitney et al. 2019, Graniero et al. 2021). Therefore, while data are consistent within this study, $\delta^{13}C_{bulk}$ offsets could be species or genera specific. It is possible that such differences are related to shell mineralogy (calcite vs. aragonite) or shell microstructure (nacreous, prismatic or homogenous), and/or to the specific composition of structural proteins and other organics in shell.

Molar abundance data between shell and muscle tissue (Fig. 2.4) revealed distinct compositions. We found shell matrix protein was similar to that reported in many structural proteins (Hare et al 1991, McMahon et al. 2018). In contrast the more equal abundances between AAs in muscle adductor is also fairly typical of muscle tissue with the notable exception of the very large Glu contribution (McMahon et al. 2010, McMahon et al. 2015, Whitney et al. 2019).

In contrast, the significant variations observed in several AAs in shell mol% distributions between the genera is likely related to the unique compositions typical of structural

proteins, as well as differences in overall shell matrix. It is well known that the organic matrix composition varies based on shell mineralogy and microstructure (Marin & Luquet 2004, Kobayashi & Samata 2006). Mollusks can mineralize calcium carbonate as calcite (the more stable form), as well as aragonite (less stable form). While oysters primarily build their shells as prismatic and foliated calcite, mussels mineralize two discrete layers of calcite and aragonite, an outer prismatic calcite layer and inner nacreous aragonite layer. These differences in shell mineralogy are also associated with species-specific proteins, as reflected in the different AA molar abundances (Agbaje et al. 2018). Ala and Gly are the most abundant AAs in nacreous aragonite and Gly the most abundant AA in prismatic calcite (Kobayashi & Samata 2006), which is consistent with our findings in mussel and oyster shells. Overall, the more variable and highly specific AA composition of shell, compared to the generally similar composition of soft tissues may in part account for differences in bulk stable isotope offsets noted above. These observations also suggest that mol% weighted AA isotope proxies (e.g. THAA and $\delta^{13}C_{\text{baseline}}$, discussed below) may give more representative values when comparing between tissue types or across different species.

2.4.2 Seasonal Observations

Seasonal biogeochemical cycles along central coastal California are primarily marked by a strong upwelling season in the Spring (Hickey et al. 1998). Annual to decadal oscillations such ENSO and PDO, however, can affect the degree or intensity of all these seasonal events (Pennington & Chavez 2017). Such dynamics raise the question if seasonal or ENSO related perturbations may be recorded and discernible in mollusk shell, or in soft tissue sampled at higher frequency. It's important to understand possible seasonal variation recorded in shell for paleo reconstructions because it suggests isotopic signals are primarily recording a single season versus an average integration over a year or several years.

Our $\delta^{13}C$ and $\delta^{15}N$ POM records did not show seasonal variations, however this is likely a function of low sampling frequency coupled with the inherent lack of integration in a time-point POM sample. We collected seawater monthly at the littoral site and seasonally at the estuarine site; phytoplankton bloom events would not be captured by infrequent time-point sampling. To capture seasonal phytoplankton trends, we suggest POM sampling weekly or biweekly.

In contrast, while bivalves integrate on timescales of months to years (Gorokhova & Hansson 1999), clear seasonality was nevertheless detected in bivalve tissues. Both $\delta^{15}N_{bulk}$ and $\delta^{15}N_{baseline}$ (i.e. $\delta^{15}N_{Phe}$) were lowest in summer for both ecosystems in both muscle tissue and shell. Along the coast, low summer $\delta^{15}N$ values are likely a function of incomplete utilization of the nitrate pool, typical of strong upwelling periods. However, it was somewhat surprising that both tissue types recorded the same seasonal signal in $\delta^{15}N$, since muscle tissue turnover rates in bivalves are near annual (e.g., Hawkins 1985), while whole shell represents the lifetime of the individual. In this study, as noted above, bivalves were collected between 55-60cm, which correlates to 1 to 2 years old (Coe & Fox 1942, Harger 1970b). The small sizes likely are why we observed a summer seasonal signal in shell, consistent also with the expectation that bivalves do not grow at a constant rate year-round, but rather growth rate is coupled to phytoplankton abundance. For example, Hawkin and Bayne (1985) showed that N utilization rates and protein assimilation rates vary seasonally in *Mytilus edulis*, highest in spring/early summer (Bayne et al. 1988, Kreeger et al. 1995).

Bivalve tissue $\delta^{13}C$ values, on the other hand, did not show a clear pattern between seasons at either environment (Fig. 2.3, Table 2.3). Along the CA margin, $\delta^{13}C$ signatures in mussels are a function of relative local plankton productivity with latitude (Vokhshoori et al. 2014). Seasonality has previously been documented in $\delta^{13}C$ of *Potamocorbula amurensis* in the SF Bay. Here, winter and early spring $\delta^{13}C$ were depleted in ^{13}C (-25 to -22‰), indicative of non-diatom food source likely linked to freshwater flow (Cloern 1996). However, that study of *P. amurensis* was in the southern SF Bay, a marine lagoon and fundamentally different

than the northern SF Bay (an estuary). Southern SF Bay is driven more by tidal pumping, whereas the northern SF Bay is influenced by delta inflow (Cloern 2019). Moreover, it has been shown that protein-N is more efficiently assimilated than protein-C (Kreeger et al. 1995), which could be an additional factor in the apparent greater sensitivity of the $\delta^{15}N$ record to seasonality. Overall, our data show that seasonality in $\delta^{15}N$ values can be detected in shell protein, largely driven by the productive summer upwelling season however this was not observed in the $\delta^{13}C$ record, suggesting, at least in our dataset, that $\delta^{13}C_{bulk}$ are impacted by seasonal variation of dominant phytoplankton groups (diatom vs. dinoflagellate) typical along the CA coast.

2.4.3 Bulk and CSI-AA Ecological Isotope Proxies between tissue types

We tested several common isotope-based ecological proxies in both soft tissue and shell protein were for possible offsets in shell signatures relative to soft tissue, and to evaluate if consistent corrections could be applied to shell matrix samples for paleoecological reconstructions. These include niche width from bulk isotopes, and from CSI-AA baseline $\delta^{13}C$, baseline $\delta^{15}N$, modeled primary producer resource contribution, and trophic level.

2.4.3.1 Niche width bulk isotope ecological proxy

Isotopic niche width (or niche breadth) is a means to investigate the intra- and inter-individual variation of organism ecological characteristics (Newsome et al. 2007). This is a widely used measure typically based on $\delta^{13}C_{bulk}$ and $\delta^{15}N_{bulk}$ data, and is informative for understanding community composition and structure, as well as resource use (Bearhop et al. 2004). *M. californianus* had a very narrow ecological niche width, in contrast to *M. edulis* and *O. Lurida*, whose niche widths were much broader (Fig. 2.2). Between tissue types, standard ellipse area and total area were identical for all three species, indicating that community structure and resource use is consistent within the isotope turnover times of soft tissue and shell. As noted in the previous section, Monterey Bay littoral production is dominated by two microalgal groups (e.g. diatoms and dinoflagellates; Fischer et al. 2020), as also reflected in

littoral mussel $\delta^{13}C_{EAA}$ data (Vokhshoori et al. 2014). However, mussels can additionally feed on bacteria and organic debris (Coe & Fox 1942). While it is therefore possible for littoral mussels to feed on a broad range of suspended particulate organic sources, the narrow niche width observed suggests that at a community level food resources are either consistently well-mixed or dominated by a few primary producer types.

In contrast, the estuarine ecosystem niche widths were very broad for $\delta^{15}N$ and $\delta^{13}C$ in both *O. Lurida* and *M. edulis*, and also had different niches in carbon space (Fig. 2.2). In SF Bay, and delta/estuarine systems in general, it is more difficult to trace the origins of organic matter sources with bulk isotopes, because the diversity in primary production sources is much greater, including terrestrial riparian, freshwater phytoplankton, salt marsh and marine phytoplankton. Further, for many of these sources there is substantial isotope variability within each source group, such that bulk isotope values are often broad and overlapping (Cloern et al. 2002).

There are therefore two possible hypotheses that can explain the offset in $\delta^{13}C$ niche space between *O. lurida* and *M. edulis* in the estuary. First, the offset could be a difference in diet between the two bivalve species. Indeed, *O. lurida* and *M. edulis* do occupy different tidal depths; *O. lurida* are low tide to subtidal dwellers (-10 to 1m; Baker et al. 2005) whereas *M. edulis* occupy the mid-tide zone (2.9 to 3.2 m; Suchanek 1978). The lower $\delta^{13}C$ values in *O. lurida* could therefore be from a higher proportion of resuspended sediment containing degraded terrestrially derived organic matter resources (Peterson et al. 1985, Peterson & Fry 1987). A second possibility could be characteristic organic composition differences between the species, for example, the percent glycogen stores in the muscle adductor tissue. In contrast to most other animals who store energy as lipid, mollusks store it in glycogen, such that $\delta^{13}C_{bulk}$ values reflect differences in relative glycogen content (Patterson & Carmichael 2016). A higher glycogen content in oysters would be consistent with higher C:N ratios observed in oyster soft tissue w (3.5) vs. *M. edulis* (3.1) (data repository).

Overall, such differences in isotopic niche width between the bivalve species is important to consider when choosing a bioarchive species for historical reconstructions. Depending on the types of environmental perturbation (e.g. drought, damming or eutrophication), one would expect a species with a narrow niche width to be more impacted, and therefore potentially a more sensitive proxy for past change. However, most important finding for main goals of this study was that niche widths preserved in isotopes of shell matrix protein were indistinguishable from those in muscle soft tissue in all three species. This suggests that representative niche width can be derived from well preserved shell for historical and archaeological studies.

2.4.3.2 CSI-AA Baseline $\delta^{13}C$ and $\delta^{15}N$ values

Because baseline isotope reconstruction is one of the main goals in palaeoecological and palaeoclimatological studies, we tested first whether compound-specific isotope baseline signals in soft tissue are faithfully transferred into shell, and further examined whether $\delta^{15}N_{baseline}$ and $\delta^{13}C_{baseline}$ from POM matched those integrated into both tissue types (Fig. 2.6). $\delta^{15}N_{baseline}$ and $\delta^{13}C_{baseline}$ from CSI-AA are integrated isotope proxies for inorganic nitrogen source (typically $\delta^{15}N_{NO3}$) and for $\delta^{13}C$ of primary production, respectively.

The observation that $\delta^{13}C_{baseline}$ and $\delta^{15}N_{baseline}$ from CSI-AA of shell protein overlapped with soft tissue values in both ecosystems indicates that EAAs are in fact transferred from adductor muscle to shell protein unchanged. Therefore, we conclude that no calibration or correction is required for CSI-AA baseline isotope signals in the biomineral fraction. These findings validate the use of shell samples as bioarchives which can accurately record information of past changes in sources and cycling of nitrogen to coastal ecosystems, as long as the shell matrix protein is well-preserved. Moreover, the isotopic offset in $\delta^{13}C_{bulk}$ niche space between *O. Lurida* and *M. edulis* is not reflected in $\delta^{13}C_{Baseline}$ records, as might be expected. While this study cannot pinpoint the exact biological mechanism, the fact that the

$\delta^{13}C_{EAA}$ match closely between the two estuarine bivalve species might suggest that observed differences in $\delta^{13}C_{bulk}$ might be a function of resynthesis of the non-essential amino acids.

Finally, in order to directly ground-truth baseline isotope signals incorporated into bivalves from their presumed sources, we also compared monthly seawater POM bulk isotopic composition with bivalve baseline isotope values in both soft tissue and shell matrix protein (Fig. 2.6). We hypothesized that our $\delta^{13}C_{baseline}$ and $\delta^{15}N_{baseline}$ in bivalve tissue would directly match sampled values of local seawater POM at each site, seasonally in soft tissue, and on an integrated timescale for shell. While similarity in $\delta^{15}N_{baseline}$ values observed between POM and both tissue types support this hypothesis for both environments, the persistent mismatch observed in $\delta^{13}C_{baseline}$ values suggest important selective sorting of food particles. Such sorting is well known in filter-feeders and could be linked to particular particle diameter (Defossez & Hawkins 1997), to higher organic content (Newell & Jordan 1983, Prins et al. 1991) or to chemical deterrence produced by the primary producer to avoid predation (Levinton et al. 2002). The specific observed $\delta^{13}C$ offsets from POM (Fig. 2.6) therefore is likely linked to the specific mixture of primary producer sources of our POM samples in each system, coupled to their relative food value.

In the littoral ecosystem, suspended POM is predominantly a mixture of phytoplankton, macroalgae (kelp), bacteria and detrital material. $\delta^{13}C$ of kelp can vary widely along the central CA coast (-24 to -15‰; Foley & Koch 2010), as do phytoplankton (-28 to -12‰, Rau et al. 2001), however average $\delta^{13}C$ of kelp are consistently enriched in ^{13}C relative to phytoplankton (Duggins et al. 1989). In addition, seaweeds contain chemical compounds that deter filter-feeders (polyphenolics). Macrophytes like kelp, common in the intertidal environment, also have substantially elevated C:N ratios, which in addition to high phenolic content likely decreases food value relative to single-celled algae (Levinton et al. 2002). While bivalves are known to filter-feed and ingest aged kelp where polyphenolics concentrations are significantly reduced, if available, bivalves will preferentially select phytoplankton to ingest (Levinton et al. 2002.

In the estuarine ecosystem the much larger and far more variable mismatch between $\delta^{13}C_{baseline}$ and POM suggests a far wider variety of non-utilized ^{13}C-enriched sources. This is consistent with the much greater diversity of OM sources in the estuarine environment; however, it is also more difficult to pinpoint specific sources leading to this offset. Freshwater POM is more negative (-28±1.9‰) than estuarine-marine POM (-24±2.2‰) (Cloern et al. 2002), and since northern SF Bay is highly influenced by freshwater inflow from the Sacramento-San Joaquin River Delta system, bivalves in this complex system are likely dynamically receiving organic matter sources for both inputs. Bivalves will adjust the particle diameter they filter-feed with changes in tides as a function of optimal organic content (Dozey & Brown 1992). The wide range of $\delta^{13}C_{baseline}$ (5‰) and wide niche breadth (Fig. 2.2) in both estuarine bivalve species suggests that individuals utilize a combination of sources.

Finally, the specific CSI-AA $\delta^{13}C_{baseline}$ equation used will also have an impact on these results. Several $\delta^{13}C_{baseline}$ equations have been proposed from lab cultured phytoplankton (Vokhshoori et al. 2014), as well as for sinking (surface exported) POM in the Monterey Bay (Shen et al. 2021) (Fig. S7). The slope we derived from our $\delta^{13}C_{AA}$ POM data (Fig. S6) was very similar to that reported by Shen et al. (2021). For this reason, we use Shen et al. (2021) equation to reconstruct $\delta^{13}C$ baseline values. However, where Shen et al. (2021) did not adjust for mol% (Fig. S7), our $\delta^{13}C_{EAA}$ values were mol% adjusted since soft tissue and shell protein have such different AA abundance distribution (Fig. 2.4). Overall, because there is a persistent mismatch between recorded baseline $\delta^{13}C$ signals from bivalve tissues and sampled POM, as noted above likely due to bivalves selective sorting of particles with different source $\delta^{13}C$ values (Ward & Shumway 2004), it is not possible to determine which equation is more correct for this application.

2.4.4.3 CSI-AA Resource contribution

Resource contribution to bivalve diet was tested between soft tissue and shell matrix protein using a Bayesian mixing model, to determine if the biomineral fractions can be used to

reconstruct relative algal and other primary production sources with application for reconstructing primary producer community structure through time. This potential has been demonstrated in deep-sea corals (McMahon et al. 2015, 2018), mussel soft tissue from both the surface (Vokhshoori et al. 2014), and deep-sea chemosynthetic environments (Vokhshoori et al. 2021), however to our knowledge the approach has never been tested in any shell matrix. The analysis depends on a "training set" of representative primary producers for a given environment having diagnostic $\delta^{13}C_{EAA}$ signatures. Larsen et al. (2009, 2013) showed that biosynthesis EAA biosynthesis carries unique "fingerprints," and since animals cannot synthesize their own EAAs, $\delta^{13}C_{EAA}$ values pass from source to consumer without alteration.

For the littoral environment (using the Larsen et al. 2013 training set), our analysis predicted identical sources, within error, for both shell and soft tissue (Figure 7). This confirms that MixSIAR is consistent with expectations from EAA CSI-AA results above. The specific sources predicted (80% of *M. californianus* diet was microalgae, followed by about 10% each from macroalgae and bacteria) is also consistent with prior non-Bayesian resource partition results from *M. californianus* soft tissue (Vokhshoori et al. 2014).

In the estuarine environment, our endmember primary producer sources were algae, bacteria and plants (training sets compiled from Larsen et al. 2013 and Tipple et al. *submitted*). The MixSIAR again indicated identical results within error in shell and muscle tissue, further confirming the application of the validity of the $\delta^{13}C_{AA}$ approach for reconstructions using both oyster and mussel shell. The specific resource partitioning showed that *M. edulis* and *O. Lurida* to be feeding the same ratio of resources (Fig. 2.7; 60% algae, 20% bacteria and 25% plants). This result is consistent with the expectations based on $\delta^{13}C_{bulk}$ data discussed above, showing directly that bivalve diets between estuarine and littoral environments are very different. At the same time, this result highlights the potential of $\delta^{13}C_{AA}$ MixSIAR approach to bypass the limitations of $\delta^{13}C_{bulk}$ in systems with complex organic sources and indicate specific mixtures of primary production sources important in different systems.

4.3.4 Trophic Level CSI-AA ecological proxy

The final ecological proxy tested was trophic level, using first the "canonical" CSI-AA trophic level equation (TL_{CSIA}) proposed by Chikaraishi et al. (2009). Accurate quantification of trophic level values is key for reconstructing past ecosystems, as it can help shed light on trophic chain length of past food webs and associated nutrient abundance (Chavez et al. 2003), as well as the underpinnings of $\delta^{15}N_{bulk}$ values. For archives which are based on POM (e.g. sediments, deep-sea corals and filter-feeders) TL_{CSIA} is typically interpreted in terms of the relative trophic structure of the plankton community, which in turn relates to relative nutrient abundance as well as climate-driven community changes (Shen et al. 2021).

However, other structural tissues as shown in deep-sea gorgonian corals has demonstrated that tissue-specific calibrations are required, due to apparent isotope routing between soft tissue and structural protein (McMahon et al. 2018, Shen et al. 2021). Therefore, a main goal was to test if similar corrections are needed in bivalve shell. Moreover, past work with bivalves suggests that the canonical TL_{CSIA} equation (with standard TDF values) does not return reasonable trophic level values for mollusks (Vokhshoori & McCarthy, 2014, Choi et al. 2018, Ek et al. 2018). Therefore, we hypothesized that existing TDF values are not appropriate for mollusk soft tissue, and that additional corrections maybe be required to obtain accurate TL_{CSIA} from shell.

Our results strongly bear out both of these hypotheses (Fig. 2.8). First, our soft tissue results are consistent with those published previously (Vokhshoori & McCarthy 2014), showing that the common TDF of 7.6‰ (Chikaraishi et al. 2009) is far too high for filter-feeding mollusks. The 7.6‰ value represents the average isotope enrichment per trophic level (TDF) between $\delta^{15}N_{Glu}$ and $\delta^{15}N_{Phe}$, originally derived from controlled feeding studies of grazing zooplankton feeding on phytoplankton (McClelland & Montoya 2002), and later confirmed by a wider range of marine grazers and consumers (Chikaraishi et al. 2007). However, none of this original work included filter-feeders, and subsequent work has shown that TDF values in fact can be highly variable between different organisms, based on both diet and specific N metabolism pathways

(McMahon & McCarthy 2016). While knowing the TL of most consumers *a-priori* is often difficult, for filter-feeding mollusks it is simplified by their predominantly algal diet, and so can be assumed to be very close to TL = 2.

Based on this assumption we use our CSI-AA data to define an empirical TDF value for filter-feeding mollusks. Here, average $TDF_{glu\text{-}phe}$ ($\Delta^{15}N_{Glu} - \Delta^{15}N_{Phe}$) was 3.4‰, substantially below the canonical 7.6‰, and also below the revised average $TDF_{glu\text{-}phe}$ value recently proposed by McMahon and McCarthy (2016): 6.6‰. $TDF_{glu\text{-}phe}$ values have generally been found to be strongly linked to diet composition, N excretion pathway, number of trophic steps (McMahon & McCarthy 2016, McMahon et al. 2015, Germain et al. 2013) and different metabolic pools of protein in specific species can also be important (Chikaraishi et al. 2007). As an example, several gastropods have shown "compressed" TDFs (Choi et al. 2018). The authors hypothesized compressed TDFs in some invertebrate species may be tied to protein-rich mucus, and specifically be a function of metabolic flux required to deaminate AAs related to production and turnover of high-protein structural components (i.e. proteinaceous mucus, byssal threads, squid ink, etc.). Following on this work, empirically derived TDF values from our study are not unreasonable. Further, while TDF values in gastropods seem to vary between species, TDF values in filter-feeding bivalves studied here seem to far more consistent (Fig. 2.8), irrespective of if they produce byssal threads (mussels) or not (oysters).

Further, our shell CSI-AA data indicates that an additional correction is required to account for isotope routing, consistent with past results from structural protein in deep-sea corals (McMahon et al. 2018). Specifically, as noted above the $\delta^{15}N_{Glu}$ values in shell were consistently 1.6±1.1‰ higher, while there was no significant difference observed in $\delta^{15}N_{Phe}$ values between tissue types (Fig. 2.5). While the value we observed was consistent across all samples, we also note that the 1.6‰ *enrichment* in the shell compared to soft tissue, however in deep-sea gorgonian corals there is a 3.5 ‰ *depletion* in structural protein compared to the metabolically active polyp tissue, which the authors attribute the offset in corals differential deamination/transamination during protein synthesis (McMahon et al. 2018.)

Figure 8 synthesizes the need for new bivalve specific CSI-AA parameters, while illustrating the impact using traditional values vs. our newly proposed constants on TL_{CSIA} estimates. Using only the "literature" TDF value (7.6‰) both tissue types greatly underestimated expected TL for a primary consumer, (1.4 and 1.7 muscle tissue and shell, respectively; Fig. 2.8), again consistent with prior data (Vokhshoori & McCarthy 2014). While TL estimates in shell approach reasonable values (1.7 ± 0.1), this is essentially an artifact of the isotopic routing enrichment in $\delta^{15}N_{Glu}$ values demonstrated above.

Therefore, here we propose new TL_{CSIA} equations which are specific for soft tissue and shell protein in marine bivalves (Fig. 2.8), incorporating our new empirically derived TDF value of 3.4‰, with an additional fractionation factor (e) for shell $\delta^{15}N_{Glu}$ of 1.6‰. Using the proposed new relationships returns trophic level values of 2.0 ± 0.1 in soft muscle tissue, and 2.0 in ± 0.2 in shell protein. What is most important here is not the value of 2.0, since this is in some sense fixed by our assumptions, but rather it is the very low variations using the same constants across both multiple species and environments (Fig. 2.8). This similarity suggests that in fact the same compressed and uniform TDF values reflect bivalve filter-feeders generally, despite differences in bulk isotope values and in food resources indicated by MixSIAR modeling.

2.5 Conclusions

We investigated the fidelity of bivalve shells as bioarchives for paleoecological reconstruction, comparing a suite of ecological isotope proxies between the well-characterized, soft muscle tissue and shell matrix protein in three bivalve species from two coastal ecosystems. We found that while shell matrix protein $\delta^{13}C_{bulk}$ and $\delta^{15}N_{bulk}$ values were consistently higher than muscle soft tissue in all three species, the trophic niche widths calculated from bulk isotope data was indistinguishable. For CSI-AA derived ecological proxies, we found $\delta^{13}C_{baseline}$, $\delta^{15}N_{baseline}$ and estimation of resource contribution using MixSIAR in shell match very closely those derived soft tissue. However, using canonical TL_{CSIA} equations

and constants, we found trophic level to be substantially underestimated in both tissue types. Based on our new data set, we therefore propose a new empirical TDF value (3.4‰) for filter-feeding mollusks, and additional ε value (1.6‰) required for correction of TL_{CSIA} data from shell, due to isotope routing which from our data appears to be consistent with suspension-feeding gastropods. Importantly, the narrow range of variation observed TL_{CSIA} values using our new relationships across species and estuarine/ littoral environments suggests these average values are accurate and widely applicable.

These results highlight the importance of conducting isotope calibration studies on any proposed new bioarchive. Because the isotopic offsets in structural proteins is apparently not universal between organisms, we suggest that the correction factors for bioarchives structural protein are likely to be specific to organism type. Finally, the new empirical bivalve specific TDF values indicated by our new data, as well as past literature (3.4‰) is substantially below TDF ranges observed for other ammonia excreting, marine primary consumers, although it is consistent with ranges of TDF values observed in some gastropods. We suggest that direct bivalve feeding experiments should be done to further explore TDF values in filter-feeding mollusks.

Overall, the results enable the use of well-preserved bivalve shell for archaeological and geological studies, in particular using CSI-AA data. Bivalve shell represents one of the most promising bioarchives for understanding ocean change in coastal regions, since sessile filter-feeders record biogeochemical cycling at localized nearshore environments. Coastal upwelling ecosystems are particularly physically and biologically dynamic (Chavez and Messie 2009), and responses to climatic perturbations can be challenging to study with tradition offshore archives. Therefore, the data here can be used to develop bivalve shells as bioarchives, opening up entirely new suite of tracers to directly connect food web responses to physical oceanographic changes in the historical and geologic past.

Acknowledgements

We appreciate Chela Zabin from the Smithsonian Environmental Research Center for permission to collect bivalves from San Francisco Bay survey sites. We thank UC Santa Cruz's Stable Isotope Lab staff, Stephanie Christensen, Dyke Andresen and Colin Carney for assistance in bulk and amino acid isotope analysis. And we are grateful to Nancy Prouty for feedback on an earlier version of this manuscript. This work was funded by the University of California, Santa Cruz Future Leaders of Coastal Science Award.

References

Agbaje, O.B.A., Ben, S.I., Zax, D.B., Schmidt, A., Jacob, D.E. (2018) Biomacromolecules within bivalve shells: Is chitin abundant? *Acta Biomater*. 80, 176–187

Ambrose, S.H. (1990) Preparation and characterization of bone and tooth collagen for isotopic analysis. *Journal of Archaeological Science* 17: 431–451.

Ambrose, S.H., Norr, L. (1992) On stable isotopic data and prehistoric subsistence in the Soconusco region. Current Anthropology 33(4): 401–404

Baker, P. (1995) Review of ecology and fishery of the Olympia oyster, Ostrea lurida with annotated bibliography. *Journal of Shellfish Research* 14:501–518

Batista, F.C., Ravelo, A.C., Crusius, J., Casso, M.A., McCarthy, M.D. (2014) Compound specific amino acid $\delta^{15}N$ in marine sediments: a new approach for studies of the marine nitrogen cycle. *Geochimica et Cosmochimica Acta* 142:553–569.

Bayne, B.L., Hawkins, A.J.S., Navarro, E. (1988) Feeding and digestion in suspension-feeding bivalve molluscs: The relevance of physiological compensations. *Am. Zool*. 28: 147–159.

Bearhop, S., Adams, C.E., Waldron, S., Fuller, R.A., Macleod, H. (2004) Determining trophic niche width: a novel approach using stable isotope analysis. *Journal of Animal Ecology* 73:1007–1012.

Bograd, S.J., Schroeder, I., Sarkar, N., Qiu, X., Sydeman, W.J., Schwing, F.B. (2009) Phenology of coastal upwelling in the California Current. *Geophys Res Lett* 36, L01602, doi:10.1029/2008GL035933

Canuel, E.A., Cammer, S.S., McIntosh, H.A., Pondell, C.R. (2012) Climate change impacts on the organic carbon cycle at the land-ocean interface. *Annu. Rev. Earth Planet. Sci*. 40:685–711

Chavez, F.P., Ryan, J., Lluch-Cota, S.E., Ñiquen, M. (2003) From anchovies to sardines and back: multidecadal change in the Pacific Ocean. *Science* 299, 217–221.

Chavez, F.P., Messie, M. (2009) A comparison of eastern boundary upwelling ecosystems. *Prog. Oceanogr*. 83:80–96

Chikaraishi, Y., Kashiyama, Y., Ogawa, N.O., Kitazato, H., Ohkouchi, N. (2007) Metabolic controls of nitrogen isotope composition of amino acids in marine macroalgae and gastropods: implications for aquatic food web studies. *Marine Ecology Progress Series.* **342**, 85–90.

Chikaraishi, Y., Ogawa, N.O., Kashiyama, Y., Takano, Y., Suga, H., Tomitani, A., Miyashita, H., Kitazato, H., Ohkouchi, N. (2009) Elucidation of aquatic food-web structure based on compound-specific nitrogen isotopic composition of amino acids. *Limnology & Oceanography: Methods*. **7**, 740–750.

Cloern., J.E. (1996) Phytoplankton bloom dynamics in coastal ecosystems: a review with some general lessons from sustained investigation of San Francisco Bay, California. *Rev. Geophysics*, 34:127–168

Cloern, J.E., Canuel, E.A., Harris, D. (2002) Stable carbon and nitrogen isotope composition of aquatic and terrestrial plants of the San Francisco Bay estuarine system. *Limnol Oceanogr* 47:713–729

Cloern., J.E., Jassby, A.D, Schraga, T.S., Nejad, E., Martin, C. (2017) Ecosystem variability along the estuarine salinity gradient: Examples from long-term study of San Francisco Bay. *Limnol. Oceanogr*. doi:10.1002/lno.10537

Cloern, J.E. (2018) Patterns, pace, and processes of water quality variability in a long-studied estuary. *Limnol. Oceanogr.* doi:10.1002/lno.10958

Coe, W.R., Fox, D.L. (1942) Biology of the California sea-mussel (*Mytilus californianus*) – influence of temperature, food supply, sex and age in the rate of growth. *J. Exp. Zool*. 90(1):1-30

Defossez, J.M., Hawkins, A.J.S. (1997) Selective feeding in shellfish: size-dependent rejection of large particles within pseudofaeces from Mytilus edulis, *Ruditapes philippinarum* and *Tapes decussatus*. *Mar Biol* 129: 139±147

Duggins, D.O., Simenstad, C.A., Estes, J.A. (1989) Magnification of secondary production by kelp detritus in coastal marine ecosystems. *Science* (Washington, D.C.) 245:170-173

Ek, C., Holmstrand, H., Mustajärvi, L., Garbaras, A., Bariseviciute, R., Sapolaite, J., Sobek A., Gorokhova, E. and Karlson, A. M. (2018) Using compoundspecific and bulk stable isotope analysis for trophic positioning of bivalves in contaminated Baltic Sea sediments. Environ. Sci. Technol. 52, 486-4868.

Ellis, G.S., G. Herbert, D. Hollander. 2014. Reconstructing carbon sources in a dynamic estuarine ecosystem using oyster amino acid $\delta^{13}C$ values from shell and tissue. J Shellfish Res. 33:217-225

Fischer, A.D., McGaraghan, A., Hayashi, K., Kudela, R.M. (2020). Return of the “age of dinoflagellates”: Drivers of unusual dinoflag-ellate dominance in northern Monterey

Bay examined using automated imaging flow cytometry. Limnology and Oceanography, 65, 2125–2141. https://doi.org/10.1002/lno.

Foley, M.M., Koch, P.L. (2010) Correlation between allochthonous subsidy input and isotopic variability in the giant kelp Macrocystis pyrifera in central California, USA. *Mar Ecol Prog Ser* 409:41−50

Germain, L., Koch, P.L., Harvey, J., McCarthy, M.D. (2013) Nitrogen isotope fractionation in amino acids from harbor seals: implications for compound-specific trophic position calculations. *Marine Ecology Progress Series* 482:265–277.

Gorokhova, E., Hansson, S. (1999) An experimental study on variations in stable carbon and nitrogen isotope fractionation during growth of Mysis mixta and Neomysis integer. Can J Fish Aquat Sci 56:2203−2210

Graniero, L.E., Grossman, E.L., O'Dea, A. (2016) Stable isotopes in bivalves as indicators of nutrient source in the Bocas del Toro Archipelago, Panama. Peerj 4, e2278.

Graniero, L.E., Gillikin, D.P., Surge, D., Kelemen, Z., Bouillon, S. (2021) Assessing $\delta^{15}N$ values in the carbonate-bound organic matrix and periostracum of bivalve shells as environmental archives. *Palaeogeogr. Palaeoclimatol. Palaeoecol*. 564, 110108.

Hansen JA. (2011) A comparison of pre-treatment methods for $\delta^{15}N$ analysis in mollusk shells. MS thesis. University of Alabama,

Hare, E.P., Fogel, M.L., Stafford, T.W., Mitchell, A.D., Hoering, T.C. (1991) The isotopic composition of carbon and nitrogen in individual amino acids isolated from modern and fossil proteins. *Journal of Archaeological Science* 18, 277–292.

Harger, J.R.E. (1970b) Comparison among growth characteristics of two species of sea mussels, *Mytilus edulis* and *Mytilus californianus*. *Veliger* 13(1):44-56

Hawkins, A., Navarro, E. (1988) Feeding and digestion in suspension-feeding bivalve molluscs: the relevance of physiological compensations. *American Zoologist*, 28,147-159.

Hawkins, A. (1985) Relationships between the synthesis and breakdown of protein, dietary absorption and turnovers of nitrogen and car- bon in the blue mussel, Mytilus edulis L. *Oecologia* 66:42–49

Hawkins, A.J.S., Bayne, B.L. (1985) Seasonal variation in the relative utilization of carbon and nitrogen by the mussel Mytilus edulis: budgets, conversion efficiencies and maintenance requirements. *Mar. Ecol. Prog. Ser*. 25, 181–188.

Hickey, B.M. (1998) Coastal oceanography of western North America from the tip of Baja California to Vancouver Island. In: Robinson AR, Brink KH (eds) The sea, the global coastal ocean, Vol 11. John Wiley & Sons, New York, NY, p 345−393

Howland, M.R., Corr, L.T., Young, S.M.M., Jones, V., Jim, S., Van Der Merwe, N. J., Mitchell, a. D., and Evershed, R. P. (2003). Expression of the dietary isotope signal in the compound-specific ?13C values of pig bone lipids and amino acids. *International Journal of Osteoarchaeology* 13, 54–65.

Jackson, A.L., Inger, R., Parnell, A.C., Bearhop, S. (2011) Comparing isotopic niche widths among and within communities: SIBER - stable Isotope Bayesian Ellipses in R. *Journal of Animal Ecology*. **80**(3), 595–602.

Jacox, M.G., Fiechter, J., Moore, A.M., Edwards, C.A. (2015a), ENSO and the California Current coastal upwelling response, *J. Geophys. Res. Oceans*, 120, 1691–1702, doi:10.1002/2014JC010650

Jassby A.D., Cloern, J.E., Powell, T.M. (1993) Organic carbon sources and sinks in San Francisco Bay—variability induced by river flow. *Mar Ecol Prog Ser* 95:39–54

Kobayashi, I., Samata, T. (2006) Bivalve shell structure and organic matrix. *Mater. Sci. Eng. C* 26, 692–698. (doi:10.1016/j.msec.2005.09.101)

Kreeger, D.A., Hawkins, A.J.S., Bayne, B.L., Lowe, D.M. (1995) Seasonal variation in the relative utilization of dietary protein for energy and biosynthesis by the mussel *Mytilus edulis*. *Mar Ecol Prog Ser* 126:177-184

Larsen, T., Taylor, D.L., Leigh, M.B., O'Brien, D.M. (2009) Stable isotope fingerprinting: a novel method for identifying plant, fungal, or bacterial origins of amino acids. *Ecology* 90:3526−3535

Larsen, T., Ventura, M., Andersen, N., O'Brien, D.M., Piatkowski, U., McCarthy, M.D. (2013) Tracing carbon sources through aquatic and terrestrial food webs using amino acid stable isotope fingerprinting. *PLoS ONE* 8, e73441.

Levinton, J.S., Ward, J.E., Shumway, S.E. (2002) Feeding responses of the bivalves Crassostrea gigas and Mytilus trossulus to chemical composition of fresh and aged kelp detritus. *Mar. Biol*. 141:367–376

Marin, F., Luquet, G. (2004) Molluscan shell proteins. *CR Palevol*. 3, 469–492. (doi:10.1016/j.crpv.2004.07.009)

McCarthy, M.D., Benner, R., Lee, C., Fogel, M.L. (2007) Amino acid nitrogen isotopic fractionation patterns as indicators of heterotrophy in plankton, particulate, and dissolved organic matter. *Geochimica et Cosmochimica Acta.* **71**, 4727– 4744.

McClelland. J.W., Montoya, J.P. (2002) Trophic relationships and the nitrogen isotopic composition of amino acids in plankton. *Ecology*. **83**, 2173–2180.

McMahon, K.W., Fogel, M.L., Elsdon, T.S., Thorrold, S.R. (2010) Carbon isotope fractionation of amino acids in fish mus- cle reflects biosynthesis and isotopic routing from dietary protein. *J Anim Ecol* 79:1132−1141

McMahon, K.W., Guilderson, T.P., Sherwood, O.A., Larsen, T., McCarthy, M.D. (2015c) Millennial- scale plankton regime shifts in the subtropical North Pacific Ocean. *Science* 350:1530–1533.

McMahon, K.W., McCarthy, M.D. (2016) Embracing variability in amino acid $\delta^{15}N$ fractionation: mechanisms, implications, and applications for trophic ecology. *Ecosphere*. **7**(12)1-26.

McMahon, K.W., Williams, B., Guilderson, T.P., Glynn, D.S., McCarthy, M.D. (2018) Calibrating amino acid $\delta^{13}C$ and $\delta^{15}N$ offsets between polyp and protein skeleton to develop

proteinaceous deep-sea corals as paleoceanographic archives. *Geochemica et Cosmochimica Acta* 220, 261-275.

Misarti, N., Gier, E., Finney, B., Barnes, K., McCarthy, M. (2107) Compound-specific amino acid $\delta^{15}N$ values in archaeological shells: Assessing diagenetic integrity and potential for isotopic baseline reconstruction. *Rapid Commun. Mass. Spectrom*. 31:1881-1891.

Newell, R.I.E., Jordan. S.J. (1983) Preferential ingestion of organic material by the American oyster Crassostrea virginica. *Mar Ecol Prog Ser* 13:47-53

Nielsen, J. M., Popp, B.N., Winder, M. (2015) Meta- analysis of amino acid stable nitrogen isotope ratios for estimating trophic position in marine organisms. *Oecologia*178:1–12.

O'Donnell, T.H., Macko, S.A., Chou, J., Davis-Hartten, K.L., Wehmiller, J.F. (2003) Analysis of $\delta^{13}C$, $\delta^{15}N$, and $\delta^{34}S$ in organic matter from the biominerals of modern and fossil Mercenaria spp. *Org. Geochem*. 34, 165–183. (doi:10.1016/S0146- 6380(02)00160-2)

Ohkouchi, N., and others. (2017) Advances in the application of amino acid nitrogen isotopic analysis in ecological and biogeochemical studies. *Org. Geochem*. 113: 150–174.

Patterson, H.K., Carmichael, R.H. (2016) The effect of lipid extraction on carbon and nitrogen stable isotope ratios in oyster tissues: Implications for glycogen-rich species. *Rapid Commun. Mass Spectrom.*, 30, 2594–2600

Peterson, B.J., Howarth, R.W., Garritt, R.H. (1985) Multiple stable isotopes used to trace the flow of organic matter in estuarine food webs. *Science* 227: 1361-63

Peterson, B.J., Fry, B. (1987) Stable isotopes in ecosystem studies. *Annual Review of Ecology and Systematics*, 18: 293-320

Pennington, J. T., Chavez, F.P. (2017) Decade-scale oceanographic fluctuation in Monterey Bay, California, 1989–2011. *Deep-Sea Res. Part II Top. Stud. Oceanogr*. 151: 4–15.

Prins, T.C., Smaal, A.C., Pouwer, A.J. (1991) Selective ingestion of phytoplankton by the bivalves Mytilus edulis L. and Cerastoderma edule (L.). Hydrobiol Bull 25: 93±100

Rau, G.H, Chavez, F.P., Friederich, G.E. (2001) Plankton $^{13}C/^{12}C$ variations in Monterey Bay, California: Evidence of non-diffusive inorganic carbon uptake by phytoplankton in an upwelling environment. *Deep Sea Res. I* 48: 79–94.

Suchanek, T.H. (1978) The ecology of Mytilus edulis L. in exposed rocky intertidal communities. *J. Exp. Mar. Biol. Ecol*. 31: 105–120

Shen, Y., Guilderson, T.P., Sherwood, O.A., Castro, C.G., Chavez, F.P., McCarthy, M.D. (2021) Amino Acid $\delta^{13}C$ and $\delta^{15}N$ Patterns from Sediment Trap Time Series and Deep-Sea Corals: Implications for Biogeochemical and Ecological Reconstructions in Paleoarchives. *Geochimica et Cosmochimica Acta* 297: 288–307.

Sherwood, O.A., Guilderson, T.P., Batista, F.C., Schiff J.T., McCarthy, M.D. (2014) Increasing subtropical North Pacific Ocean nitrogen fixation since the Little Ice Age. *Nature* 505, 78–81.

Silfer, J.A., Engel, M.H., Macko, S.A., Jumeau, E.J. (1991). Stable carbon isotope analysis of amino acid enantiomers by conventional isotope ratio mass spectrometry and combined gas chromatography/isotope ratio mass spectrometry. *Analytical Chemistry* 63, 370–374.

Sobczak, W.V., Cloern, J.E., Jassby, A.D., Muller-Solger, A.B. (2002) Bioavailability of organic matter in a highly disturbed estuary: The role of detrital and algal resources. *PNAS* 99(12):8101-8105

Stenton-Dozey, J.M.E., Brown, A.C. (1992) Clearance and retention efficiency of natural suspended particles by the rockpool bivalve Venerupis corrugatus in relation to tidal availability. *Mar Ecol Prog Ser* 82.175-186

Stock, B.C., Semmens, B.X. (2016) MixSIAR GUI User Manual.https://doi.org/10.5281/zenodo. 47719. https://github.com/brianstock/MixSIAR/, Version 3.1.

Suchanek, T.J. (1978) The ecology of Mytilus edulis L. in exposed rocky intertidal communities. *J. Exp. Mar. Biol.Ecol*. 31:105-120.

Tieszen, L.L., Boutton, T.W., Tesdahl, K.G., Slade, N.A. (1983) Fractionation and turnover of stable carbon isotopes in animal tissues: implications for $\delta^{13}C$ analysis of diet. *Oecologia*. 57:32-37

Tipple, B.J., Christensen, S., Ianiri, H.L., McCarthy, M.D., Vokhshoori, N.L. (submitted) Stable carbon isotope amino acids fingerprints of estuarine and freshwater macrophyte and terrestrial primary producers, PANGAEA.

Versteegh, E.A.A., Gillikin, D.P., Dehairs, F. (2011) Analysis of $\delta^{15}N$ values in mollusk shell organic matrix by elemental analysis/isotope ratio mass spectrometry without acidification: an evaluation and effects of long-term preservation. *Rapid Communications in Mass Spectrometry*, 25,675–680.

Vokhshoori, N.L., McCarthy, M.D. (2014) Compound-specific $\delta^{15}N$ amino acid measurements in littoral mussels in the California upwelling ecosystem: a new approach to generating baseline $\delta^{15}N$ isoscapes for coastal ecosystems. *PLoS oNE* **9**:e98087.

Vokhshoori, N.L., Larsen, T., McCarthy, M.D. (2014) Reconstructing $\delta^{13}C$ isoscapes of phytoplankton production in a coastal upwelling system with amino acid isotope values of littoral mussels. *Mar Ecol Prog Ser* 504:59−72

Vokhshoori, N.L., McCarthy M.D., Close H.G., Demopoulos A.W. J., Prouty N.G. (2021). New geochemical tools for investigating resource and energy functions at deep-sea cold seeps using amino acid $\delta^{15}N$ in chemosymbiotic mussels (Bathymodiolus childressi). *Geobiology*, 00, 1–17. https://doi.org/10.1111/gbi.12458

Ward, J. E., Shumway, S.E. (2004) Separating the grain from the chaff: particle selection in suspension and deposit feeding bivalves. *J. Exp. Mar. Biol. Ecol*. 300, 83–130

Watanabe, S., Kodama, M., Fukuda, M. (2009) Nitrogen stable isotope ratio in the manila clam, Ruditapes philippinarum, reflects eutrophication levels in tidal flats. *Marine Pollution Bulletin*, 58, 1447–1453.

Whitney, N.M., Johnson, B.J., Dostie, P.T., Luzier, K., Wanamaker, A.D. (2019) Paired Bulk Organic and Individual Amino Acid $\delta^{15}N$ Analyses of Bivalve Shell Periostracum: A Paleoceanographic Proxy for Water Source Variability and Nitrogen Cyclin Processes. *Geochimica Et Cosmochimica Acta* 254: 67–85. doi:10.1016/j. gca.2019.03.019.

Wolf, N., Newsome, S.D., Peters, J., Fogel, M.L. (2015) Variability in the routing of dietary proteins and lipids to consumer tissues influences tissue specific discrimination. *Rapid Communications in Mass Spectrometry* 29:1448–1456.

Zupcic-Moore, J.R., Ruiz-Cooley, R.I., Paliza, O., Koch, P.L., McCarthy, M.D. (2017) Using stable isotopes to investigate foraging variation and habitat use of sperm whales from northern Peru. *MEPS*, 579, 201–212. https://doi.org/10.3354/meps12281

Supplemental Materials

Table S1. Seasonal bulk $\delta^{13}C$ and $\delta^{15}N$ values for seawater particulate organic matter of size fractions: Nitex (>53 μm) and GFF (<0.7 μm) from two coastal environments, Littoral (Santa Cruz, CA) and Estuary (Northern San Francisco Bay).

Littoral Seawater POM				
Season	$\delta^{13}C_{GFF}$	$\delta^{15}N_{GFF}$	$\delta^{13}C_{Nitex}$	$\delta^{15}N_{Nitex}$
spring	-19.41	7.89	-19.02	8.39
summer	-18.76	8.09	-17.72	9.13
fall	-18.97	11.19	-18.47	10.70
winter	-18.84	8.65	-18.00	8.76
Estuarine Seawater POM				
Season	$\delta^{13}C_{GFF}$	$\delta^{15}N_{GFF}$	$\delta^{13}C_{Nitex}$	$\delta^{15}N_{Nitex}$
spring	-21.41	8.41	-19.68	9.50
summer	-22.42	NA	-20.92	9.45
fall	-21.40	7.75	-23.22	12.72
winter	-23.69	10.70	-22.99	11.01

Table S2. Seasonal and average (±1 SD) bulk $\delta^{13}C$ and $\delta^{15}N$ offsets (tissue – POM) between seasonal values of bivalve tissue (soft muscle and shell matrix protein) in three species – Littoral *Mytilus Californianus*, Estuarine *Ostrea Lurida* and Estuarine *Mytilus edulis* – from GFF fraction of seawater particulate organic matter (<0.7µm) collected from two coastal environments: Littoral (Santa Cruz, CA) and Estuary (Northern San Francisco Bay). *Summer Estuarine $\delta^{15}N$ offset from Nitex fraction (>0.53µm).

Littoral Mussel POM Offset				
Season	$\delta^{13}C_{muscle}$	$\delta^{13}C_{shell}$	$\delta^{15}N_{muscle}$	$\delta^{15}N_{shell}$
spring	3.84	4.88	3.20	4.29
summer	3.27	4.00	2.46	3.71
fall	3.46	4.78	-0.05	0.82
winter	3.14	4.38	2.49	3.55
Average	3.43	4.51	2.03	3.09
SD	0.30	0.40	1.42	1.55

Estuarine Oyster POM Offset				
Season	$\delta^{13}C_{muscle}$	$\delta^{13}C_{shell}$	$\delta^{15}N_{muscle}$	$\delta^{15}N_{shell}$
spring	-2.19	-2.07	4.27	5.26
summer	-1.05	1.23	1.61*	2.77*
fall	-1.64	1.00	5.54	6.24
winter	0.64	3.23	2.30	3.45
Average	-1.06	0.85	3.43	4.43
SD	1.23	2.19	1.80	1.60

Estuarine Mussel POM Offset				
Season	$\delta^{13}C_{muscle}$	$\delta^{13}C_{shell}$	$\delta^{15}N_{muscle}$	$\delta^{15}N_{shell}$
spring	1.24	3.00	3.63	5.77
summer	-0.38	2.08	1.87*	2.77*
fall	-1.34	0.91	4.18	4.84
winter	1.74	3.77	2.40	2.68
Average	0.32	2.44	3.02	4.02
SD	1.43	1.23	1.07	1.54

Figure S1. SIBER ellipse area for two tissue types, shell matrix protein and soft muscle tissue, for three species of bivalve in this study: Littoral *Mytilus Californianus* (dark blue), Estuarine *Ostrea Lurida* (pink) and Estuarine *Mytilus edulis* (light blue)

	CA mussel adductor	Blue mussel adductor	Olympia oyster adductor	CA mussel shell	Blue mussel shell	Oyster shell
TA	1.491	5.031	6.8241	0.907	3.808	5.257
SEA	0.323	2.398	1.685179	0.306	1.484	2.215
SEAc	0.329	2.548	1.733327	0.323	1.576	2.400

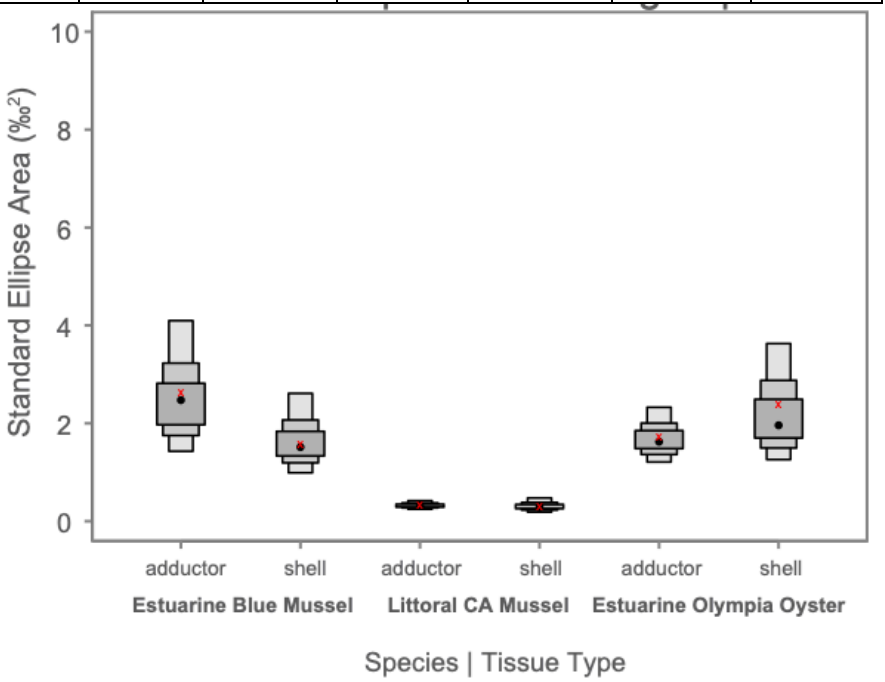

Figure S2. Molar abundance difference between shell matrix protein and soft muscle tissue for three species of bivalve in this study: Littoral *Mytilus Californianus* (dark blue), Estuarine *Ostrea Lurida* (pink) and Estuarine *Mytilus edulis* (light blue)

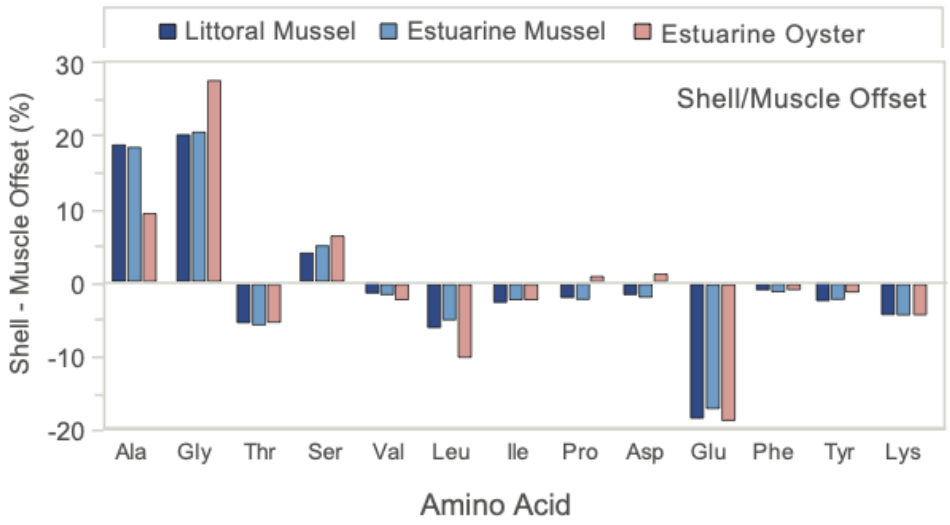

Figure S3. Raw seasonal essential amino acid $\delta^{13}C$ values of three bivalve species (A) Littoral *M. californianus* (circle), (B) Estuarine *O. Lurida* (triangle) and (C) Estuarine *M. edulis* (square) in two tissue types: muscle tissue (filled symbol) and shell (open symbol). Seasons are as follows: Spring (pink), Summer (blue), Fall (yellow) and Winter (green).

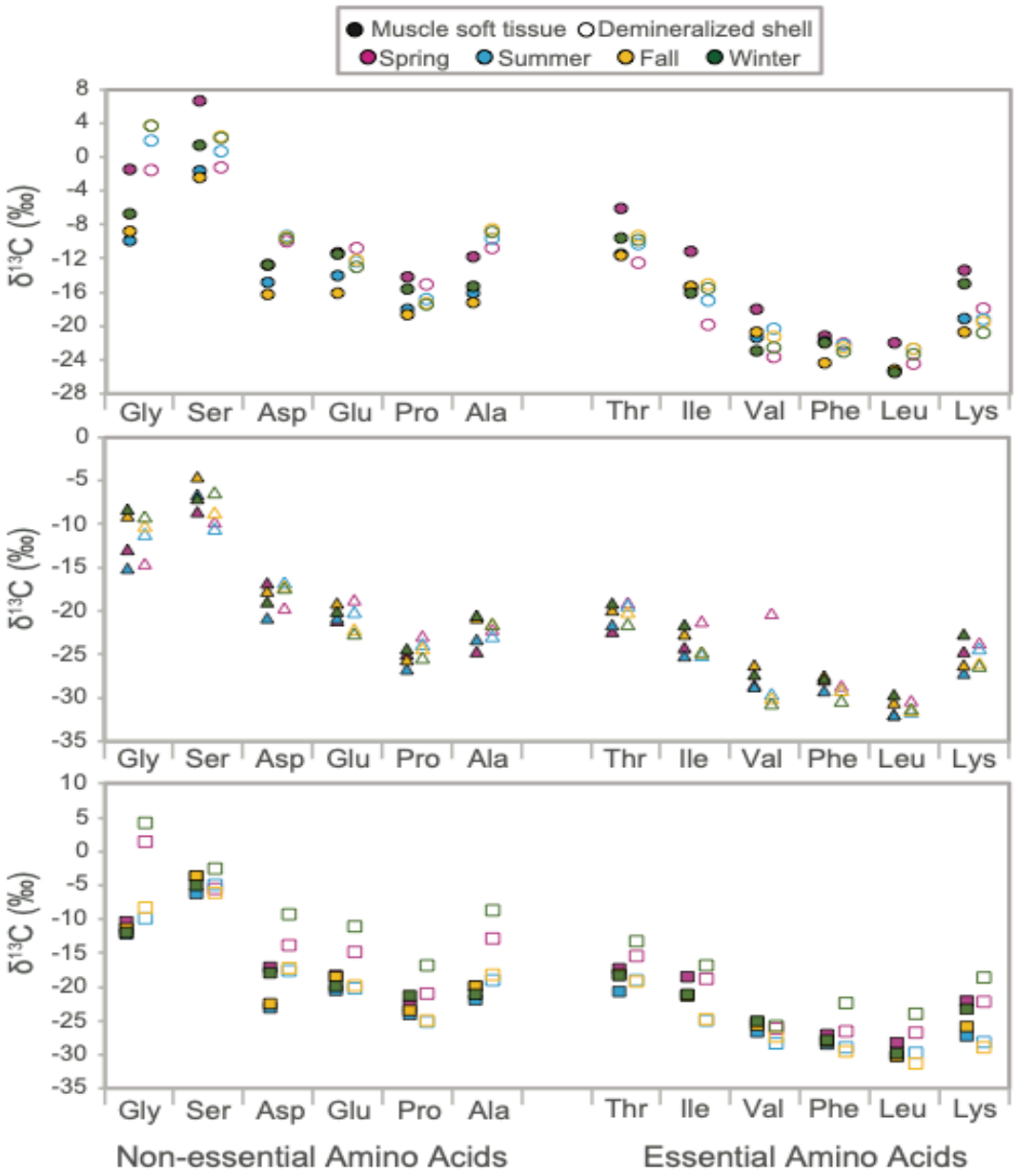

Figure S4. Raw seasonal amino acid $\delta^{15}N$ values of three bivalve species (A) Littoral *M. californianus* (circle), (B) Estuarine *O. Lurida* (triangle) and (C) Estuarine *M. edulis* (square) in two tissue types: muscle tissue (filled symbol) and shell (open symbol). Seasons are as follows: Spring (pink), Summer (blue), Fall (yellow) and Winter (green).

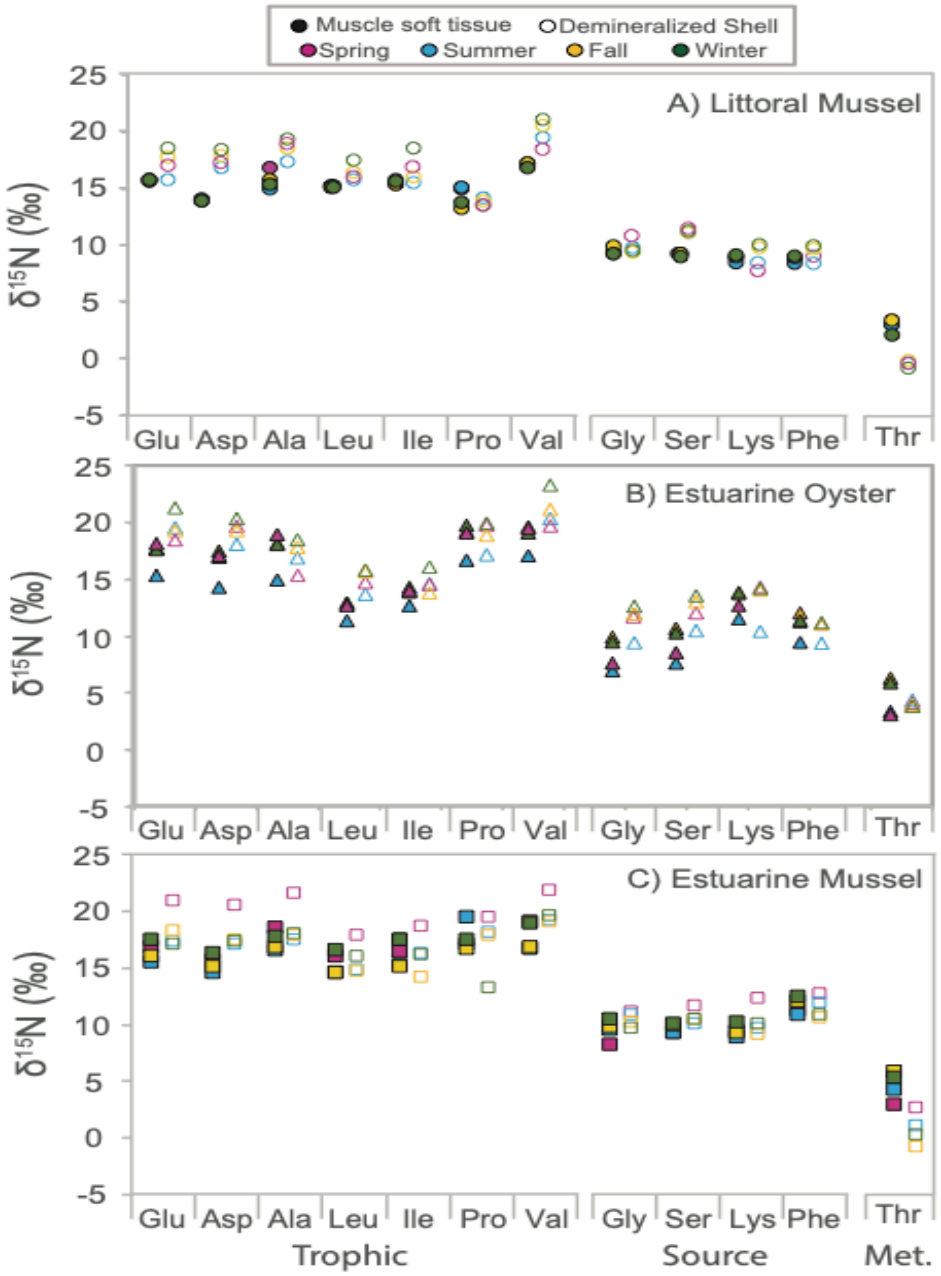

Figure S5. Raw seasonal amino acid $\delta^{13}C$ values in POM for the Estuarine ecosystem (filled circle and Littoral ecosystem (open circle). Seasons are as follows: Spring (pink), Summer (blue), Fall (yellow) and Winter (green).

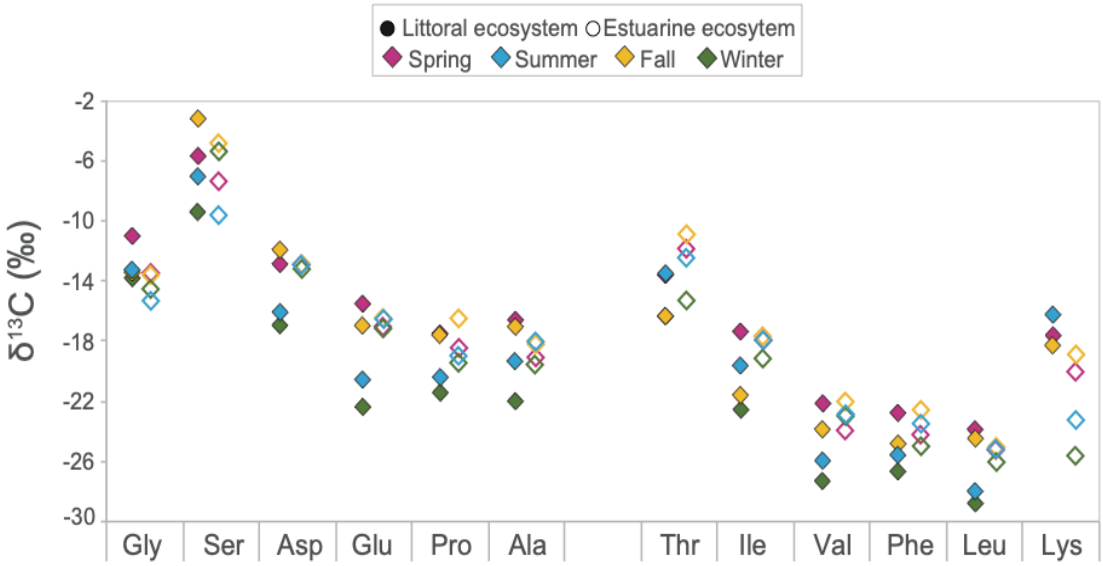

Figure S6. Linear relationship between measured bulk $\delta^{13}C$ and mol% adjusted EAA $\delta^{13}C$ in seawater POM (GFF) from the Monterey Bay and Northern San Francisco Bay (n = 8).

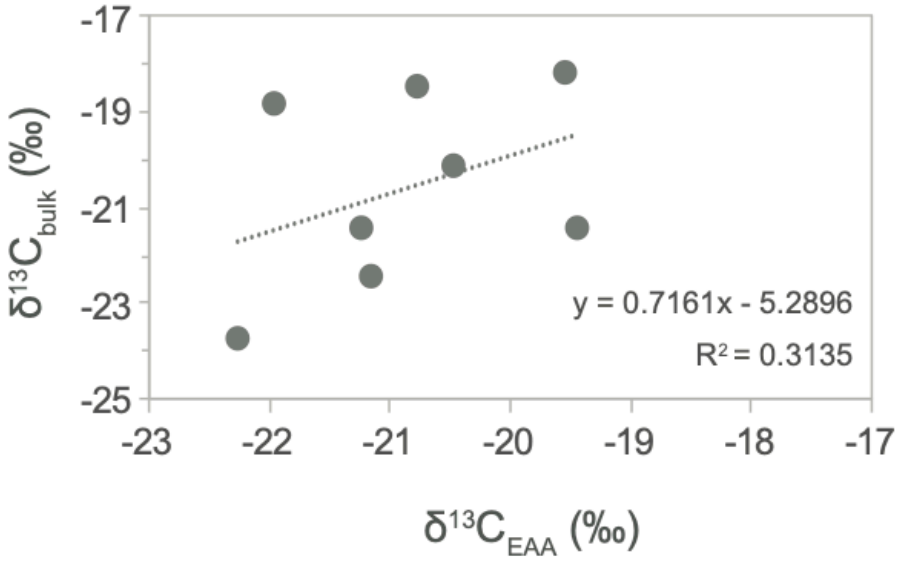

Figure S7. $\delta^{13}C$ and $\delta^{15}N$ baseline biplot for Littoral and Estuarine bivalves soft muscle tissue and shell matrix protein using the equations proposed by Vokhshoori et al. 2014 mol% adjusted (And B) and Shen et al. 2021 not mol% adjusted (C and D).

Vokhshoori et al. 2014 $\delta^{13}C$ baseline equation mol% adjusted (y = 0.9237x + 0.1312)

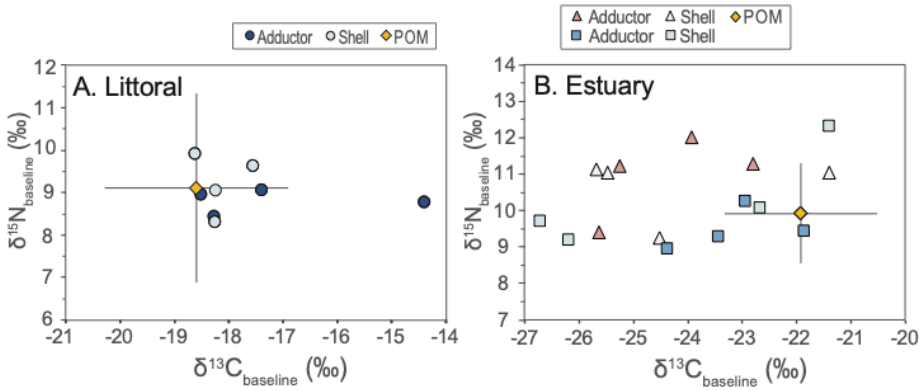

Shen et al. 2021 $\delta^{13}C$ Vaseline equation, not mol% adjusted (y = 0.754x – 5.864)

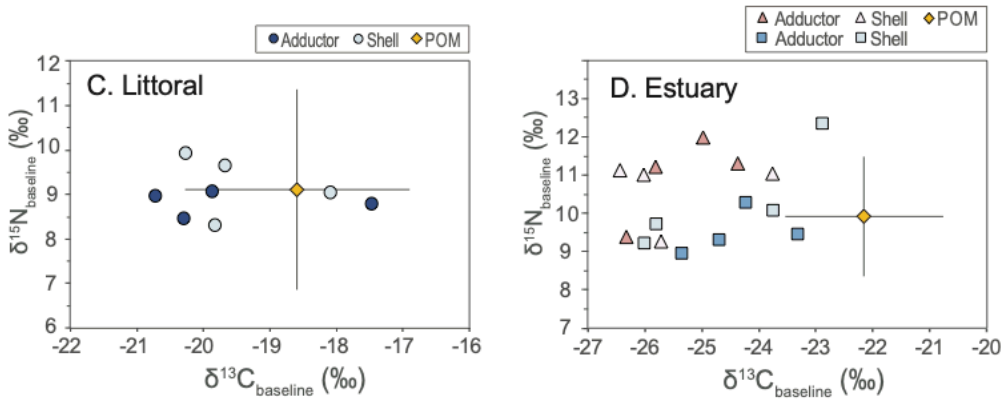

Chapter 3

Preservation of amino acid isotope proxies in diagenetically altered shells

"Language is our gift and our responsibility. I've come to think of writing as an act of reciprocity with the living land. Words to remember old stories, words to tell new ones, stories that bring science and spirit back together to nurture our becoming people made of corn."

- Robin Wall Kimmerer, *Braiding Sweetgrass*

Preservation of stable isotope signatures of amino acids in diagenetically altered Middle to Late Holocene archaeological mollusc shells

Natasha L. Vokhshoori, Torben Rick, Todd Braje, Matthew D. McCarthy

Abstract: Stable isotope proxies measured in the proteinaceous fraction of archaeological mollusc shell potentially preserves important ecological information for reconstructing past trophic and climatic conditions of nearshore environments. A major issue, however, is controlling for diagenetic alteration in shells that can alter the isotope values. "Bulk" stable isotope values of nitrogen ($\delta^{15}N$), and especially carbon ($\delta^{13}C$) have been shown to shift strongly with increasing C:N ratios in degraded shell, resulting in unreliable values. Here, we examine the stability of an entirely new set of potential shell paleo-proxies, compound-specific isotopes of amino acids (CSI-AA), examining both carbon ($\delta^{13}C$-AA) and nitrogen ($\delta^{15}N$-AA) patterns and values from the insoluble protein fraction of mussel shells from the California Channel Islands. Archaeological shell samples ranged in age (6,100 to 250 cal BP) and depositional environments (e.g. exposed coastal bluff, at depth, etc.) exhibiting a wide range of degradation states. Archaeological shell data was directly compared with the same proxies and data types from modern shells of the same species and region. Our results show C:N ratios can be regarded as a "master variable" to indicate relative degradation state of shell organic matter. Modern shell C:N ratios ranged from 2.8 to 3.5, while those in archaeological shell were substantially elevated, ranging from 3.4 to 9.5. C:N ratios exhibited strong negative correlations with bulk $\delta^{13}C$ values, weight % C and weight %N, and significant but weak correlation with $\delta^{15}N$ values, together showing the impact of diagenesis on bulk properties. Relative molar abundances revealed that Glycine and Alanine, the most abundant AAs in insoluble shell protein, progressively decreased with increasing C:N ratio. An additional "cleaning" step using weak NaOH helped to remove possible contaminants (e.g. surrounding sediments, terrestrial organic matter) without altering bulk values in some samples but was overall inconsistent in restoring bulk values to expected ranges. In contrast, CSI-AA data was

relatively unaltered, even in the most degraded shell samples. Normalized CSI-AA values in archaeological shell was well-preserved, matching overall expected patterns of modern mussel shell. Specific isotope proxies for "baseline" (δ^{15}N-Phenylalanine and average δ^{13}C-Essential AAs) were also not statistically different from modern across all C:N groupings. While there were some differences in a few specific AA isotope values with degradation (i.e. Glycine and Serine), in contrast, Glutamic Acid and Phenylalanine, the two AA most commonly used to calculate trophic level, were not altered. We conclude that while bulk isotopes, particularly δ^{13}C, are likely to be unreliable in degraded archaeological shells with C:N ratios higher than ~4.0, isotope proxies from CSI-AA can still be used even in samples with highly elevated C:N ratios (>7.0) to reconstruct past climatic and ecological conditions of the nearshore marine environment.

3.1 Introduction

Mollusc shells are often among the most abundant skeletal hard parts preserved in coastal archaeological sites, representing one of the most promising potential bioarchives for reconstructing past local, coastal palaeoecological and palaeoceanographic conditions (Andrus 2011, Prendergast and Stevens 2014, Leng and Lewis 2016). In the face of a rapidly changing climate due to a combination of anthropogenic carbon dioxide emissions, habitat loss and pollution, marine ecosystems, especially oceanographically dynamic regions such as eastern boundary coastal upwelling systems, have shown to have widely different responses to climatic perturbations. A most recent example was the 2014-2016 marine heatwave (McClatchie et al. 2016), had huge ecological damage in the Pacific Northwest, but coastal communities in southern California were far less impacted (Sakuma et al. 2016). The need for bioarchives that can reconstruct highly detailed, local conditions is important for understanding how different coastal communities might respond to climatic perturbations in the historical and geologic past.

In marine shell, sea surface temperature reconstructions from oxygen isotopes ($\delta^{18}O$) are commonly performed in the carbonate fraction, however, a small but significant percentage of shell is also composed of proteinaceous organic matter. The insoluble organic matter content in bivalve shell is primarily in the form of glycoproteins and trace amounts of polysaccharides (Hattan et al. 2001) with a much higher C:N ratio (Hudson 1967). The isotopic and organic chemical composition of this organic matter fraction at the molecular level arguably represents far more diverse paleo-proxy potential, but to date is far less developed.

Stable isotope proxies from carbon ($\delta^{13}C$) and nitrogen ($\delta^{15}N$) measured in shell matrix protein of ancient bivalves can record highly detailed ecological information for reconstructing past trophic and climatic conditions of nearshore environments; this is because sessile filter-feeding bivalves are passive recorders of water column organic matter sources, thus integrating key isotopic signals into their tissues (Lorrain et al. 2002, Vokhshoori and McCarthy 2014), including the biomineral fraction (Ellis et al. 2014, Graniero et al. 2016, Graniero et al. 2021, Vokhshoori et al. *in review*) .

A major potential issue with shell matrix protein, however, is controlling for diagenetic alteration. Post-depositional conditions can expose shells to both physical and chemical weathering where the porous nature of shell carbonate also allows organic contamination and post depositional alteration to occur (Sykes et al. 1995). This can result in partial hydrolysis of the shell causing degradation of indigenous organic compounds (e.g. glycoproteins) either out of the shell matrix, or intrusion of exogenous compounds from the surrounding environment (e.g. terrestrial C_3 or C_4 plants), overall altering the organic content composition and isotope values (Silfer et al. 1994, Sykes et al. 1995, Misarti et al. 2017). Another possible mechanism for alteration is biological reworking of the organic content. For example, heterotrophic bacteria have been shown to change the amino acid molar content of organic matter, and therefore likely to also alter bulk carbon and nitrogen isotope signatures (Macko et al. 1987, Lehmann et al. 2002). In bulk, or whole tissue, $\delta^{15}N$ and especially $\delta^{13}C$ values, have shown to change dramatically with increasing C:N ratios either from diagenetic alteration or contamination, thus

resulting in unreliable values (Ambrose 1990, Ambrose & Norr 1992, O'Donnell et al. 2003). However, in recent years compound-specific isotopes analysis (CSIA) has become a widely used leading edge technique for biogeochemical and paleoecological reconstructions, however the preservation CSIA data has never been directly investigated in diagenetically altered insoluble shell matrix protein of archaeological mollusc shells.

Compound-specific isotopes of amino acids (CSI-AA) of both in carbon ($\delta^{13}C_{AA}$) and nitrogen ($\delta^{15}N_{AA}$) has proven to overcome multiple issues with traditional bulk isotope data. CSI-AA is increasingly used in ecological, biogeochemical and oceanographic studies for tracing food chain length (Choy et al. 2015, Loick-Wilde et al. 2018), reconstructing primary producer groups (Larsen et al. 2013, McMahon et al. 2015), and tracing inorganic nitrogen sources (Sherwood et al. 2011, Vokhshoori & McCarthy 2014). Whereas bulk isotope values inherently represent a mixture of the isotope signatures of all carbon and/or nitrogen containing compounds, CSI-AA measures only amino acids, the molecular constituents that make up proteins. By isolating a select group of molecules, with known biochemical pathways and predictable isotopic fractionation patterns (Ohkouchi et al. 2017), we may directly compare AA isotope signatures of ancient shell to its modern analog. If CSI-AA signatures are well-preserved in ancient shell samples, these molecular-isotope paleo-proxies can potentially be applied to reconstruct changes in local ocean biogeochemistry and primary production at archaeological sites worldwide.

Here, we directly address the problem of diagenesis for the first time by comparing modern CSI-AA data to ancient archaeological shell samples over a wide range of degradation states. We measured the elemental, molecular and stable isotope values of both $\delta^{13}C$ and $\delta^{15}N$ in bulk and CSI-AA within the insoluble protein fraction of mussel shells (*Mytilus californianus*) from modern and archaeological shells excavated from California Channel Islands ranging in age (6,100 to 250 cal BP) and depositional environments (e.g. exposed coastal bluff, buried strata, etc.). The overarching questions for this study are first how well amino acid isotope signatures are preserved in diagenetically altered archaeological shells on multimillennial

timescales, and second if CSI-AA data can transcend many of the known issues of bulk stable isotope values in degraded shell material, potentially providing more accurate and far more diverse range of paleo-isotope information.

3.2 Materials and Methods

3.2.1 Sample collection, context, and processing

Data for modern *Mytlilus californianus* shells was compiled from Vokhshoori et al. *in review*. Briefly, live whole individuals of *M. californianus* were collected from Santa Cruz, CA (36°57'2 N, 122°2'39 W) between February 2018 to January 2019. Archaeological mussel shells were excavated from midden sites around the Channel Islands and mainland Santa Barbara area (Table 3.1) and were also obtained from collections at the Santa Barbara Museum of Natural History.

Table 3. 1 Sample information

Archaeological Site	Provenience	Location	Age (Cal BP)	Time Period	Bulk Analyses (n)	CSIA Analyses (n)
-	-	Santa Cruz	0	Modern	33	4
CA-SMI-470	Unit 2	San Miguel Island	460-250	Historic	10	2
CA-SBA-4194	Level 3, 40-50cm	Pt. Conception	730-565	Historic	10	3
CA-SBA-4187	Main midden, 50L	Pt. Conception	790-655	Historic	10	4
CA-SMI-481	East Dune ?	San Miguel Island	945-380	MLT	10	2
CA-SMI-481	Unit 1, Level 3	San Miguel Island	1020-920	Late	10	0
CA-SMI-481	Unit 1b	San Miguel Island	1260-920	Late	10	2
CA-ANI-2	Unit 1/2	Anacapa Island	3250-2750	Early - EZ	10	3
CA-SRI-191	Unit 1	Santa Rosa Island	6120-5840	Early - Eyb	10	4

Upon retrieval, bivalve shells were taken to the lab for sample processing and preparation for isotope analysis. For modern bivalves, soft tissue parts were discarded. Then all shells were scrubbed clean using a wired bristle brush and scalpel to remove periostracum and other large dirt particles. Shells were then soaked in a dilute bleach (NaClO) solution for 1 hr, sonicated in nano-pure water, and dried in an oven overnight at 60ºC. Each shell was then

crushed using a mortar and pestle, sieved through a 5µm screen, and 1000 mg weighed into a labelled 20x150 mm borosilicate vials. To extract the acid insoluble organic matter (OM) fraction, samples were acidified with a weak 1N HCl by pipetting 1mL increments until shell was completely dissolved (~35 mL); samples were stored in the fridge overnight to complete the reaction. After acidification, OM fraction was isolated by filtration onto 22mm 0.7 GF/F Whatman filters, rinsed thoroughly with nano-pure water, and dried overnight at 60ºC. Sample yields were calculated based on total dry mass, a fraction was set aside for bulk $\delta^{13}C$ analysis, and the remaining amount was used for CSIA of AAs on a selected subset of shell samples.

3.2.2 NaOH clean test

For a subset of shell samples (data repository), we tested an additional NaOH cleaning protocol, targeted to remove potential contamination by intrusion of exogenous OM, including plant matter and/or humic acids, performed following the protocol proposed by Ambrose (1990). Again, ~1000mg or the remaining amount of whole crushed shell demineralized in 20x150 mm borosilicate vials. After complete demineralization and rinsing with nanopore water, each sample was submerged in ~35mL of 0.125M NaOH at room temperature for 20 to 24 hours and rinsed to neutrality with nano-pure water. Between rinses, samples were centrifuged at 3000 RPM for 5 minutes, the supernatant was pipetted off and disposed of. Samples dried overnight at 60ºC and sample yields were calculated.

3.2.3 Bulk Stable Isotope Analysis

Stable carbon and nitrogen isotope ratios of the organic fraction were measured on a Carlo Erba 1108 elemental analyzer coupled to a Thermo Finnigan Delta Plus XP isotope ratio mass spectrometer (EA-IRMS). Measurements of carbon and nitrogen stable isotopes were made on separate sub samples, since acid demineralization has been shown to alter $\delta^{15}N$ values (Schalcher & Connolly 2014). Samples were weighed (~0.5mg of demineralized shell

for $\delta^{13}C$ analysis and ~35mg of whole crushed shell for $\delta^{15}N$ analysis) and packed in 3x9 mm tin capsules. Within-run analytical error was assessed via repeated analysis of internal proteinaceous reference materials (Pugel and Acetanilide) and was estimated to be ±0.2‰ for both $\delta^{13}C$ and $\delta^{15}N$. Isotopes values are reported using delta (δ) notation in parts per thousand (‰): $\delta^{13}C$ or $\delta^{15}N = [(R_{sample}/R_{standard}) - 1]$, where R is the ratio of heavy to light isotope of the sample (R_{sample}) and standard ($R_{standard}$) respectively referenced to that of atmospheric N_2 (air) for $\delta^{15}N$ and Vienna PeeDee Belemnite (PDB) for $\delta^{13}C$.

3.2.4 Amino Acid Stable Isotope Analysis

Demineralized shell OM was analyzed for amino acid isotope analysis of nitrogen and carbon following established McCarthy Lab protocols (e.g. Batista *et al.*, 2014). Briefly, ~3 to 5 mg of bivalve demineralized shell was weighed into 8 mL hydrolysis vials, submerged in 1-2 mL of 6N HCl, purged with N_2 gas to remove oxygen, and hydrolyzed for 20 h at 110°C. After hydrolysis, samples were cooled to room temperature and stored in a -4°C freezer until further processing. Samples were then purified using cation-exchange chromatography with the DOWEX 50WX8-400 resin. Before dry down, purified filtrate was spiked with Norleucine as an internal standard.

$\delta^{15}N$-AA and $\delta^{13}C$-AA values were measured as trifluoroacetyl isopropyl ester (TFA-IP) derivatives. After drying hydrolysates at 60°C under N_2, amino acid isopropyl esters were prepared with a 1:4 mixture of acetyl chloride:isopropanol at 110°C for 60 min and then aceytlated using a 1:1 mixture of dichloromethane (DCM) and trifluoroacetic anhydride (TFAA) at 110°C for 10 min (Silfer et al. 1991). Samples were again dried and re-dissolved in ethyl acetate for amino acid analysis. AA isotopes values were measured using a Thermo Trace gas chromatograph coupled to a Finnegan Delta-Plus IRMS and GCC III (isoLink) at the University of California Santa Cruz Stable Isotope Laboratory (Santa Cruz, CA; https://sites.google.com/ucsc.edu/sil). Using this method, we measured $\delta^{15}N$ and $\delta^{13}C$ values

of the following AAs: alanine (Ala), glycine (Gly), threonine (Thr), serine (Ser), valine (Val), leucine (Leu), isoleucine (Ile), proline (Pro), aspartic acid (Asp), glutamic acid (Glu), phenylalanine (Phe), tyrosine (Tyr), and lysine (Lys). All samples were analyzed in triplicate. Measured $\delta^{13}C_{AA}$ values were corrected for the carbon added during derivatization following the approach of Silfer et al. (1991) and Hare et al. (1991). Final isotope value accuracy and reproducibility was checked in two ways: 1) by comparison of the internal Norleucine standard with its known values, and 2) by assessing values of an internal IAS reference material (cyanobacteria), analyzed with every sample set according to McCarthy Lab protocols. Reproducibility, as estimated with standard deviation for samples was typically less than < 0.3 ‰ (range: 0.0−0.6 ‰) for carbon and <0.5‰ (range: 0.1−1.0 ‰) for nitrogen.

3.2.5 Amino-acid diagenetic tests and statistics

Degradation Index is a quantitative approach for directly relating the reactivity of organic material, as indicated by changes in amino acid composition (Dauwe et al. 1999). The heterogenous composition (i.e. amino acid molar abundance) of shell protein can potentially lead to selective preservation of more stable (or less available) molecular compounds. While Dauwe and subsequent authors have applied DI to marine organic matter and interpreting excursions only in the negative direction as microbial degradation, we apply this technique to shells and infer any major excursion from modern shell as the benchmark in the negative or positive direction as indication of diagenesis or degradation:

$$DI = \Sigma \left[var_i - Avg.\ var_i / SD\ var_i \right] \times fac.coef \qquad (1)$$

where var_i is the original (non-normalized) mole percentage of amino acid, Avg. var_i and SD var_i are the mean and standard deviation of modern shells in our dataset and fac.coef is the factor coefficient for amino acid *i* (Dauwe et al. 1999).

In order to evaluate the preservation of $\delta^{15}N_{AA}$ metabolic patterns, we normalized measured $\delta^{15}N_{AA}$ values by subtraction from the average $\delta^{15}N$ (or $\delta^{13}C$) values of total

hydrolysable amino acids (THAA). This adjustment allows modern $\delta^{15}N_{AA}$ patterns to be directly compared to AA data from other time periods or depositional environments:

$$\text{Normalized } \delta^{15}N \text{ (or } \delta^{13}C) = \delta^{15}N \text{ AA} - \delta^{15}N \text{ THAA (or } \delta^{13}C \text{ THAA)} \quad (2)$$

where $\delta^{15}N_{THAA}$ (or $\delta^{13}C_{THAA}$) is the average of all measured AAs (Ala, Gly, Thr, Ser, Val, Leu, Ile, Pro, Asp, Glu, Phe and Lys).

Finally, an additional CSI-AA based degradation index, more specific to microbial alteration on amino acid isotope values, is the ΣV parameter, originally proposed by McCarthy et al. (2007). It is a $\delta^{15}N_{AA}$-based proxy for measuring total microbial AA resynthesis, and is based on the average deviation of individual $\delta^{15}N$ values of trophic amino acids from the mean $\delta^{15}N$ value of trophic amino acids. We calculated ΣV values here using seven trophic amino acids (Glu, Asp, Ala, Val, Leu, Ile, and Pro):

$$\Sigma V = 1/n\Sigma Abs(\chi i) \quad (3)$$

where χ is the deviation of each trophic AA = $\delta^{15}N_{AA}$ − Avg. $\delta^{15}N$ (Glu, Asp, Ala, Val, Leu, Ile, and Pro), and n is the number of amino acids used in the calculation.

CSI-AA based trophic level (TL_{CSIA}) was calculated as an additional check on two important AAs that are used in the equation: $\delta^{15}N_{Phe}$ and $\delta^{15}N_{Glu}$. We use the modified TL equation for molluscs. The original equation, TL_{CSIA}, is the algal-based approach proposed by Chikaraishi et al. 2009. Our $TL_{CSIA\text{-}mollusc}$ accounts for a different trophic discrimination factor (TDF) specific to mollusc soft tissue as well as an additional fractionation to shell matrix protein:

$$TL_{CSIA\text{-}mollusc} = 1 + [\ (\delta^{15}N_{Glu} - \delta^{15}N_{Phe} - \beta) / (TDF_{Glu\text{-}Phe} - \varepsilon_{shell})\ ] \quad (4)$$

where $\delta^{15}N_{Glu}$ and $\delta^{15}N_{Phe}$ represent the stable nitrogen isotope values of bivalve Glu and Phe, respectively, β represents the difference in $\delta^{15}N$ between Glu and Phe of primary producers (3.4‰ for aquatic cyanobacteria and algae; McClelland and Montoya 2002; Chikaraishi et al. 2009), $TDF_{Glu\text{-}Phe}$ 3.4‰ ($TL_{CSIA\text{-}mollusc}$; Vokhshoori et al. *in prep*), and ε_{shell} represents the observed fractionation (1.6‰) due to isotopic routing to the shell protein biomineral fraction.

Statistical analyses, t-tests, ANOVAs and PCAs, were performed in R (v.3.3.1) with RStudio interface (v.0.98.1028).

3.3 Results

3.3.1 Shell matrix protein yields

Sample yields were calculated as amount of acid insoluble protein recovered per gram of non-demineralized shell (Table 3.2). Modern sample yields were high. For every gram of crushed shell, average acid insoluble protein yield was 7.9 ± 0.7 mg/g (range 6.7 - 9.3 mg/g (*n* = 28). Archaeological shell protein recovery was more variable. Samples from all time periods from San Miguel Is. had the highest average yields (4.0 to 5.6 mg/g) and the lowest yields were from Anacapa (2.6 ± 1.1 mg/g), Santa Rosa (1.5 ± 0.7 mg/g) and Pt. Conception (2.4 ± 0.7 mg/g).

Table 3. 2 Bulk elemental information grouped by site/location.

		Shell Protein Yields (per gram)					Weight % Carbon					Weight % Nitrogen				C:N			
Location	Time Period	n	Mean	±	Max	Min	n	Mean	±	Max	Min	Mean	±	Max	Min	Mean	±	Max	Min
Santa Cruz	Modern	28	7.9	0.7	9.3	6.6	33	38.0	3.5	43.4	26.8	13.1	1.3	14.7	8.6	3.0	0.2	3.5	2.8
Pt. Conception	Historic	3	2.4	0.7	3.1	1.8	19	12.3	11.9	39.9	3.8	3.2	3.8	12.5	0.8	5.3	1.4	9.5	3.6
San Miguel Island	Historic	2	5.6	0.3	5.8	5.3	10	39.8	1.1	41.0	37.2	13.1	0.8	14.1	11.8	3.6	0.2	4.0	3.4
San Miguel Island	MLT	2	4.4	0.2	4.6	4.3	10	41.3	1.6	44.5	39.6	13.3	0.6	14.3	12.6	3.6	0.1	3.8	3.5
San Miguel Island	Late	5	4.0	1.4	5.5	1.8	20	34.6	12.2	45.3	3.3	10.2	4.0	14.2	0.8	4.1	0.6	5.7	3.5
Anacapa Island	Early - EZ	5	2.6	1.1	3.9	1.2	10	20.9	12.4	42.8	7.7	5.9	3.7	12.6	2.0	4.2	0.3	4.6	3.9
Santa Rosa Island	Early - Eyb	7	1.5	0.7	2.1	0.2	10	4.5	1.3	7.0	2.5	1.0	0.2	1.4	0.7	5.1	0.6	5.8	3.9

3.3.2 Elemental and bulk isotope values in shell matrix protein

Modern shell protein C:N ratios were the low compared to archaeological shell from all time periods and islands. Mean C:N ratios for modern shell protein as 3.0 ± 0.2, ranging from 2.8 to 3.5. Archaeological shell C:N ratios ranged from 3.4 to 9.5 and varied strongly across

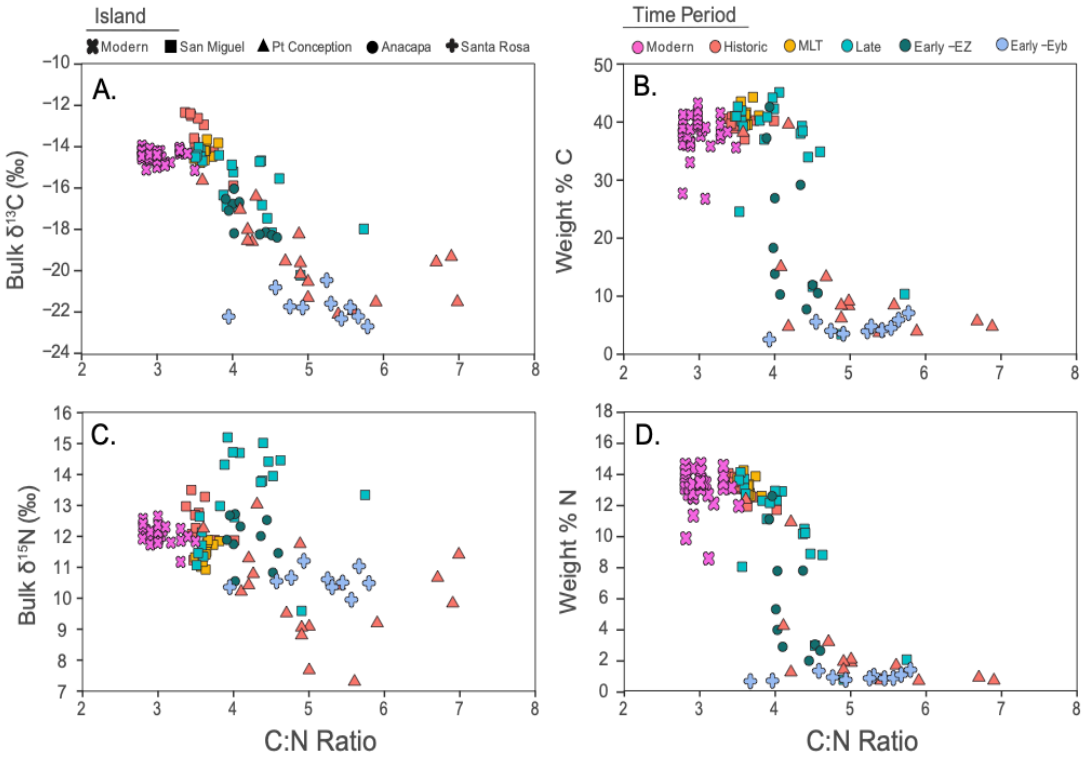

Figure 3. 1 Bulk isotope results organized by island (symbol shape) and time period (filled color); see legend on figure. Organic fraction C:N ratios of individual mussel shells plotted by A) bulk $\delta^{13}C$, B) weight %C, C) bulk $\delta^{15}N$ and D) weight %N.

different island depositional locations. The Pt. Conception and Santa Rosa sites had the highest mean C:N ratios, 5.3 ± 1.4 and 5.1 ± 0.2, respectively, followed by Anacapa, with average values of 4.2 ± 0.3. Finally, shells from the San Miguel Is. (Historic, MLT and Late Periods) site had the lowest C:N ratios, 3.8 ± 0.3.

Table 3. 3 Bulk isotopic information grouped by location/site.

			Bulk' $\delta^{13}C$ (‰)				Bulk $\delta^{15}N$ (‰)			
Location	**Time Period**	n	Mean	±	Max	Min	Mean	±	Max	Min
Santa Cruz	Modern	33	-14.5	0.3	-13.9	-15.1	12.1	0.3	12.6	11.2
Pt. Conception	Historic	19	-19.5	1.9	-15.6	-22.1	10.4	1.5	13.1	7.3
San Miguel Island	Historic	10	-13.5	1.1	-12.3	-15.9	12.5	0.7	13.5	11.2
San Miguel Island	MLT	10	-14.3	0.4	-13.7	-14.8	11.5	0.3	11.9	10.9
San Miguel Island	Late	20	-15.8	1.7	-14.0	-20.2	13.2	1.5	15.2	9.6
Anacapa Island	Early - EZ	10	-17.4	0.9	-16.0	-18.4	11.9	0.7	12.7	10.5
Santa Rosa Island	Early - Eyb	10	-21.8	0.7	-20.5	-22.7	10.6	0.4	11.2	10.0

Bulk $\delta^{13}C$, weight %C (wt%C), bulk $\delta^{15}N$ and weight %N (wt %N) all showed consistent decreases with increasing C:N values (Tables 2 and 3, Fig. 1). For $\delta^{13}C$ values, regression of $d^{13}C$ vs. C:N was significant in archaeological shell (P < 000.1, R^2=0.63) (Fig. 1a), in contrast modern $\delta^{13}C$ values showed no trend with C:N (P = 0.41, R^2= 0.0) and range of values were also narrow (-15.1 to -13.9‰). $\delta^{13}C$ values from all sites had a narrow range (2‰), except for Late Period San Miguel Is. (-20 to -14‰) and Historic Pt. Conception (-22 to -15‰). Wt %C also displayed a significant negative correlation with C:N (P < 000.1, R^2 = 0.60), while again within modern shell alone the regression was not significant (P = 0.80, R^2 = 0.0) (Fig. 1b). However, while $\delta^{13}C$ decreased linearly, the wt %C data show a bimodal distribution (Fig. S1a), where one group centered around 40% wt %C and the second group around 10%.

Bulk $\delta^{15}N$ values also significant negative trend with C:N, however far weaker than that observed for $\delta^{15}N$ (P = 0.0001, R^2 = 0.13). In addition, there was also a very weak but significant trend in the modern group (P = 0.03, R^2 = 0.15) (Fig. 3.1c). Wt %N showed a similar significant regression with C:N ratio to wt %C (Fig. 3.1d) (P<0.0001; R^2 = 0.71), also displaying a bimodal distribution where most data around 14 wt %N, and a second smaller group of data clustered around 3 wt %N (Fig. S1b). Finally, the relationship between bulk $\delta^{15}N$ values and wt %N yield was also significant (P = 0.008, R^2 = 0.26), with the modern group again not have any significant trend when analyzed independently (P= 0.7).

Weight percent organic recoveries were also a significant driver of isotope values (Fig. 2). For both carbon and nitrogen, as wt % decreased, $\delta^{13}C_{bulk}$ values also decreased (R^2= 0.78, P<0.0001), as did $\delta^{15}N_{bulk}$ values, however with far more variation and weaker regression (R^2= 0.26, P<0.0001). Overall, we found wt %C and wt %N both show a strong correlation with C:N ratios, where both carbon and nitrogen yields decreased to much lower concentrations below a C:N threshold of ~ 4 (Fig. 3.1). At the lowest end of organic yields, stable isotope values clearly also shift (Fig. 3.2). For carbon, shells with less than ~20% C show clear and linear decreases in $\delta^{13}C$ values, while for nitrogen, as with almost all data described above, trends are far less clear, however $\delta^{15}N$ values are more erratic at less than ~ 4% N.

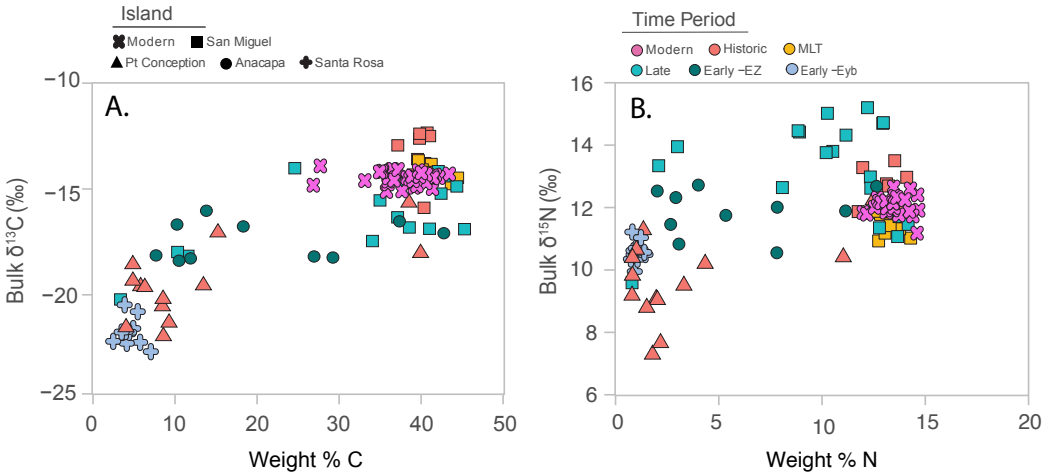

Figure 3. 2 Elemental weight percent and bulk isotope values, A) Weight %C versus bulk $\delta^{13}C$ and B) weight %N versus bulk $\delta^{15}N$, organized by island (symbol shape) and time period (filled color); see legend on figure.

A principle component analysis (PCA) synthesizes the main variables driving difference in the bulk dataset in statistical space (Fig. 3.2). Our five input variables were: $\delta^{13}C$ values, $\delta^{15}N$ values, wt %C, wt %N and C:N ratios. PCA showed shell samples clustered according to island. However, within this general pattern data from some sites/ islands were tightly clustered (Modern, San Miguel Is. Historic and MLT, Santa Rosa), while others showed far more scatter (Anacapa, Pt. Conception) (Fig. 3). The first principle component explained 79.8% of the variance and separated the older shells (Anacapa and Santa Rosa) from the more recent time period shells, with the exception of shells from Pt. Conception (Historic period). The second principle component explained 13.2% of the variance and separated Modern shells from San Miguel Is. (Historic and Late period). A total of 93% of the variance was explained by the first two axes. $\delta^{15}N_{bulk}$ had the longest vector length reflecting highest contribution in building the ordination of PC 2 axis. Wt %C and $\delta^{13}C$ variables directly overlapped, reflecting a strong covariance/correlation of the two variables. The near orthogonal angle between $\delta^{15}N_{bulk}$ with all the other variables, suggests that $\delta^{13}C$, wt %C and C:N are generally uncorrelated with $\delta^{15}N_{bulk}$ change. Moreover, parallel but opposing of wt %C and $\delta^{13}C_{bulk}$ vectors with C:N reflects a strong negative correlation.

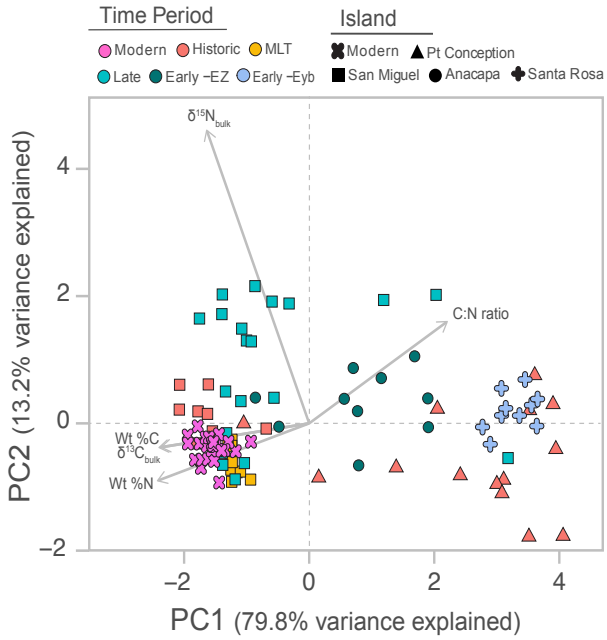

Figure 3. 3 Principle component analysis of bulk isotope and elemental results ($\delta^{13}C$, $\delta^{15}N$, weight %C, weight %N and C:N ratio) of modern and archaeological shells (see legend for time periods and island). Values in parentheses are the percentage variation accounted by the first and second principal components. The first principal component (PC1) separates modern and San Miguel Is. from the other sites, and the second principal component (PC2) separates San Miguel Is. (Late) from the rest of the sites. The vector lengths show that $\delta^{15}N$ and C:N were the most important variables for explaining variations in the first two PCs.

3.3.3 NaOH clean test

A subset of insoluble protein fractions from archeological shell of varying C:N ratios were treated with 0.125M NaOH (see methods) to test for potential removal of contamination from lipids, terrestrial matter and/or humics, which could cause lower than expected $\delta^{13}C_{bulk}$ values and/or higher than expected C:N ratios. Results were plotted as the difference between treatment and non-treated fractions by subtraction of Post-NaOH from Pre-NaOH values for $\delta^{13}C_{bulk}$, wt %C, $\delta^{15}N_{bulk}$ and wt %N against C:N ratio (Fig.4). In general, “improvement” (i.e. a shift in values toward this expected for modern shell, e.g., increased wt % and decreased C:N ratios) from NaOH treatment was variable (Fig.4). In general, starting sample mass may have

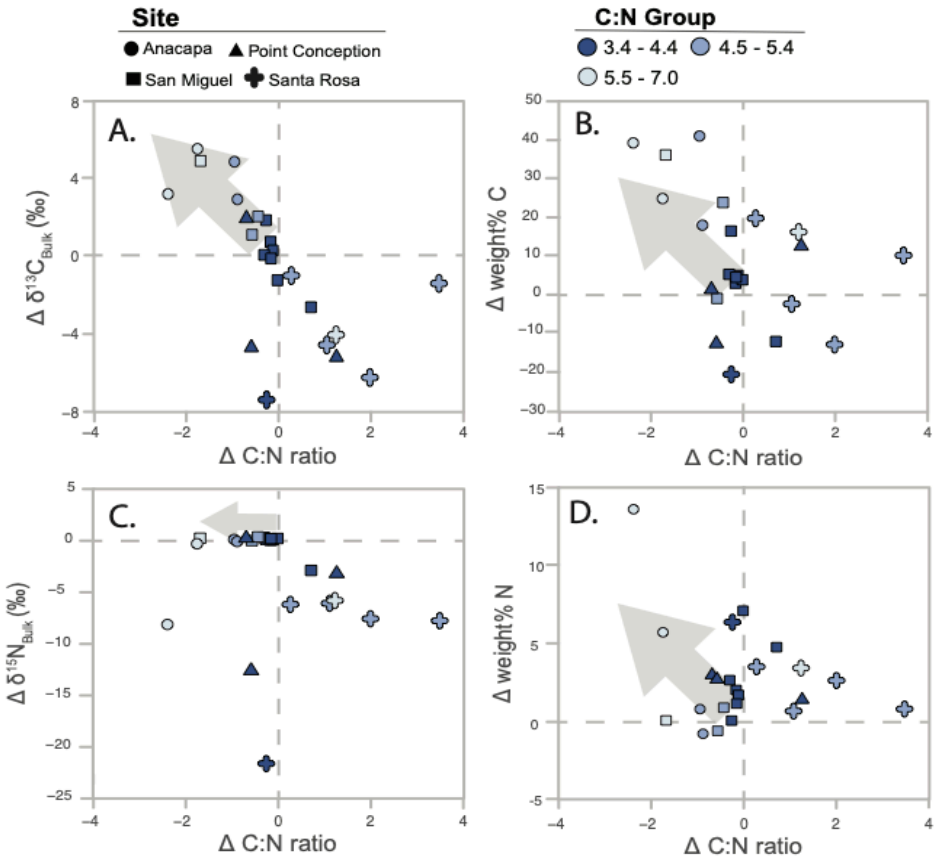

Figure 3. 4 Bulk isotope and elemental results between Pre- and Post- treatment with 0.125M NaOH to test potential contaminant compounds (e.g. lipids and humics; see Methods) in shells. Figures show the difference of post-treatment subtracted from pre-treatment for A) bulk $\delta^{13}C$, B) Weight %C, C) $\delta^{15}N_{bulk}$ and D) Weight %N plotted by difference in C:N ratio, organized by island (symbol shape) and C:N group (filled color); see legend on figure. Dotted lines indicate intersection of no change for reference and grey arrow, also for reference, indicates direction of "improvement". Where improvement is change from the treatment in the direction of modern, unaltered shell protein values, i.e. wt% C=40%, wt%=15%, C:N=3, $\delta^{13}C$ values become less negative and $\delta^{15}N$ values don't change.

altered the outcome of the result for some of these shells (Fig. 3.5, Fig. 3.S2). Figure 5 compares sample mass with the difference in our elemental and isotopic results and clearly shows that samples that were less than ~400µg show dramatic deterioration, C:N increased and weight %C and N and $\delta^{13}C$ decreased. This is especially noticeable in the change in $\delta^{15}N$ values, there was an exponential decrease in isotope values with decreasing sample mass. For those shells whose C:N ratios decreased, wt %C and $\delta^{13}C_{bulk}$ increased, while $\delta^{15}N_{bulk}$ values did not change.

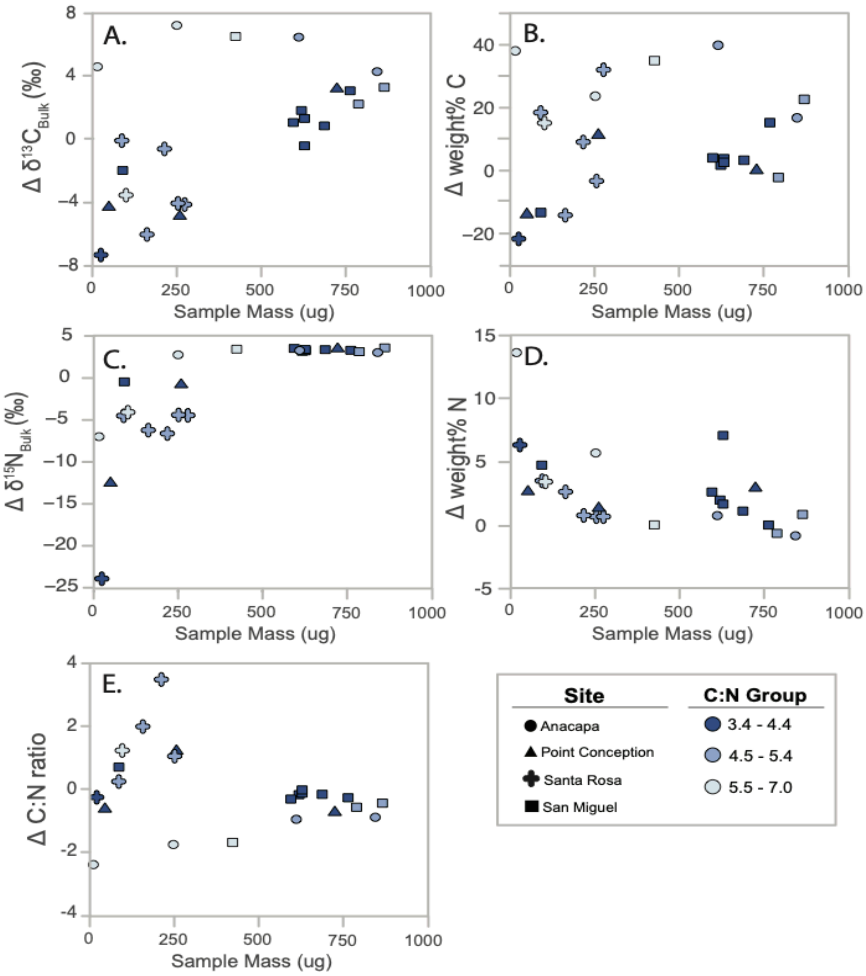

Figure 3. 5 Influence on sample mass on NaOH cleaning test results. Figures show the difference of post-treatment subtracted from pre-treatment for A) bulk $\delta^{13}C$, B) Weight %C, C) $\delta^{15}N_{bulk}$ and D) Weight %N plotted by starting sample mass(µg), organized by island (symbol shape) and C:N group (filled color); see legend on figure.

3.3.4 Amino acid Molar abundance distribution

Relative molar abundance data for modern and archaeological shells were grouped based on progressive decreases in their C:N ratio (2.5–3.3, 3.4–4.3, 4.4–5.4, 5.5–7.0) (Fig. 3.6a). In all modern and archaeological shell, Ala and Gly were the two most abundant AAs, followed by Ser and Asp, irrespective of C:N ratio. However, in contrast Ala and Gly mol% progressively decreased with increasing C:N ratios. Compared to modern mol% of Gly, Group 4.4-4.5 and 5.5-7.0 were also distinct (ANOVA, $F_{3,20} = 27.74$, $P<0.0001$). Ser mol% was different in all three

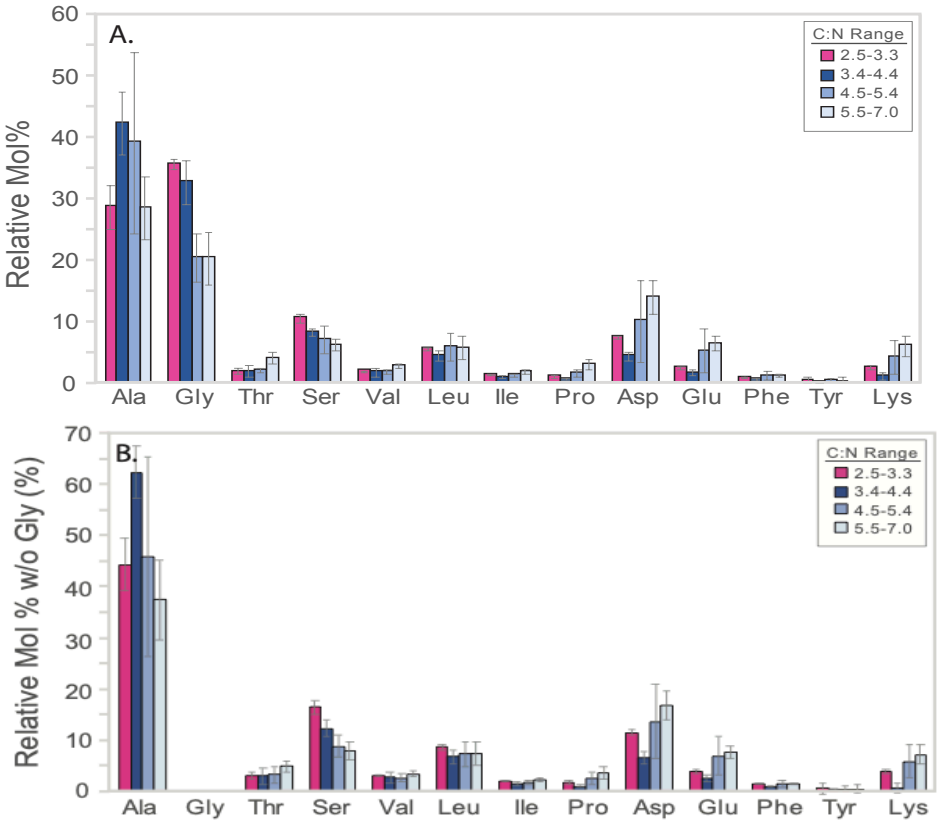

Figure 3.6 Molar abundance of each individual shell sample of glycine and alanine to demonstrate relative change with increasing C:N, organized by C:N group 2.5 - 3.4 (Modern; n = 4), 3.5 - 4.4 (n = 9), 4.5 – 5.4 , 5.5 – 7.0 for A) glycine, B) alanine (without glycine),

groups compared to modern ($F_{3,20}$ = 11.15, P = 0.0001). In Group 5.5-7.0 Pro Mol% was different from modern (Tukey HSD t-test $P < 0.01$), as was Glu ($P < 0.05$) and Lys ($P < 0.05$). Amino acid molar distributions showed similar pattern changes with higher C:N ratios when normalized with and without Glycine (Fig. 3.6b): Specifically, Ala and Ser decreased with increasing C:N, while Asp and Lys increased.

Finally, we also more closely examined the molar abundance changes of the two most abundant amino acids, Gly and Ala across the data set, to understand how these mol% values shifted with increasing C:N ratio (Fig. 3.7). Since our molar abundance data is relative to the AAs measured, as above we calculated Ala mol% abundance with and without Gly, to look at possible Ala mol% change independently. Mol% Gly steeply declines from values characteristic

of modern shell when C:N ratios are higher than ~4.5. In contrast, mol% Ala *increases* with increasing C:N initially, relative to modern shell values, then falls levels similar or lower to modern values in shells with C:N ratios 5.5 or higher. The ratio of Ala:Gly reflects these changes. Ala is lower than Gly in modern, fresh shell protein (Ala:Gly ~0.8) but increases in the archaeological shells (Ala:Gly 1.0 to 2.5).

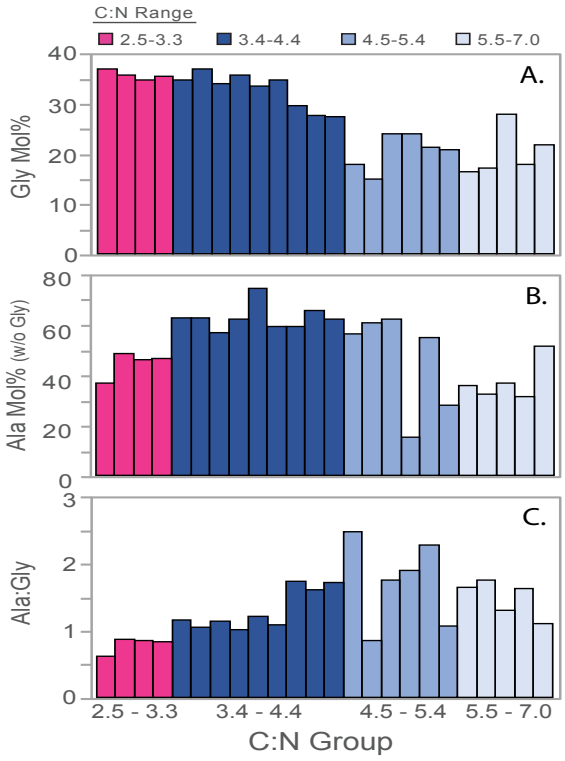

Figure 3.7 Molar abundance of each individual shell sample of glycine and alanine to demonstrate relative change with increasing C:N, organized by C:N group 2.5 - 3.4 (Modern; n = 4), 3.5 - 4.4 (n = 9), 4.5 – 5.4 , 5.5 – 7.0 for A) glycine, B) alanine (without glycine), and C) the ratio of Ala to Gly (Fig. 6A)

3.3.5 Normalized amino acid carbon and nitrogen isotope values

Amino acid carbon and nitrogen isotope values were normalized to $\delta^{13}C_{THAA}$ and $\delta^{15}N_{THAA}$, respectively and then plotted in terms of C:N grouping defined above (Fig. 8). Measured non-normalized averages can be found in Tables 5 and 6. This normalization to THAA removes the influence of potential baseline changes, allowing direct comparison of AA

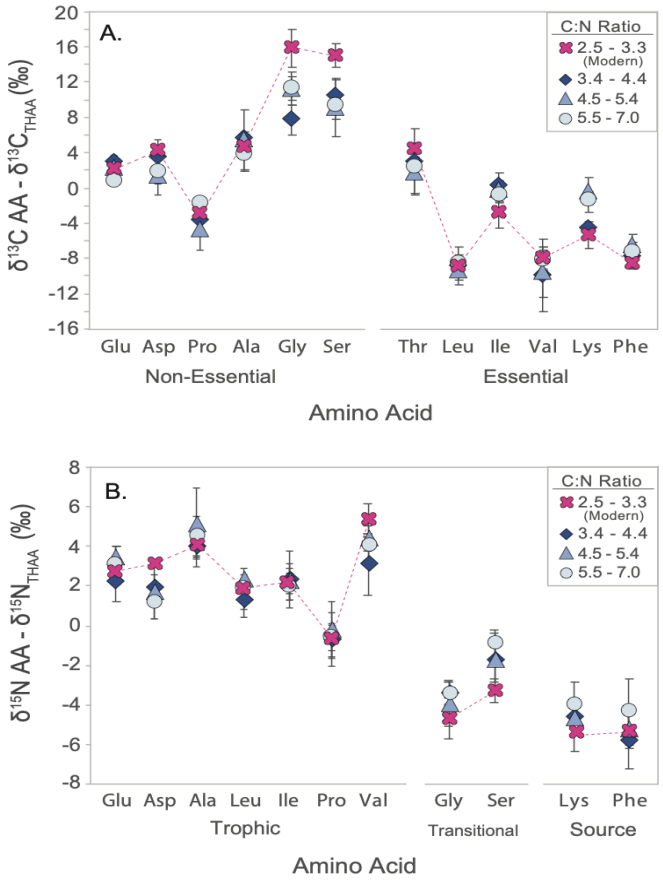

Figure 3.8 Normalized A) $\delta^{13}C_{AA}$ and A) $\delta^{15}N_{AA}$ values in shell matrix protein of *Mytilus californianus* grouped by the C:N ratio. Normalization is by the subtraction of $\delta^{15}N_{THAA}$ or $\delta^{13}C_{THAA}$ (where THAA is the average of Ala, Gly, Thr, Ser, Val, Leu, Ile, Pro, Asp, Glu, Phe, Lys. C:N groupings are as follows: 2.5 - 3.4 (Modern; n = 4), 3.5 - 4.4 (n = 9), 4.5 – 5.4 (n = 5), 5.5 – 7.0 (n = 6). Dotted line follows the mean value of modern shell. Error bars indicate ±1 standard deviation.

biosynthetic *patterns* between modern/unaltered shell and archaeological shell. In contrast with the bulk record, there were few differences in the carbon and nitrogen AA patterns in either modern or archaeological across the C:N groupings examined. In the carbon record (Fig. 8a), for the non-essential amino acids (NAA) the largest differences were observed, with $\delta^{13}C_{Gly}$

and $\delta^{13}C_{Ser}$ the most offset between normalized archaeological shell vs. modern data, with $d^{13}C$ values more negative for both AA. Specifically, when compared to modern patterns, within range C:N 3.4-4.4 , the $\delta^{13}C_{Gly}$ was significantly lower by 8.2‰ (Tukey HSD t-test *P*=0.001), in C:N 4.5-5.4 range $\delta^{13}C_{Ser}$ was 6.0‰ lower and $\delta^{13}C_{Asp}$ 2.9‰ lower (*P*=0.04 and *P*=0.02), and in C:N range 5.5-7.0 $\delta^{13}C_{Asp}$ was 2.5 ‰ lower (*P*=0.05). In contrast, the essential amino acids (EAA) patterns were far more similar: $\delta^{13}C_{Ile}$ was statistically ~2.5‰ higher in from modern in two C:N ranges (3.4 - 4.4 and 4.5 - 5.4 ; *P*<0.001). There was also a weak difference in $\delta^{13}C_{Lys}$ values were 5‰ higher in one C:N group (4.4 - 5.4 ; *P*=0.02) relative to modern.

$\delta^{15}N$ amino acid isotope patterns between modern and archeological shell also showed little difference (Fig. 3.6b). Two consistent differences were observed: $\delta^{15}N_{Asp}$ values were always lower in archaeological shell compared to modern (2.3 to 2.6 ‰) and $\delta^{15}N_{Ser}$ values were slightly higher (0.7 to 1.1‰) than modern. Statistically, C:N group 5.4-7.0 showed the most differences compared to modern in the following AAs: $\delta^{15}N_{Thr}$ (*P*=0.01), $\delta^{15}NS_{er}$ (*P*=0.02) and $\delta^{15}N_{Asp}$ (*P*=0.02). C:N group 3.4-4.4 also showed some differences, although weaker, in $\delta^{15}N_{Thr}$ (*P*=0.04) as well as $\delta^{15}N_{Val}$ (*P*=0.02). Notably, however, there were no significant differences in $\delta^{15}N_{Glu}$ and $\delta^{15}N_{Phe}$, two AAs that are used in ecological isotope proxies for reconstructing Trophic Level and $\delta^{15}N_{baseline}$ (Vokhshoori et al. *in review*).

3.3.6 Amino acid based diagenetic parameters

We calculated a number of specific metrics for degradation and diagenesis, including $mol\%_{AA}$, DI and ΣV parameters. The widely used Degradation Index (DI; eqn. 1), a measure of characteristic AA mol% shifts away from “fresh” organic matter with degradation in marine environments (Dauwe et al. 1999). Here, DI was defined in terms of changes based on modern shell matrix protein “starting” abundances (Fig. 3.9; Methods section 2.5). Multiple shell specimens were indicated as highly “degraded” via the DI index; however, this DI data did not fall out clearly as a function of C:N ratios (Fig. 3.9). Santa Rosa Is. samples had the highest

overall DI values (2 or greater). In contrast, shells from the Pt. Conception site, while having the highest C:N ratios, showed no DI excursion away from modern values.

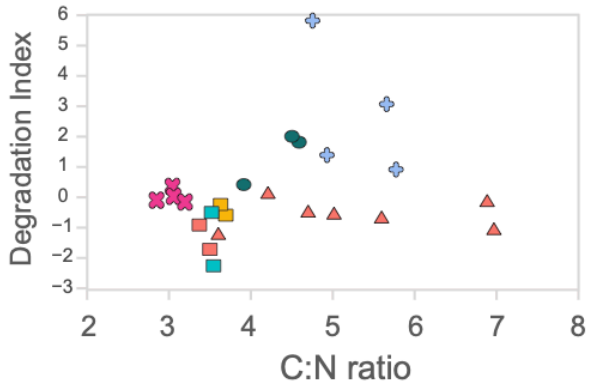

Figure 3.9 Degradation index of amino acid molar abundance (see Methods for calculation) versus C:N ratio grouped by site (symbols) and time period (filled colors).

For $\delta^{13}C_{AA}$ we tested the relationship between mol% adjusted NAA (Fig. 3.10a) and EAA (Fig. 3.10b) with C:N ratio. Mol% adjusting, meaning the isotope value is weighted to the percent abundance of that AA, can potentially test if shifts on $\delta^{13}C_{bulk}$ values is driven by the isotopic composition from NAAs, EAAs or both. We found a significant decreasing trend in $\delta^{13}C_{NAA}$ values ($R^2 = 0.34$, $P = 0.0017$), but not in $\delta^{13}C_{EAA}$ values ($R^2 = 0.08$, $P=0.184$) with C:N ratio.

For $\delta^{15}N_{AA}$ we also examined ΣV, TL_{CSIA} and $\delta^{15}N_{phe}$ vs $\delta^{15}N_{bulk}$. The microbial resynthesis index, ΣV of all archaeological shells fell close to the range of Modern ΣV values (Fig. 3.11a): modern ΣV ranged between 1.2 to 1.6 while archaeological shells were on average 1.4 ± 0.3 (range from 0.9 to 1.9). TL_{CSIA} showed a similar tight range, with values also similar to those in modern shell (Fig. 3.11b), where TL_{CSIA} of modern shells ranged between 1.8 and 2.0 while archaeological shells were on average 1.9 ± 0.2 and ranged from 1.6 to 2.3, excluding

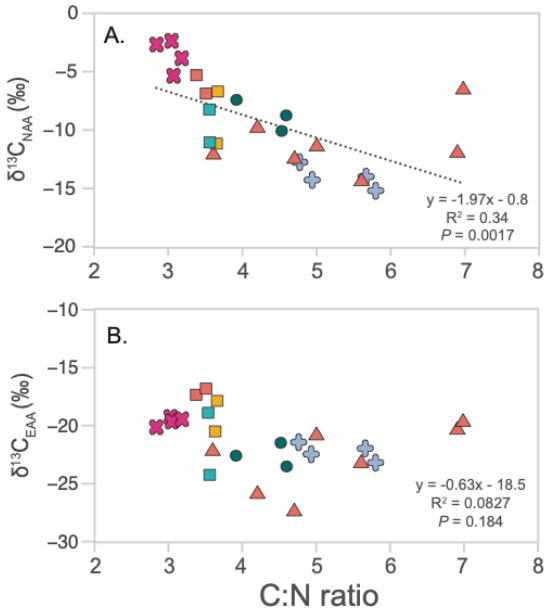

Figure 3.10 Mean mol% adjusted A) $\delta^{13}C$ of the non-essential amino acids (NAA; Ala, Gly, Ser, Asp, Pro and Glu) and B) $\delta^{13}C$ of the essential amino acids (EAA, Thr, Val, Leu, Ile, Phe and Lys) versus C:N ratio grouped by site (symbols) and time period (filled colors) and the dotted line is the linear regression of the data, equation, R^2 and p-value noted on the figure.

two outlying values that fell outside of the ±0.4 propagated error, one from Pt. Conc. (1.5) and Late Period San Miguel Is (2.5). We also tested the preservation of $\delta^{15}N_{Phe}$ values, our proxy for $\delta^{15}N_{baseline}$ values, and again found no trend with C:N ratios.

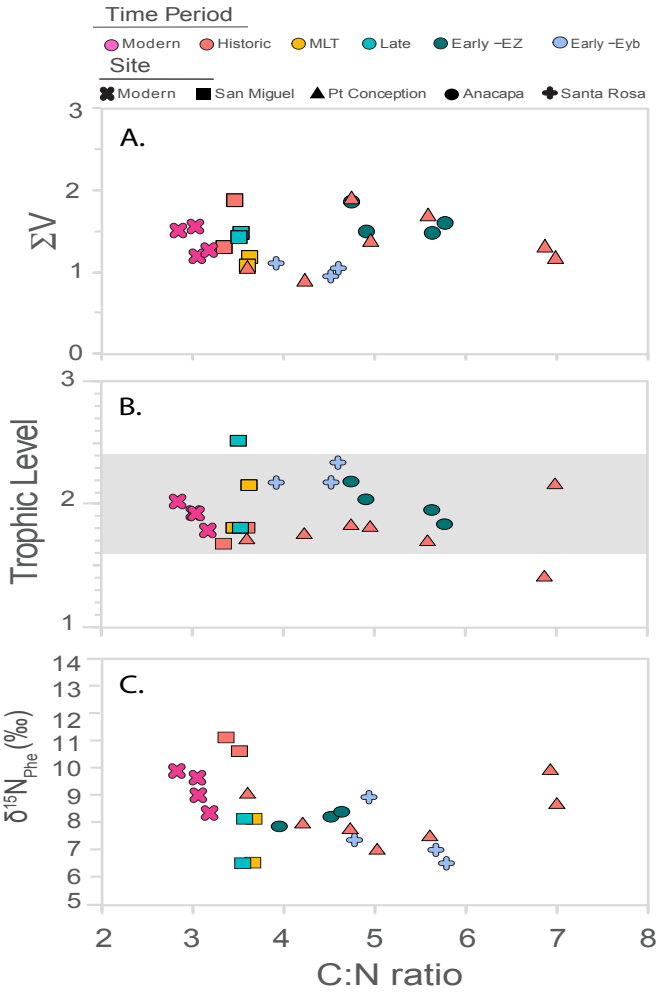

Figure 3.11 Nitrogen parameters as additional checks for testing the preservation of isotope values. A) ΣV is the microbial synthesis index, values that hover between 1 and 2 suggest no alteration to the average $\delta^{15}N$ values of trophic AAs. B) Trophic Level is a basic check on two key amino acids, Glu and Phe, used in the TL calculation, where the grey shading indicates ± 0.4 error propagated error in the calculation. TL estimations that fall outside of this range are might altered in their $\delta^{15}N_{glu}$ and/or $\delta^{15}N_{phe}$ value. And C) $\delta^{15}N_{phe}$ our proxy for $\delta^{15}N_{baseline}$ values, also shows no trend with C:N indicating good preservation of this proxy.

3.4 Discussion

This study investigates the bulk and amino acid isotope patterns in the acid insoluble fraction of shell matrix protein of archaeological bivalve shells from a suite of time periods and depositional environments. We first explore how diagenesis may have altered the organic fraction of our shells at the elemental and molecular level (e.g. weight %C and %N, mol%$_{AA}$),

and then evaluate possible effects on our isotope records in the context of a number of established diagenetic parameters. Diagenetic alteration to bulk isotope values in structural proteins such as bone and shell is well-documented (Ambrose & Norr 1992, O'Donnell 2003), and was significant in our dataset (Fig. 3.1). There are several mechanisms that drive this alteration including physical processes, chemical reactions, and biological resynthesis (Mitterer 1993, Macko et al. 1994). However, fidelity of the CSI-AA record is largely underexplored within the acid insoluble fraction of archaeological shell; most CSI-AA research has focused on the molecular characterization and isotope patterns in the soluble protein fraction of fossil shell (Weiner 1975, Weiner 1983, Robbins & Ostrom 1995, Penkman et al. 2008) with particular focus on comparison of D- and L- enantiomers of amino acid isotope signatures (Engel et al. 1994, Silfer et al. 1994, O'Donnell et al. 2007). These two organic fractions in the shell matrix have different organic concentrations (Hudson 1967), organic composition and AA molar distribution (Kobayashi & Somata 2006, Marie et al. 2007) as well as preservation potential (Sykes et al. 1995, Penkman et al. 2008), and thus should be considered separately. In archaeological bioarchives, where the insoluble protein fraction is more readily preserved than in fossil shells, prior work suggests preservation of isotope values from CSI-AA is more promising (Misarti et al. 2017) and can overcome the obstacle of diagenesis in the bulk isotope record. We also test the possibility of exogenous contamination as a possible cause for elemental and isotopic excursions in bulk material (Ambrose 1990).

3.4.1 Mechanisms of diagenesis in archaeological shell matrix protein

Shell protein matrix can undergo significant alteration over time due to physical processes, chemical reactions and biological resynthesis (Mitterer 1993, Macko et al. 1994, Sykes et al. 1995). Our archaeological shell samples underwent a range of diagenetic alteration based on several indicators that most closely correlated with C:N ratios. For this reason, we compare a suite of paleo-proxies and diagenetic parameters to this "master variable" C:N ratio.

Organic matter yields lower than modern (~8mg/1g shell) clearly indicates removal of shell matrix protein relative to inorganic components, however it does not indicate if this removal is physical or biological. The major physical processes to affect protein concentrations in shell are leaching and contamination. Leaching and contamination have opposite effects on the amino acid concentration and composition. Leaching decreases amino acid concentrations, while contamination has the potential to increase amino acid concentrations. Fundamentally, however, leaching and contamination are caused by the same mechanism; water infiltrates the permeable pores of the shell and mobilizes indigenous organic compounds. This intruding aqueous phase not only can remove organic compounds from the shell matrix, but it can also introduce exogenous compounds from surrounding sediments, or depositional environment (Sykes et al. 1995). While our archaeological shells did show progressively decreasing OM yields, it still does not fully negate the possibility of contamination, which we discuss further, below (section 4.2). Acid dissolution for the organic content of mollusc shell yields two fractions, soluble (5-10%) and insoluble (90-95%) organic content (Hudson 1967). The soluble fraction is thought to be bound within the *intra*-crystalline matrix (Crenshaw 1972) and the insoluble fraction is found in the *inter*-crystalline shell matrix. Under diagenetic conditions, such as leaching or chemical hydrolysis from water inflow, the *inter*-crystalline matrix is more susceptible to loss of amino acids and/or exchange of organic material from the surrounding environment, i.e. contamination of the indigenous organic material within the shell; while the *intra*-crystalline matrix is largely protected from this exposure. This is why the soluble protein is best preserved and used in fossil molluscs, and also explains the loss in the insoluble sample material in our dataset.

We also explored the possibility of biological degradation using a number of complimentary parameters. We first examined shifts in the CSI-AA based ΣV parameter (Fig. 3.9; McCarthy et al. 2007), widely used in testing bacterial degradation of organic matter in marine systems. This parameter has been proposed as specific for microbial resynthesis, even if total quantities of AA remain unchanged, and is based on $\delta^{15}N$ values of the trophic amino

acid groups. Since trophic AAs fractionate in predictable magnitudes and patterns with trophic transfer (e.g. McClelland & Montoya 2002), deviations from well-known patterns are due bacterial reworking (McCarthy et al. 2007, Calleja et al. 2013, Batista et al. 2014), producing ΣV values > ~2. Using modern shells as a benchmark for ΣV value of "fresh, unaltered" shell protein, the observation that archaeological shell ΣV was within the same range as modern shells suggests that bulk property shifts in degraded shells are not a function of microbial resynthesis of most proteins. Further, microbial reworking of organic matter typically leaves an obvious fingerprint in amino acid molar composition. For example, *increased* Gly concentrations have long been recognized as a hallmark of bacterial degradation of marine OM (Dauwe et al., 1999; Yamashita and Tanoue, 2003; Kaiser and Benner, 2009). In our data, however, the fact that Gly mol% *decreased* extensively supports the conclusion from ΣV that shell protein alteration, even in the most degraded shells, was not a microbial source.

While physical removal from leaching or chemical hydrolysis potentially explains the total loss of organic material (i.e. protein yield, weight %C and weight %N), it does not readily explain why $\delta^{13}C$ values dramatically decrease with C:N ratio increase, or (to a lesser extent) $\delta^{15}N$ values shifts with C:N changes. In order for the bulk isotope values and C:N ratios to change there must be selective loss of certain AAs within the organic content.

If selective loss of certain compounds is the main mechanism for bulk changes in shell matrix protein, this then poses the question of how altered the remaining biomolecules are. Insoluble organic matter in shells is primarily composed of silk-like proteins rich is glycine and alanine and a small percentage of saccharides in the form of chitin or its monomer glucosamine (Kobayashi & Samata 2006, Marie et al. 2007, Agbaje et al. 2018; Fig. 6a). An individual matrix is thought to be composed of an inner layer of chitin, bounded by silk-like insoluble proteins on which are bound the acidic soluble matrix material (Weiner et al. 1983), having a physical structure somewhat like a sandwich (Risk et al. 1997). Even if there was major loss of proteins (C:N ~ 3.0), it would also have to be substantial enough such that the isotopic and molecular

difference in chitin composition (C:N ~ 6) remaining would overwhelm the signal. However, given that saccharides make up less than 1% of the insoluble organic content (Agbaje et al. 2018), this explanation seems very unlikely.

The explanation for the strong decrease we observed in Gly mol% is not fully clear. We note that analogous CSI-AA measurements on sub-fossil deep-sea proteinaceous corals recently found a very similar trend of strongly decreased Gly, but minor ΣV or other AA changes (Glynn et al. *in prep*). These authors hypothesized loss of Gly was from spontaneous aqueous decarboxylation, a well-known chemical reaction that cleaves the C-N bond via abiotic hydrolysis. This decarboxylation hypothesis is consistent with prior NMR spectra data of fossil shells investigating the insoluble organic matrix, showing that C-N functional groups in proteins show most pronounced diminishment (Risk et al. 1997).

Another possibility is selective loss of certain AAs (Macko et al. 1994), similar to what we observe for Gly. As noted above, relative molar abundance distributions showed a 56% decrease in Gly mol% with increasing C:N (Fig. 3.6a), and also a clear decrease in Ala (even if Gly was removed from the calculation; Fig. 3.6b), such that mol% ratio of Ala:Gly shifts from 0.8 in modern shell, up to 2.5 in archaeological shells (Fig. 3.7). Given such large changes, it might be hypothesized that loss of Gly, Ala, and to a lesser extent Ser (Fig. 3.6) could be responsible for the dramatic change in bulk $\delta^{13}C$ values and C:N ratios, as demonstrated in fossil bone collagen (Tuross et al. 1988).

The $\delta^{13}C$ values of these amino acids, together with their mol% changes, supports this idea. In decreasing order mol% Gly, Ala, Ser and Asp are the four most abundant amino acids; they also have the highest relative $\delta^{13}C$ values, where Gly and Ser $\delta^{13}C$ values are markedly higher than the rest (Fig. 3.8).Using Gly as an example for how much influence it can have on bulk values, a simple calculation of THAA $\delta^{13}C$ values normalized to $mol\%_{AA}$ shows a 3.1‰ ± 1.2 decrease in $\delta^{13}C_{THAA}$ values when Gly is completely removed. Our study did not measure absolute molar abundance, so we can only speak to relative change in our dataset. Regardless,

it is clear that if shell matrix protein is almost wholly composed of silk-like proteins rich in Gly and Ala, that the bulk isotope changes observed could largely result from a substantial loss of these AAs. To our knowledge, these are novel results, as this is the first study to use CSI-AA data to directly investigate the impact of molecular level changes on bulk isotope values in insoluble ancient mollusc shell, and they strongly suggest that that changes in abundance of only a few AA, likely via physical and/or chemical alteration, may drive most change observed in bulk properties.

3.4.2 Diagenesis or contamination?

Contamination from humics, lipids and/or terrestrial C_3 plants can in fact drive C:N ratios to increase, and $\delta^{13}C$ values to decrease in archaeological samples (Ambrose1990). However, without molecular level data it is not possible to distinguish between this and impacts of compositional shifts from diagenetic alteration, since both mechanisms could produce similar elemental and isotopic signals (discussed in earlier section 4.1).

Unfortunately, “contamination” is difficult to rule out, as it depends on assuming efficacy of a specific cleaning protocol used. As noted above, our shells were exhaustively cleaned using established methods (Misarti et al. 2017). However, in order to further examine if additional exogenous organics might have survived these protocols to substantially influence our results, we then applied a further “cleaning” to a subset of shells using weak NaOH (Ambrose 1990). This approach should be particularly effective at mobilizing humic or fulvic acids. Comparing the results of the two datasets (Fig. 3.4), we hypothesize that if bulk parameters in further NaOH cleaned shell consistently shift toward expected modern shell values, this would indicate that contaminants were not removed by the standard cleaning and could be a key overlooked factor.

Overall, however, our results produced no clear pattern or shifts to suggest that contamination of base-soluble organics is not a main driver of decreasing isotope values (Fig.

3.1). Our benchmark for “improvement” in each parameter (Fig. 3.4) was essentially a change in values toward those characteristics of modern shells. More specifically, modern shell weight %C and weight %N are 35-40% and 15%, respectively; and C:N ratios range from 2.8 to 3.5. For isotopes, it is more problematic to define “improvement” in this way, especially for historical samples, since it’s unknown what the isotope value should be without *a priori* detailed background information. However, we nevertheless compared how isotope values shifted in relation to expected modern values.

Our results were variable, largely a function of the shell’s depositional environment. We found that shells from San Miguel Is. that already had low, nearly “fresh” C:N ratios (<3.8), did not change significantly in response to the NaOH cleaning. However, shells from Anacapa Is. did change substantially, typically improving into an acceptable range (C:N ratios decreased from ~6 to ~4 or less, wt %C increased from ~10% to 30-40%, concomitantly, $\delta^{13}C$ values increased). This comparison suggests that shells from Anacapa Is. likely experienced a higher degree of contamination intruded from the surrounding depositional environment and suggests that the NaOH protocol could be a very clear method to remove exogenous contamination. However, in contrast to these two relatively clear outcomes, shells from Santa Rosa Is. and Pt. Conception in all parameters were much “worse” (i.e. values moved away from expectations for fresh/modern shell; C:N ratios increased, wt %C decreased and $\delta^{13}C$ values also decreased).

Finally, however, our data also suggests that starting sample mass may have had an important effect on both bulk and elemental results (Fig. 3.5, Fig S2). For isotope analysis of the “Pre-cleaned” sample set, sample weights were all higher than 400µg, whereas with the “Cleaned” samples, due to having to split existing samples, some were much less than this, as low as 150µg. While standards were weighed out to bracket even the lower mass range, consistent relationships observed with most parameters suggest sample amounts may have been too low for reliable instrument detection in many cases.

If we consider only “cleaned” shells with a starting sample mass greater than 400µg, the results produced no change for shells that were already “reliable” and improvement for shells that had high C:N ratios. These shells with originally high C:N ratios dropped down into more acceptable C:N ranges (Fig. 3.5). Therefore, for any bulk analyses we suggest following the protocol proposed by Ambrose (1990) by including the NaOH cleaning step to remove contaminants from shells while not altering the isotope value of shells that are not contaminated, and to a sample mass of at least 400 µg. While Ambrose (1990) specifically attributes observed bulk isotopic changes in archaeological bone collagen, also rich in Gly as those we observe in our shells, to predominantly exogenous contamination, our molecular level data suggests that loss of ^{13}C-enriched AAs is driving the major decrease in $\delta^{13}C_{bulk}$ values and increased in C:N ratios.

3.4.3 Is it possible to determine when bulk isotope values are reliable?

Together, our results suggests that C:N is the most diagnostic indicator of preserved bulk isotope values. Overall, our bulk and cleaning data support the conclusions of Ambrose (1990), for determination of reliable bulk isotope values. There are several indicators for assessing the quality of an archaeological sample including wt %C, wt %N and C:N ratios.

Taken together, our results suggest, $\delta^{13}C$ and $\delta^{15}N$ values in bivalve shell can be reliably accepted with C:N ratios of less than 4.0. While modern shells range from 2.8 to 3.5, it appears that minor degradation of shell protein content doesn’t have a strong impact on the isotope values. This evidence comes from Ambrose (1990) recommended a similar, but slightly lower C:N value (3.6) as the cutoff for ancient bone collagen. While there are some similarities between these structural proteins, e.g. Gly the most abundant AA in both proteins, there are also some major differences. For example, collagen protein is an α-helix structure where shell protein is b-pleated sheets, certain terminal AAs are likely more exposed in one protein matrix over the other. Also, bone collagen is rich in lipids, labile compounds, and also those

susceptible to exogenous contamination. An incomplete removal of lipids from purified collagen will certainly drive C:N ratios to be much higher, and $\delta^{13}C$ values to be much lower.

Variations in bulk isotope values can also be a function of environmental changes. Our data set does span over nearly 7,000 years and spatially dynamic covering inshore and offshore oceanographic processes (Fig. S3). Regional sediment core record from the northern CA margin (Addison et al. 2018) and locally from Santa Monica Basin (Balestra et al. 2018) covering the Holocene do show $\delta^{13}C$ and $\delta^{15}N$ excursions in sediment organic matter. However, these excursions were small in comparison to range in isotope values we found in our bulk dataset (Fig. 3.1). Regional sediment core record of CA margin found a 1‰ shift in $\delta^{13}C_{org}$ values, and locally in the Santa Monica Basin, $\delta^{13}C$ values showed a 3‰ range over 7,000 years. In contrast, our $\delta^{13}C$ values exhibited a 10‰ range and was significantly correlated with C:N ratios. Despite likely shifts in our isotope record due to environmental signals, the range in values due to environmental perturbations is clearly not as dramatic as the observed linear decrease in $\delta^{13}C$ values we observe in our dataset. Overall, however, our dataset demonstrates the need for close examination of bulk and elemental data measured of archaeological specimens as critical for assessing potential diagenetic alterations.

3.4.4 Preservation of amino acid isotope record

Early data has suggested that even in cases where bulk properties are strongly altered, CSI-AA isotope patterns may retain intact, representing a possible way to bypass limitations in bulk properties for degraded samples. As noted above, the archaeological shells in this study were from a range of time periods and depositional environments (Table 1). Bulk properties show clearly that over time the shells underwent varying degrees of a diagenesis, and also some shells were potentially contaminated with humics and/or lipids. Here we look at several AA-based parameters for qualifying if CSI-AA produces reliable isotope results in shells whose bulk isotope values are diagenetically altered.

The almost identical overall CSI-AA patterns for carbon and nitrogen between modern and the different archaeological shells grouped by C:N ratio showed that in contrast to bulk parameters, CSI-AA data appears to almost unaffected by degradation and diagenesis, at least over the range of conditions indicated by these shell samples (Fig. 8). We note that this conclusion is based on normalized CSI-AA patterns. We normalize to THAA in order to remove shifting baseline isotope signals and allows for direct comparison of biosynthetic AA patterns between groups.

For $\delta^{13}C_{AA}$ data, the observation that the AA pattern showed no statistical differences between EAAs in modern vs. archaeological shell strongly supports this conclusion. In contrast the greater differences in NAA (Gly, Ser and Asp) is not unexpected since these AAs showed larger changes in $mol\%_{AA}$ (Fig. 3.6). The direction of isotopic change is notable as well. As explained above (section 4.1), among the most likely mechanisms shifting archaeological shell composition are physical leaching and abiotic chemical reactions. Together with the preferential loss of abundant AAs (i.e. Gly), there also seems to be a preferential loss of ^{13}C-enriched molecules in those same AAs. $\delta^{13}C_{Gly}$ and $\delta^{13}C_{Ser}$ have the highest carbon isotope values, so preferential physical loss of those AAs (i.e. leaching) would decrease bulk isotope values, but compounding that effect is likely hydrolysis breaking peptide bonds into smaller peptides or free AAs and/or defunctionalization (decarboxylation) where there is a loss of amino acid functional groups (Mitterer 1993), that is removing ^{13}C-enriched compounds and resulting in Gly and Ser about 4‰ more negative than modern normalized $\delta^{13}C$ values.

We therefore investigated whether these low, diagenetically altered AAs affected average $\delta^{13}C_{NAA}$ and $\delta^{13}C_{EAA}$ values. For $\delta^{13}C_{AA}$, preservation of carbon isotope values in the essential amino acids are the most important for biogeochemical proxies, since this group best records baseline production $\delta^{13}C$ values (Shen et al. 2021, Vokhshoori et al. *in review*). Further, $\delta^{13}C_{EAA}$ can also be used to “fingerprint” primary producer types at the base of a food web (Larsen et al. 2013, Vokhshoori et al. 2014), or quantify the combination food resources

of a consumer's diet (Stock and Semmens 2016). Therefore, we evaluated the trend between mol% adjusted $\delta^{13}C_{NAA}$ and $\delta^{13}C_{EAA}$ values and C:N ratios (Fig. 10).

As expected, $\delta^{13}C_{NAA}$ significantly decreased with increasing C:N, but the $\delta^{13}C_{EAA}$ did not, confirming that $\delta^{13}C_{EAA}$ signatures are well-preserved, even in much older shells. This observation is consistent with the fact that the most degraded AAs, (i.e. those with substantial decreases in mol%) are all NAAs.

For $\delta^{15}N_{AA}$ biosynthetic pattern, the fact that archaeological shells also closely match the average modern pattern (Fig. 8) strongly supports a similar conclusion. Following the same logic, if leaching of Gly results in more negative $\delta^{13}C_{bulk}$ values, then it's relatively low $\delta^{15}N$ values would have an increased net effect on $\delta^{15}N_{bulk}$ values. However, it is also harder to connect mechanistically the patterns in $\delta^{15}N_{AA}$ to that observed in the $\delta^{15}N_{bulk}$ record in our data. While we found a significant decreasing trend in $\delta^{15}N_{bulk}$ with C:N ratios, most $\delta^{15}N$ values were tightly clustered by site (Fig.1c). Instead of clearly "decreasing" $\delta^{15}N$ values, it appears $\delta^{15}N_{bulk}$ values become more erratic at higher C:N ratios. This high variability in $\delta^{15}N$ values with high C:N ratios has also been observed in bone collagen (Ambrose1990) and fossil mollusc shell O'Donnell et al. 2003).

Finally, we also looked at other N parameters to assess preservation of key amino acids used in reconstructing certain ecological proxies: ΣV, TL and $\delta^{15}N_{baseline}$. As discussed above (section 4.1), the ΣV parameter of the archaeological shells tightly clustered around modern values. This suggests that there were no major isotopic alterations in the trophic AAs associated with microbial resynthesis. Regarding the fidelity of $\delta^{15}N$ values in two key AAs, Glu and Phe, we calculated TL using a mollusc-specific TL equation (Vokhshoori et al. *in review*). We found archaeological shell TL values fell within the error of reliable TL estimations, with the exception of a couple samples (SMI-481 B5 and Dune1 S2). We also evaluated isotope values based on the correlation of $\delta^{15}N_{Phe}$ and C:N ratios and found no trend indicating $\delta^{15}N_{phe}$ is reliable for $\delta^{15}N_{baseline}$ reconstructions.

Overall, it's difficult to determine if variable $\delta^{15}N$ values are a function of weight %N (Fig. 3.2) or progressive loss of certain AAs. We did not observe major differences in Ala or Gly with respect to their $\delta^{15}N$ value (Fig. 3.8). While prior work has been done to artificially degrade shells by exposing them to various temperatures and chemicals, this largely focused on AA concentrations on the *soluble* protein fraction (Sykes et al. 1995, Penkman et al. 2008). Future work could artificially degrade shells with specific intentions of measuring CSI-AA in the *insoluble* shell protein fraction. This could address isotopic shifts with loss of certain AAs for both carbon and nitrogen.

3.5 Conclusions

This research lays the foundation for using bivalve shell and other mollusc invertebrates as bioarchives at coastal archaeological sites for addressing paleo-environmental and paleo-ecological questions that might not otherwise been possible with traditional bulk isotope methods. We investigated the fidelity of isotope signatures in the insoluble shell matrix protein of archaeological mollusc shells, with specific focus on preservation of isotope signals from compound-specific isotopes of amino acids. In bulk isotopes, it is challenging to disentangle sources signals from trophic effects, and in ancient archives there is the compounded challenges of diagenesis. Our data showed that incorporating an additional NaOH base cleaning step to remove potential contaminants can improve most shell's bulk values, while not altering the isotope values of non-contaminated shells. In addition, our data indicates that where bulk isotope values were diagenetically altered, especially for $\delta^{13}C$, both $\delta^{13}C_{AA}$ and $\delta^{15}N_{AA}$ patterns, values, and proxy reconstructions were well preserved, even in the most degraded shell samples. There were a few exceptions; $\delta^{13}C_{Gly}$ and $\delta^{13}C_{Ser}$ and $\delta^{13}C_{Asp}$ values seemed to be altered, likely contributing to lower than average bulk $\delta^{13}C$ values in degraded shells. However, these three AAs are all non-essential AAs. In contrast, average $\delta^{13}C_{EAA}$ values showed no alteration with C:N ratios, indicating that common CSI-AA baseline

and primary production fingerprinting applications can be reliably reconstructed. With $\delta^{15}N_{AA}$, preservation of $\delta^{15}N$ values were observed across all AAs. Our N-based parameters (e.g. ΣV, TL, $\delta^{15}N_{Phe}$ vs $\delta^{15}N_{bulk}$) clearly demonstrated that key AAs used in paleo-proxies for trophic level and baseline nitrogen reconstructions are preserved.

Overall, CSI-AA signals were very well preserved in even the most degraded shell samples, as indicated by most altered C:N ratios, whereas bulk isotopes signals were dramatically altered. With CSI-AA becoming increasingly available and the developments of ecological proxies, bivalves as bioarchives presents an entirely new realm in paleo-climatological research for studying how past changes in climate affected nearshore ecosystem structure specific to that local geographic region. Potential for new information includes not only bypassing the limitations of degradation in bulk isotope work, but also applying the rapidly expanding potential of CSI-AA proxies for determining specific changes in coastal production, nutrient sources, plankton assemblages, and biogeochemical cycling of both C and N. Based on NMR data, Risk and co-authors (1997) found insoluble organic matter intact from bivalve shells as old as 37,000 years. This suggests highly detailed, local coastal climatological records can be reconstructed anywhere mollusc shells are preserved.

Acknowledgements

Fieldwork for this project was supported by Channel Islands National Park and The Nature Conservancy. We are thankful for the generosity of Santa Barbara Natural History Museum for supplying the archaeological shells in this study. We also thank the Santa Ynez Band of Chumash Indians Elders Council for consultation related to this project. We thank Dyke Andreasen and Colin Carney (UCSC-SIL) for assisting with bulk isotopic analyses, and deeply grateful to Stephanie Christensen for assistance with CSI-AA analysis and always making sure the instruments were humming. This study was supported by National Science Foundation (BCS 2115154 and 2115145 to T.R. and M.D.M).

References

Agbaje, O.B.A.; Ben, S.I.; Zax, D.B.; Schmidt, A.; Jacob, D.E. Biomacromolecules within bivalve shells: Is chitin abundant? Acta Biomater. 2018, 80, 176–187

Ambrose SH. 1990. Preparation and characterization of bone and tooth collagen for isotopic analysis. Journal of Archaeological Science 17: 431–451.

Ambrose SH, Norr L. 1992. On stable isotopic data and prehistoric subsistence in the Soconusco region. Current Anthropology 33(4): 401–404.Baker, P. 1995. Review of ecology and fishery of the Olympia oyster, Ostrea lurida with annotated bibliography. Journal of Shellfish Research 14:501–518

Andrus, C. F. T. 2011. Shell midden sclerochronology. Quat. Sci. Rev. 30, 2892–2905.

Batista, F. C., A. C. Ravelo, J. Crusius, M. A. Casso, and M. D. McCarthy. 2014. Compound specific amino acid δ15N in marine sediments: a new approach for studies of the marine nitrogen cycle. Geochimica et Cosmochimica Acta 142:553–569.

Calleja M. L., Batista F., Peacock M., Kudela R. and McCarthy M. D. 2013. Changes in compound specific delta N-15 amino acid signatures and D/L ratios in marine dissolved organic matter induced by heterotrophic bacterial reworking. Mar. Chem. 149, 32–44.

Chikaraishi Y, Ogawa NO, Kashiyama Y, Takano Y, Suga H, Tomitani A, Miyashita H, Kitazato H, Ohkouchi N (2009) Elucidation of aquatic food-web structure based on compound-specific nitrogen isotopic composition of amino acids. *Limnology & Oceanography: Methods*. **7**, 740–750.

Choy, C. A., B. N. Popp, C. Hannides, and J. C. Drazen. 2015. Trophic structure and food resources of epipelagic and mesopelagic fishes in the North Pacific Subtropical Gyre ecosystem inferred from nitrogen isotopic compositions. Limnology and Oceanography 60:1156–1171.

Crenshaw M. A. 1972. The soluble matrix from Mercenaria mercenaria shell. Biomin. 6, 611.

Dauwe, B., Middelburg, J. J., Herman, P. M. J., and Heip, C. H. R.(1999) Linking diagenetic alteration of amino acids and bulk organic matter reactivity, Limnol. Oceanogr., 44, 1809–1814,

Engel, M.H., Goodfriend, G.A., Qian, Y.R., Macko, S.A. 1994. Indigeneity of organic-matter in fossils-a test using stable-isotope analysis of amino-acid enantiomers in Quaternary mollusk shells. Proceedings of the National Academy of Sciences of the United States of America 91, 10475–10478.

Erlandson JM, Rick TC, Braje TJ, Casperson M, Culleton B, Fulfrost B, Garcia T, Guthrie DA, Jew N, Kennett D, Moss ML, Reeder L, Skinner C, Watts J, Willis L. 2011. Paleoindian seafaring, maritime technologies, and coastal foraging on California's Northern Channel Islands. Sci (331) 6021: 1181–1185

Glynn, D., M.D. McCarthy. *in prep*. Preservation of fossil deep sea coral proteinaceous skeleton, bulk and compound-specific amino acid C and N isotope paleo-proxies on multi-millennial timescales.

Hare, E. P., Fogel, M. L., Stafford, T. W., Mitchell, A. D., and Hoering, T. C. 1991. The isotopic composition of carbon and nitrogen in individual amino acids isolated from modern and fossil proteins. Journal of Archaeological Science 18, 277–292.

Hattan SJ, Laue TM, Chasteen ND (2000) Purification and characterization of a novel calcium-binding protein from the extrapallial fluid of the mollusc, Mytilus edulis. J Biol Chem 276, 4461–4468

Hudson J. D. (1967) The elemental composition of the organic fraction, and the water content of some recent and fossil mollusc shells. Geochim. Cosmochim. Acfa 31, 2361-2378.

Kaiser, K. and Benner, R.(2009) Biochemical composition and size distribution of organicmatter at the Pacific and Atlantic times-series stations. Mar. Chem., 113, 63–77

Kobayashi, I. & Samata, T. 2006 Bivalve shell structure and organic matrix. Mater. Sci. Eng. C 26, 692–698. (doi:10.1016/j.msec.2005.09.101)

Larsen T., Ventura M., Andersen N., O'Brien D. M., Piatkowski U. and McCarthy M. D. 2013. Tracing carbon sources through aquatic and terrestrial food webs using amino acid stable isotope fingerprinting. PLoS ONE 8, e73441.

LeBlanc, C. 1989. Terrestrial input to estuarine bivalves as measured by multiple stable isotopes tracers. PhD diss., McMaster University. 201 pp.

Lehmann, M. F., Bernasconi, S. M., Barbieri, A., and McKenzie, J. A. (2002) Preservation of organic matter and alteration of its carbon and nitrogen isotope composition during simulated and in situ early sedimentary diagenesis, Geochim. Cosmochim. Ac., 66(20), 3573–3584, 2002.

Leng, M.J., Lewis, J.P. 2016 Oxygen isotopes in Molluscan shell: Applications in environmental archaeology, Environmental Archaeology, 21:3, 295-306,

Macko, S. A., M. L. Fogel-Estep, M. H. Engel, and P. E. Hare. 1987. Isotopic fractionation of nitrogen and carbon in the synthesis of amino acids by microorganisms. Chemical Geology 65:79-92.

Marie B, Luquet G, Pais De Barros J-P, Guichard N, Morel S, Alcaraz G, Bollache L & Marin F (2007) The shell matrix of the freshwater mussel Unio pictorum (Paleoheterodonta, Unionoida). Involvement of acidic polysaccharides from glycoproteins in nacre mineralization. FEBS J 274, 2933–2945

McCarthy MD, Benner R, Lee C, Fogel ML (2007) Amino acid nitrogen isotopic fractionation patterns as indicators of heterotrophy in plankton, particulate, and dissolved organic matter. *Geochimica et Cosmochimica Acta.* **71**, 4727– 4744.

McClelland JW, Montoya JP (2002) Trophic relationships and the nitrogen isotopic composition of amino acids in plankton. *Ecology*. **83**, 2173–2180.

McMahon, K. W., T. P. Guilderson, O. A. Sherwood, T. Larsen, and M. D. McCarthy. 2015c. Millennialscale plankton regime shifts in the subtropical North Pacific Ocean. Science 350:1530–1533

Misarti N, Gier E, Finner B, Barnes K, McCarthy M (2107) Compound-specific amino acid $\delta^{15}N$ values in archaeological shells: Assessing diagenetic integrity and potential for isotopic baseline reconstruction. Rapid Commun. Mass. Spectrom. 31:1881-1891.

Mitterer, R.M., 1993. The diagenesis of proteins and amino acids in fossil shells. In: Engel, M.H., Macko, S.A. (Eds.), Organic Geochemistry. Plenum Press, New York, pp. 739–753.

O'Donnell TH, Macko SA, Chou J, Davis-Hartten KL, Wehmiller JF. 2003 Analysis of δ13C, $\delta^{15}N$, and $\delta^{34}S$ in organic matter from the biominerals of modern and fossil Mercenaria spp. Org. Geochem. 34, 165–183. (doi:10.1016/S0146- 6380(02)00160-2)

O'Donnell, T. H., S. A. Macko & J. Wehmiller. 2007. Stable carbon isotope composition of amino acids in modern and fossil Merce- naria. Org. Geochem. 38:485–498.

Ohkouchi, N., Chikaraishi, Y., Close, H. G., Fry, B., Larsen, T., Madigan, D. J., McCarthy, M. D., McMahon, K. W., Nagata, T., Naito, Y. I., Ogawa, N. O., Popp, B. N., Steffan, S., Takano, Y., Tayasu, I., Wyatt, A. S. J., Yamaguchi, Y. T., & Yokoyama, Y. (2017). Advances in the application of amino acid nitrogen isotopic analysis in ecological and biogeochemical studies. Organic Geochemistry, 113, 150–174.

Ostrom, P.H., Zonneveld, J.P. & Robbins, L.L. (1994) Organic geochemistry of hard parts – Assessment of isotopic variability and indigeneity. Palaeogeography, Palaeoclimatology, Palaeoecology, 107, 201–212

Penkman, K. E. H., Kaufman, D. S., Maddy, D. & Collins, M. J. 2008 Closed-system behaviour of the intra-crystalline fraction of amino acids in mollusc shells. Quat. Geochronol. 3, 2–25

Prendergast, A.L., Stevens, R.E. 2014. Molluscs (Isotopes): Analyses in Environmental Archaeology. In: Smith C. (eds) Encyclopedia of Global Archaeology. Springer, New York, NY. https://doi.org/10.1007/978-1-4419-0465-2_2162

Robbins, L. L. & P. H. Ostrom. 1995. Molecular isotopic and bio- chemical evidence of the origin and diagenesis of shell organic material. Geology 23:345–348.

Schlacher TA, Connolly RM (2014) Effects of acid treatment on carbon and nitrogen stable isotope ratios in ecological samples: a review and synthesis. Methods in Ecology and Evolution, 5, 541–550.

Shen, Yuan, Thomas P. Guilderson, Owen A. Sherwood, Carmen G. Castro, Francisco P. Chavez, and Matthew D. McCarthy. 2021. "Amino Acid Δ13C and Δ15N Patterns from Sediment Trap Time Series and Deep-Sea Corals: Implications for Biogeochemical and Ecological Reconstructions in Paleoarchives." Geochimica et Cosmochimica Acta 297: 288–307. https://doi.org/10.1016/j.gca.2020.12.012.

Sherwood, O. A., Guilderson, T. P., Batista, F. C., Schiff, J. T., & McCarthy, M. D. 2014. Increasing sub-tropical North Pacific ocean nitrogen fixation since the Little Ice Age. Nature, 505, 78–81. https://doi. org/10.1038/nature12784

Silfer, J. a., Engel, M. H., Macko, S. a., and Jumeau, E. J. 1991. Stable carbon isotope analysis of amino acid enantiomers by conventional isotope ratio mass spectrometry and combined gas chromatography/isotope ratio mass spectrometry. Analytical Chemistry 63, 370–374.

Silfer, J.A., Qian, Y., Macko, S.A., Engel, M.H., 1994. Stable carbon isotope compositions of individual amino acid enantiomers in mollusk shell by GC/C/IRMS. Organic Geochemistry 21 (6/7), 603–609.1065

Stock, B.C., Semmens, B.X. (2016) MixSIAR GUI User Manual.https://doi.org/10.5281/zenodo. 47719. https://github.com/brianstock/MixSIAR/, Version 3.1.

Tuross, N., Fogel, M. L. & Hare, P. E. (1988). Variability in the preservation of the isotopic composition of collagen from fossil bone. Geochimica et Cosmochimica Acta 52, 929–935.

Vanderklift MA, Ponsard S (2003) Sources of variation in consumer-diet ^{15}N enrichment: a meta-analysis. Oecologia 136:169−182

Vander Zanden, M. J. and Rasmussen, J. B. 1999. Primary consumer $\delta^{13}C$ and $\delta^{15}N$ and the trophic position of aquatic consumers. - Ecology 80: 1395-1404.

Vokhshoori NL, McCarthy MD. 2014. Compound-specific $\delta^{15}N$ amino acid measurements in littoral mussels in the California upwelling ecosystem: a new approach to generating baseline $\delta^{15}N$ isoscapes for coastal ecosystems. *PLoS oNE* **9**:e98087.

Vokhshoori, N.L., T. Larsen, M.D. McCarthy. 2014. Reconstructing $\delta^{13}C$ isoscapes of phytoplankton production in a coastal upwelling system with amino acid isotope values of littoral mussels. Mar Ecol Prog Ser 504:59−72

Vokhshoori, N. L., McCarthy M. D., Close H. G., Demopoulos A. W. J., & Prouty N. G. (2021). New geochemical tools for investigating resource and energy functions at deep-sea cold seeps using amino acid δ15N in chemosymbiotic mussels (Bathymodiolus childressi). Geobiology, 00, 1–17. https://doi.org/10.1111/gbi.12458

Vokhshoori, N.L, Rick, T., Braje, T., McCarthy, M.D. (*in review*) Calibrating bulk and amino acid $\delta^{13}C$ and $\delta^{15}N$ isotope ratios between bivalve soft tissue and shell for paleoecological reconstructions

Weiner S, Hood L (1975) Soluble protein of the organic matrix of mollusk shells: a potential template for shell formation. Science 190, 987–988

Weiner S (1983) Mollusk shell formation: isolation of two organic matrix proteins associated with calcite deposition in the bivalve *Mytilus californianus*. Biochemistry 22, 4139–4145.

Yamashita, Y.; Tanoue, E. (2003) Chemical characterization of a protein like fluorophores in DOM in relation to aromatic amino acids. Mar. Chem. 82, 255-271

Table 3.4 Average relative molar abundance grouped by site/location

		Relative Molar Abundance (%)																							
Location	**Time Period**	**n**	Ala	±	Gly	±	Thr	±	Ser	±	Val	±	Leu	±	Ile	±	Pro	±	Asp	±	Glu	±	Phe	±	Lys	±
Santa Cruz	Modern	4	28.6	3.6	35.6	0.9	1.9	0.4	10.6	0.7	2.0	0.0	5.5	0.3	1.3	0.1	1.0	0.3	7.4	0.3	2.5	0.3	0.9	0.1	2.5	0.3
Pt. Conception	Historic	7	37.0	12.0	23.8	4.4	3.0	1.8	6.9	0.9	2.1	0.8	4.0	0.9	1.3	0.7	2.3	1.5	9.9	5.1	4.6	2.3	0.9	0.4	4.0	2.7
San Miguel Island	Historic	2	40.1	1.0	35.8	1.5	2.7	0.7	8.7	0.3	1.5	0.3	4.0	0.7	1.0	0.1	0.6	0.0	4.0	0.2	1.2	0.2	0.4	0.0	NA	NA
San Miguel Island	MLT	2	37.7	1.8	34.8	1.2	2.4	0.6	8.7	0.7	1.7	0.1	5.2	0.3	1.2	0.1	0.6	0.1	5.1	0.3	1.5	0.2	0.6	0.1	0.6	NA
San Miguel Island	Late	2	39.9	2.1	34.0	0.9	1.7	1.5	8.4	0.5	2.6	1.3	5.2	0.1	0.9	0.3	0.6	0.0	4.6	0.4	1.6	0.0	0.6	0.0	NA	NA
Anacapa Island	Early - EZ	3	45.3	2.5	25.0	2.0	1.6	0.2	6.6	0.3	2.0	0.1	5.4	0.5	1.2	0.2	1.1	0.2	5.3	1.3	3.0	0.8	0.9	0.2	2.1	0.8
Santa Rosa Island	Early - Eyb	4	28.8	13.2	16.6	1.3	3.0	0.8	6.8	2.8	2.3	0.9	7.8	1.9	1.6	0.4	2.3	0.4	15.2	5.1	7.4	2.8	1.5	0.6	6.5	2.1

Table 3.5 Average amino acid $\delta^{13}C$ values grouped by site/location

			Amino Acid $\delta^{13}C$ (‰)																							
Location	**Time Period**	n	Ala	±	Gly	±	Thr	±	Ser	±	Val	±	Leu	±	Ile	±	Pro	±	Asp	±	Glu	±	Phe	±	Lys	±
Santa Cruz	Modern	4	-9.4	1.0	-1.8	2.5	-9.6	0.6	1.0	1.7	-21.9	1.5	-22.8	0.4	-16.8	2.1	-17.0	0.4	-9.7	0.7	-12.0	1.1	-22.5	0.4	-19.3	1.2
Pt. Conception	Historic	7	-12.2	2.5	-6.4	3.2	-16.9	4.3	-11.5	5.1	-27.7	4.5	-27.7	3.0	-16.7	6.3	-21.3	3.7	-15.7	4.4	-16.2	1.9	-24.7	1.2	-19.0	2.4
San Miguel Island	Historic	2	-8.0	0.9	-4.9	1.3	-8.8	0.2	0.8	1.2	-21.6	0.6	-21.6	1.4	-12.9	0.3	-16.4	1.6	-9.2	1.1	-9.8	1.5	-22.0	1.0	-21.2	0.2
San Miguel Island	MLT	2	-9.0	1.1	-9.8	5.2	-11.4	2.4	-2.7	4.0	-25.5	1.9	-21.6	0.8	-13.5	0.6	-16.5	1.0	-10.7	1.6	-10.9	1.1	-22.3	0.8	-19.5	1.8
San Miguel Island	Late	2	-10.7	0.6	-9.3	3.6	-11.9	4.1	-3.9	3.3	-23.7	4.8	-24.3	0.2	-15.6	1.7	-18.1	2.0	-11.4	0.4	-12.0	1.4	-23.7	1.4	-19.1	1.5
Anacapa Island	Early Period EZ	3	-10.3	2.0	-4.6	1.6	-12.9	2.5	-4.6	2.3	-27.2	3.2	-26.3	1.1	-16.3	0.7	-22.7	2.5	-13.9	1.0	-14.0	1.1	-23.8	0.2	-18.8	3.6
Santa Rosa Island	Early Period Eyb	4	-15.2	1.1	-8.5	0.8	-16.1	1.5	-8.2	1.9	-26.1	1.1	-26.4	0.9	-18.9	0.8	-21.4	0.8	-18.0	1.2	-17.4	1.2	-25.0	0.7	-19.1	1.1

Table 3.6 Average amino acid $\delta^{15}N$ values grouped by site/location

		Amino Acid $\delta^{15}N$ (‰)																							
Location	**Time Period**	n	Ala	±	Gly	±	Thr	±	Ser	±	Val	±	Leu	±	Ile	±	Pro	±	Asp	±	Glu	±	Phe	±	Lys	±
Santa Cruz	Modern	4	18.5	0.9	9.8	0.7	-0.5	0.3	11.2	0.2	19.8	1.1	16.3	0.8	16.7	1.3	13.7	0.3	17.5	0.7	17.2	1.2	9.2	0.7	9.0	1.3
Pt. Conception	Historic	7	15.5	1.4	8.7	1.3	3.5	2.4	10.8	0.6	16.0	1.5	13.6	1.4	13.9	1.3	11.2	1.6	13.2	1.8	15.5	1.2	8.2	1.0	8.2	0.8
San Miguel Island	Historic	2	20.3	0.9	12.4	0.5	6.2	3.4	13.2	2.2	18.0	1.6	17.6	0.1	20.8	1.3	14.1	0.5	17.8	0.2	17.8	0.1	10.8	0.3	NA	NA
San Miguel Island	MLT	2	18.4	2.3	10.1	1.7	2.9	2.2	12.5	0.3	16.0	1.9	14.1	1.1	15.0	1.3	13.8	3.2	15.6	1.3	15.6	2.3	7.4	1.1	5.9	NA
San Miguel Island	Late	2	19.3	1.3	12.1	1.1	4.0	7.0	13.8	1.1	17.3	0.7	15.6	0.9	16.5	0.9	13.2	1.0	16.5	0.6	16.4	1.4	7.3	1.1	NA	NA
Anacapa Island	Early - EZ	3	18.2	0.3	9.2	0.8	0.3	0.1	11.0	0.2	19.2	0.2	16.4	0.1	16.5	0.8	15.2	0.7	17.2	0.3	17.7	0.7	8.2	0.2	9.1	0.4
Santa Rosa Island	Early - Eyb	4	19.4	2.0	9.5	1.5	4.3	1.0	12.4	0.7	17.4	0.7	15.8	0.7	15.3	0.7	12.7	0.8	14.3	1.5	15.8	1.5	7.4	1.1	8.0	1.0

Supplemental Materials

Figure S1. Kernel density plots of A) weight %C and B) weight %N in the entire shell dataset. Notice the bimodal distribution in the weight % observed in both carbon and nitrogen.

A.

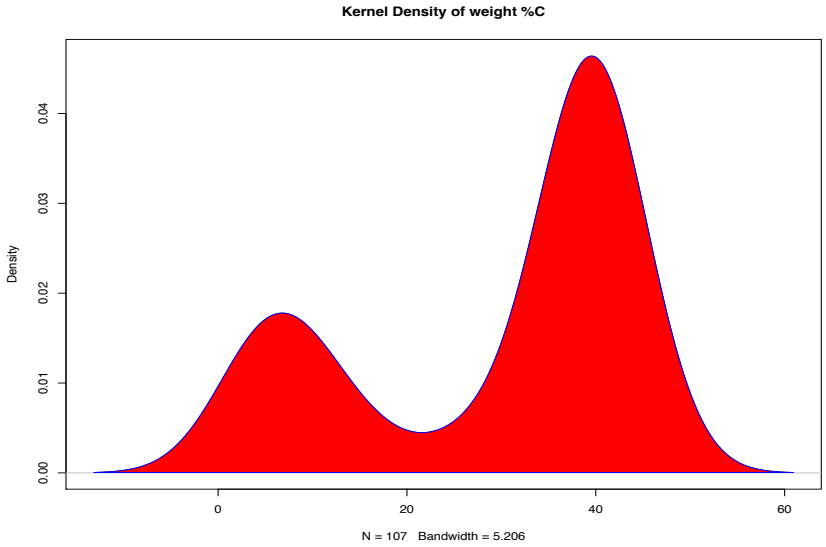

B.

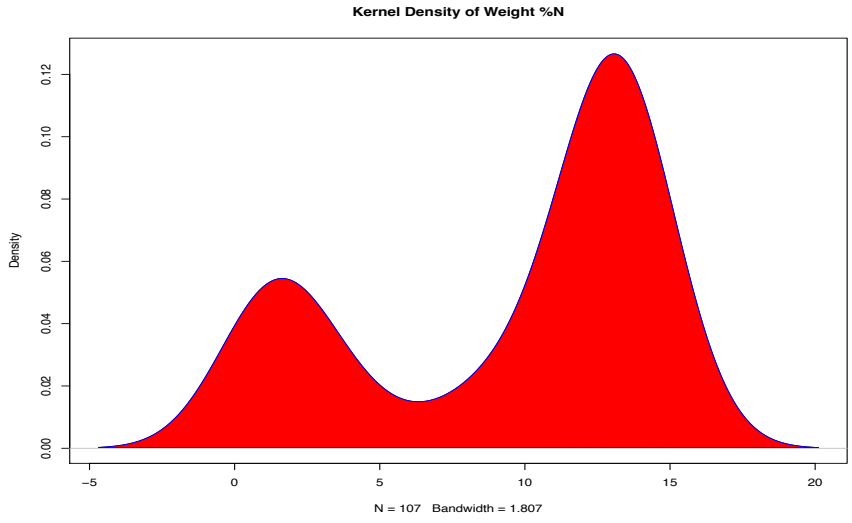

Figure S2. Principle component analysis between samples treated with NaOH clean step, and generally and samples not treated with NaOH. Notice that sample mass vector separates the two groups in PC2.

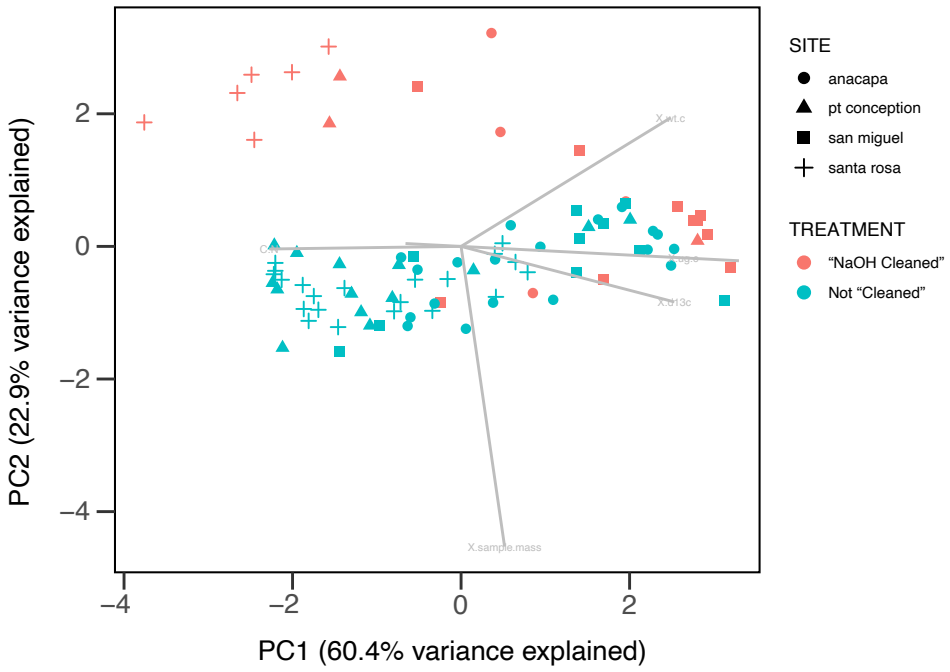

Figure S3. Map of southern California Channel Islands. Strong sea surface temperature gradient, generally corresponding to nutrient availability; ~ 4 °C decrease from inshore to offshore islands.

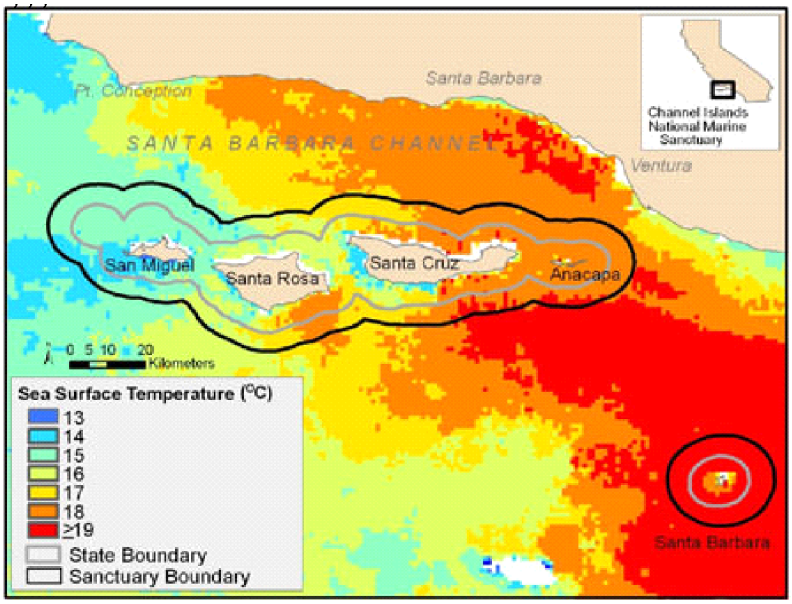

Summary

As climate change accelerates and human resource extraction expands, many parts of the ocean are already experiencing fundamental shifts at the base of ocean food webs. Trophic processes are tightly coupled to carbon and nitrogen biogeochemical cycles, for which any perturbation propagates through entire ocean ecosystems. Climate oscillations such as El Niño and Pacific Decadal Oscillation, or human-induced global planetary warming, both can therefore alter the intensity and trajectory of the atmospheric jet stream, and in turn directly impact not only total primary production, but entire ecosystem health and structure. However, to make a direct link between climate perturbations and large-scale ecosystem response is often very challenging since we cannot go forward in time, so can only be achieved by building detailed historical climate records, using chemical tracers from geologic archives.

In this dissertation I have developed and calibrated a suite of ecological isotope proxies, enabling a whole new bioarchive approach using mollusk shell for paleo-ecological and climatological reconstructions, which can directly address how climate shifts impact nutrient supply- the critical ecosystem-sustaining base of the food web. In this way, my work links sessile filter-feeding bivalves as bioarchives with leading-edge molecular-isotope tools to enable investigations related to natural and human-induced climate change to ecosystems that are highly variable and vulnerable, including coastal marine ecosystems and deep-sea chemosynthetic communities.

In Chapter 1 I developed a suite of geochemical tools using the ubiquitous seep mussel species, *Bathymodiolus childressi*, to understand nitrogen source and cycling in heterogenous deep-sea methane cold seeps. My study was the first ever to measure amino-acid nitrogen isotopes in a chemosynthetic system. With this tool, I was able to decouple nitrogen source isotope values from trophic effects in a chemosymbiotic organism, who's mixotrophic diet predominantly relies on its methanotrophic symbionts for nutrition, while still maintaining the

ability to filter-feed, and thus incorporating local and exogenous nitrogen sources into these food webs. Overall, the new CSI-AA geochemical tools I developed can be applied to other chemosymbiotic species, as well as to extinct or ancient seep shell mounds, to investigate past biogeochemical histories of any chemosynthetic ecosystem in the world's oceans.

In Chapter 2 I addressed the fundamental issue for mollusk shells to be used as a bioarchives, proper calibrations of key isotope signals from soft tissue into shell matrix must be understood. In three ubiquitous species in two common coastal environments, I show that ecological isotope proxies from bulk and CSI-AA (i.e., niche width, baseline nitrogen and carbon, trophic level and resource contribution) are transferred without alteration, and so preserved in shell matrix protein. However, I also show that existing trophic transfer calibration values are incorrect for filter-feeding mollusks in general, and so propose a new mollusk-specific trophic level equation to account for consistent compressed trophic discrimination factors in bivalve soft tissue, and enrichment fractionation factor from isotopic routing in shell.

Finally, in Chapter 3, to produce reliable historical and geological records from shell matrix protein, understanding the impact of diagenesis on isotope signals is fundamentally important. For this, I measured bulk and amino acid carbon and nitrogen isotopes in the insoluble shell matrix protein of archaeological *Mytilus californianus* shells from a wide range of time periods and depositional environments around the California Channel Islands. I show that while bulk isotopes are highly susceptible to diagenetic alteration, CSI-AA proxies are largely preserved without change. My data also provide the molecular level mechanisms driving bulk isotope diagenetic alteration in shell, at both the molar composition and molecular isotope level, than has ever been done before.

This dissertation represents a foundational step forward in CSI-AA approaches and systematics, solving past issues with mollusk data and fundamentally expanding the use of CSI-AA in a broad range of studies. The work proposed in this dissertation offers an entirely new suite of tools to ecologists wishing to reconstruct baseline nutrient sources and primary producer community structure, geobiologists investigating relative contribution of chemosynthetic

production into food webs, oceanographers concerned with rapid shifts in coastal zones, and archaeologists keen in understanding the effects of climate change on Native American coastal subsistence, culture, and socipolotical systems. My dissertation provides the bedrock for employing bivalves as bioarchives in reconstructing ecological and biogeochemical histories to help understand some of the most productive regions of our oceans, and potentially make predictions about the state of marine ecosystems in the future.